



UNIVERSITY  
OF TRENTO - Italy

Department of Materials Engineering  
and Industrial Technologies

---

---

Doctoral School in Materials Science and Engineering – XXIV cycle

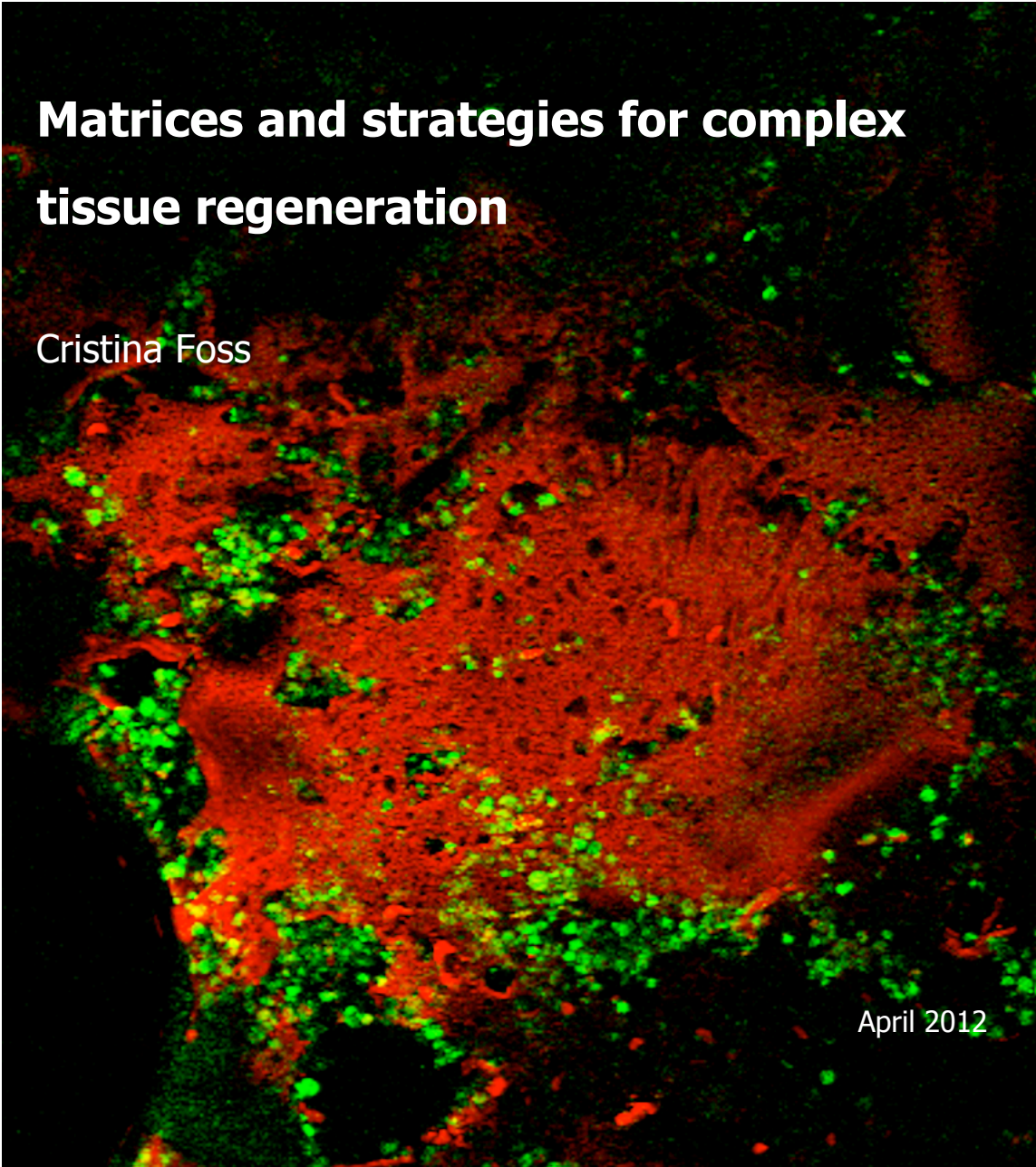
---

---

# Matrices and strategies for complex tissue regeneration

Cristina Foss

April 2012

A large, dark-field fluorescence microscopy image showing a complex, porous structure. The structure is primarily red, with numerous bright green spots and clusters scattered throughout, indicating specific components or cells within the matrix.

# Contents

<b>1</b>	<b>Introduction</b>	<b>9</b>
1.1	Definition and principles of Tissue Engineering . . . . .	9
1.2	Human joint anatomy . . . . .	14
1.3	Osteochondral defect . . . . .	19
1.4	Osteochondral Tissue Engineering . . . . .	21
1.4.1	Cartilage regeneration: materials and strategies . . . . .	22
1.4.2	Bone regeneration: materials and strategies . . . . .	24
1.4.3	Osteochondral strategies . . . . .	26
1.5	A natural polymer: silk fibroin . . . . .	32
1.5.1	Silk fibroin structure . . . . .	33
1.5.2	Silk fibroin as a multifunctional polymer . . . . .	37
1.5.3	Silk fibroin in Tissue Engineering . . . . .	38
1.5.4	Degradation and immunological response . . . . .	46
1.6	Proposed research and objectives . . . . .	47
<b>2</b>	<b>ASCs and silk fibroin scaffolds</b>	<b>51</b>
2.1	Introduction . . . . .	51
2.2	Materials and methods . . . . .	52
2.2.1	Scaffold preparation . . . . .	53
2.2.2	Isolation and culture of adipose-derived stem cells (ASCs)	54
2.2.3	Cell seeding and culture of silk fibroin/ASC constructs .	54
2.2.4	Cell seeding efficiency . . . . .	55

2.2.5	Cell viability . . . . .	55
2.2.6	Cell proliferation . . . . .	55
2.2.7	Real time PCR analysis . . . . .	56
2.2.8	Compressive mechanical properties . . . . .	56
2.2.9	Sulfated glycosaminoglycan production . . . . .	57
2.2.10	Histological analysis . . . . .	57
2.2.11	<i>In vivo</i> implantation and evaluation . . . . .	58
2.2.12	Statistical analysis . . . . .	59
2.3	Results and discussion . . . . .	59
2.3.1	Cell loading efficiency, viability and distribution . . . . .	59
2.3.2	Cell proliferation . . . . .	61
2.3.3	Chondrogenic differentiation . . . . .	61
2.3.4	Mechanical properties of <i>in vitro</i> cultured silk scaffolds . . . . .	69
2.3.5	<i>In vivo</i> repair of chondral defects . . . . .	71
2.4	Conclusions . . . . .	75
<b>3</b>	<b>Hyaluronic acid and silk fibroin</b>	<b>77</b>
3.1	Introduction . . . . .	77
3.2	Materials and methods . . . . .	81
3.2.1	Scaffold production . . . . .	81
3.2.2	Scaffold characterization . . . . .	82
3.2.2.1	Environmental Scanning Electron Microscopy . . . . .	82
3.2.2.2	Fourier Transform Infrared Spectroscopy . . . . .	82
3.2.2.3	Porosity . . . . .	82
3.2.2.4	Cross-linking degree . . . . .	82
3.2.2.5	Water content . . . . .	84
3.2.2.6	Wettability properties . . . . .	84
3.2.2.7	Mechanical properties . . . . .	84
3.2.2.8	Hyaluronic acid mapping and quantification . . . . .	85
3.2.2.9	Statistical analysis . . . . .	86
3.3	Results and discussion . . . . .	86

3.3.1	Environmental Scanning Electron Microscopy . . . . .	86
3.3.2	Fourier Transform Infrared Spectroscopy . . . . .	88
3.3.3	Cross-linking degree . . . . .	91
3.3.4	Porosity . . . . .	95
3.3.5	Wettability properties . . . . .	95
3.3.6	Water content and mechanical properties . . . . .	98
3.3.7	Hyaluronic acid mapping and quantification . . . . .	101
3.4	Conclusions . . . . .	103
<b>4</b>	<b>Chondrocytes on SF/HA scaffolds</b>	<b>105</b>
4.1	Introduction . . . . .	105
4.2	Materials and methods . . . . .	107
4.2.1	Scaffold preparation . . . . .	107
4.2.2	Hyaluronic acid loss of SF/HA scaffolds in culture medium	107
4.2.3	Isolation and culture of resting zone chondrocytes . . . . .	108
4.2.4	Cell seeding and culture of scaffold/chondrocyte constructs	108
4.2.5	Cell seeding efficiency . . . . .	109
4.2.6	Cell proliferation . . . . .	109
4.2.7	Real time PCR analysis . . . . .	109
4.2.8	Alkaline phosphatase activity . . . . .	110
4.2.9	Compressive mechanical properties . . . . .	110
4.2.10	Sulfated glycosaminoglycan production . . . . .	110
4.2.11	Statistical analysis . . . . .	111
4.3	Results and discussion . . . . .	111
4.3.1	Hyaluronic acid loss from SF/HA scaffolds in culture medium . . . . .	111
4.3.2	Effect of HA-enriched medium on chondrocyte/SF con- structs . . . . .	113
4.3.3	Cell seeding efficiency and proliferation . . . . .	117
4.3.4	Chondrogenic phenotype analysis . . . . .	118

4.3.5	GAG production and mechanical properties of chondrocyte/scaffold constructs . . . . .	122
4.4	Conclusions . . . . .	125
<b>5</b>	<b>Interface: the nanometric net</b>	<b>129</b>
5.1	Introduction . . . . .	129
5.2	Materials and methods . . . . .	133
5.2.1	Scaffold production . . . . .	133
5.2.2	Scaffold characterization . . . . .	134
5.2.2.1	Scanning electron microscopy . . . . .	134
5.2.2.2	Fourier Transform Infrared Spectroscopy . . . . .	134
5.2.2.3	Differential scanning calorimetry . . . . .	134
5.2.3	Co-culture of human articular chondrocytes and osteoblasts . . . . .	135
5.2.3.1	Cell seeding and co-culture of chondrocyte/scaffold constructs and osteoblasts . . . . .	135
5.2.3.2	Chondrocyte viability . . . . .	136
5.2.3.3	Cell proliferation . . . . .	136
5.2.4	Statistical analysis . . . . .	137
5.3	Results and discussion . . . . .	137
5.3.1	Scaffold characterization . . . . .	137
5.3.1.1	Scanning electron microscopy . . . . .	137
5.3.1.2	Fourier Transform Infrared Spectroscopy . . . . .	139
5.3.1.3	Differential scanning calorimetry . . . . .	139
5.3.2	Co-culture of human articular chondrocytes and osteoblasts . . . . .	142
5.3.2.1	Cell proliferation . . . . .	142
5.3.2.2	Chondrocyte viability . . . . .	145
5.4	Conclusions . . . . .	149
<b>6</b>	<b>Final remarks</b>	<b>151</b>

# Abstract

In the field of Tissue Engineering, a new concept has been developed in the last few years. The formation of new tissue induced by a tissue engineered system needs to be accompanied by the achievement of a complete tissue functionality and scaffold properties have to be designed following the principles of biomimetics, i.e. the complexity of the physiological environment has to be translated and reproduced in the cell-scaffold construct.

This approach is especially challenging when the interface between two tissues has to be restored. In this case, the scaffold has not only to sustain the regeneration of two different tissues, but also to ensure the regeneration of a functional interfacial zone between them. Therefore, scaffold properties must reflect the complexity of tissue boundary structures, in terms of controlled gradients in morphological, chemical and mechanical properties.

The aim of this research work was the application of these advanced principles to the regeneration of the osteochondral defect, which is a degenerative pathology involving both cartilage and bone tissue, whose current treatments are ineffective in the long term.

In this work, a multiphasic scaffold for osteochondral Tissue Engineering was produced and characterized. Silk fibroin-based 3D sponges were employed for the chondral and subchondral components for cartilage and bone regeneration, respectively, to exploit the biocompatibility and versatility of silk fibroin in Tissue Engineering applications. For the restoration of a functional interface, a nanometric net was used to separate the two components, in order

to allow a dialogue among cells between the two phases thanks to a physiological solute flow, while preventing cell migration towards the chondral site, especially of blood cells which may cause mineralization of the non-calcified cartilage.

For the chondral component, two different strategies were explored. First, pure silk fibroin sponges produced by salt leaching were combined to static or dynamic culture conditions to evaluate the chondrogenic potential of adipose-derived stem cells (ASCs). These cells have indeed many advantages for cartilage Tissue Engineering applications, such as abundance, easy accessibility, ability of self-renewal and stability during *in vitro* culture. The best differentiation of ASCs towards chondrocytes was achieved after 28 days of culture in a static environment and chondrogenic media, in terms of higher chondrogenic gene expression, new cartilage extracellular matrix deposition and increase of compressive mechanical properties. ASC/scaffold constructs were then implanted *in vivo* in a rat xiphoid critical size defect for 8 weeks and also in this case, the best outcomes in terms of new tissue volume and quality were obtained when static conditions and chondrogenic medium were employed during pre-culture.

The aim of the second strategy presented in this work was to modify silk fibroin (SF) sponges with the addition of hyaluronic acid (HA). Besides hyaluronic acid is a natural component of cartilage and contributes to its biomechanics thanks to its ability to retain a remarkable amount of water, it has been shown to modulate chondrocyte phenotype when employed in scaffolds for cartilage regeneration. Therefore, we exploited its properties producing silk fibroin/hyaluronic acid scaffolds by salt leaching at different HA concentrations, eventually cross-linked by genipin to improve HA retention. SF/HA sponges were completely characterized in terms of physical, chemical and mechanical properties and then used to culture primary chondrocytes *in vitro*. Results demonstrated that the scaffolds with the highest amount of hyaluronic acid both with and without cross-linking elicited better responses in cartilage cells with respect to pure silk fibroin sponges, in terms of chondrogenic

phenotype enhancement and new cartilage extracellular matrix deposition.

The nanometric net of the multicomponent scaffold for osteochondral regeneration was produced by electrospinning of poly-d,l-lactid acid/polyethylene glycol (PdlLA/PEG) blends. PdlLA was employed since it is a well-known biocompatible polymer and it is easy to process with this technique, while PEG was added to avoid fiber shrinkage in an aqueous environment. Nets were characterized in terms of morphology and thermal properties, then assembled to a silk fibroin sponge without any modification to their geometry. To preliminarily evaluate the biological properties of PdlLA/PEG electrospun nets, a system to co-culture chondrocytes on scaffolds with net and osteoblasts was designed and validated, so that the biochemical communications between cells could take place through the net fibers. In the future, this system will be employed to evaluate how osteoblasts can improve chondrocyte response in terms of phenotype maintenance and new cartilage tissue deposition.

The results reported in this research work will be the basis for the final design of a multicomponent scaffold which comprises the best outcomes obtained. Hence, SF/HA scaffolds which elicited the best responses on chondrocytes will be used in combination with ASCs, in order to verify their potential to sustain chondrogenesis *in vitro*. Then, they will be assembled to the nanometric net and, before moving to an appropriate *in vivo* study, the co-culture system will be employed to assess how the cellular dialogue with osteoblasts can have beneficial effects on the chondrogenic differentiation of adipose-derived stem cells.



# Chapter 1

## Introduction

### 1.1 Definition and principles of Tissue Engineering

The definition of Tissue Engineering was first established in 1988, during a conference organized by the National Science Foundation in Lake Tahoe (California). It was defined as the “application of principles and methods of engineering and life sciences toward fundamental understanding of structure–function relationship in normal and pathological mammalian tissues and the development of biological substitutes to restore, maintain, or improve functions” [1]. The aim of Tissue Engineering is therefore the regeneration of structures in the organism which have been compromised by traumas and/or pathologies implanting in the damaged site new tissue artificially produced.

The paradigm of Tissue Engineering is schematically shown in figure 1.1. Functional tissue can be fabricated starting from a scaffold, that is a tridimensional structure able to guide tissue development, eventually combined with a cell source able to regenerate the tissue. Several cell sources can be employed, from cells extracted from the patient in the damaged tissue to stem cells of different origin, cultured so that they express the suitable phenotype. Scaffolds can be made of natural and/or artificial materials and populated by cells before or after implantation. In this latter case, cells available in the

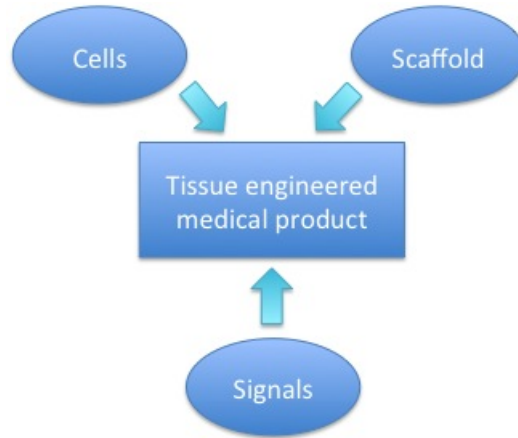


Figure 1.1: The paradigm of Tissue Engineering.

implantation site are supposed to migrate inside the 3D structure and synthesize new extracellular matrix (ECM). It is clear that, to this purpose, the chemical, physical and biological properties of the scaffold have to be designed carefully, to guide the tissue regeneration in a physiologically functional way. To improve the restoration of the tissue, specific signals can be conjugated to the material (in order to be released in the damaged site) or used during the preliminary *in vitro* culture. These signals can be chemical (such as growth factors) or mechanical (hydrostatic pressure or compressive stimulation, for instance): their aim is to help processes such as tissue morphogenesis, ECM functional distribution throughout the scaffold, cellular differentiation [1].

From the previous considerations, it becomes evident how the approach of Tissue Engineering implies the transfer of the medical treatment to a cellular level: the resources needed for tissue regeneration are introduced in the pathologic environment in a suitable configuration to optimize their activity and help the natural processes of self-repair. The main advantage (and the main challenge) of this strategy is the control of the tridimensional development of the new tissue in a functional way.

The achievement of this goal is highly dependent on many variables: the

use of a cell-free or a pre-seeded scaffold; the choice of the most appropriate cell source; the material to use to produce the scaffold; the design of the morphological, chemical and physical properties of the scaffold; the parameters to employ in the preliminary *in vitro* culture; and so on. However, all these ingredients should be chosen and combined according to a simple but not trivial principle, i.e. biomimetics. This means that the biological system to regenerate has also to be the model to design the Tissue Engineering system. It implies that the cellular behavior has to be known in detail, both during normal tissue morphogenesis and during the repair and regeneration phases when a damage or a pathology is present. In fact, only in this case we will be able to evaluate how cells can be guided towards tissue regeneration, that is, which signals have to be provided, both *in vitro* and *in vivo*.

Under this point of view, the scaffold is, besides cells, a fundamental component for tissue regeneration, since its role is to sustain and promote new tissue formation through the interaction with cells. To fabricate a scaffold, several so-called *biomaterials* have been proposed and used: polymers, metals, ceramics, composites, either natural or synthetic. The definition of biomaterial can be given in different ways, with an increasing degree of complexity: a biomaterial can be simply described as a material used to substitute a portion of a living system or put in direct contact with a biological tissue; alternatively, a biomaterial can be any material used in a medical device and able to interact with biological systems. However, one of the most complete definition may be considered the following: “any substance (other than drugs) or combination of substances, synthetic or natural in origin, which can be used for any period of time, as a whole or as a part of a system which treats, augments or replaces any tissue, organ or function of the body” [2]. The action of a biomaterial is governed by the interaction between material and organism, that is, by the reciprocal effect of the biological environment on the material and viceversa. The property which describes this interaction is called biocompatibility and is a fundamental requirement of a scaffold for Tissue Engineering.

The first definition of biocompatibility was given when implantable devices

started to be used in the clinical practice (during the years between 1940-1980), as materials that were meant to remain within an individual for a long time. Initially, efforts were focused on the events that had to be avoided and a material was considered biocompatible if and only if it was accepted by the surrounding tissues and the organism, i.e. it was non-toxic, non-immunogenic, non-thrombogenic, non-carcinogenic, non-irritant and so on [2, 3].

The same concept of biocompatibility was adopted when the first generation of biomaterials was designed for Tissue Engineering applications and any kind of reactions of the body was minimized to obtain a bioinert material. The biomaterial was thought as something invisible after implantation, but the outcomes of this approach were disappointing. Today, biomaterials are designed to be active and to establish a reciprocal dialogue with cells, in order to guide them towards the formation of new functional tissue. In this case, the concept of biocompatibility is enriched with a more complex meaning, which becomes tightly correlated to the application of the biomaterial itself. This means that it can be considered biocompatible if, after implantation, the biomaterial can interact according to its purpose, without causing any damage to the organism. Recently, a complete and exhaustive definition was given by Williams [3]: “Biocompatibility refers to the ability of a biomaterial to perform its desired function with respect to a medical therapy, without eliciting any undesirable local or systemic effects in the recipient or beneficiary of that therapy, but generating the most appropriate beneficial cellular or tissue response in that specific situation, and optimizing the clinically relevant performance of that therapy”.

On these bases, the ideal properties of a scaffold for Tissue Engineering can be outlined: besides biocompatibility (as defined above), it has to have a high tridimensional and interconnected porosity to allow cell migration, nutrient diffusion and a functional organization of new tissue; morphology has to be designed according to the physiological properties of the damaged tissue; its surface has to be chemically suitable to induce cell adhesion, proliferation and differentiation. Finally, the biodegradability of the material has to be

carefully evaluated: the scaffold has to degrade in a controlled fashion, so that the 3D structure of the scaffold can be gradually substituted with new tissue and the loss of mechanical stability is compensated by the formation of fresh ECM. Moreover, degradation products have to be biocompatible, too. Last, but not least, a scaffold needs to be implanted easily, its production should be reproducible also on a large scale for a clinical application and has to be sterilized to avoid any contaminations which may cause the failure of an implant.

After all these considerations, it appears clear that the complexity of the Tissue Engineering approach represents its major strength and its highest obstacle. Many challenges have to be handled to reach its final aim, i.e. to gradually substitute organ transplantation. However, efforts have been done towards this objective and some tissue engineered applications are today commercially available, for instance for skin regeneration to heal burns or diabetic ulcers. Many studies are currently in progress in the field of cardiovascular, urologic, neurologic, orthopedic and muscular diseases, searching new biomaterials and new scaffolds. Promising results have been obtained thanks to the development of bioreactors, i.e. systems able to provide suitable cell culture conditions in terms of nutrient flow and mechanical stimulation. Tissue formation *in vitro* has been improved, but many difficulties has still to be ridden out: stimuli have to be designed specifically according to the application and the mechanisms underlying the integration of a graft after implantation *in vivo* need to be understood [1].

Finally, a crucial remark has to be done about the economical, social and ethical impact that a clinical application of Tissue Engineering will have. Many issues need to be solved, such as the debate about the use of embryonic stem cells or the necessary requirements to start a clinical trial on humans. However, results remain promising and more and more benefits will soon be available for patients.

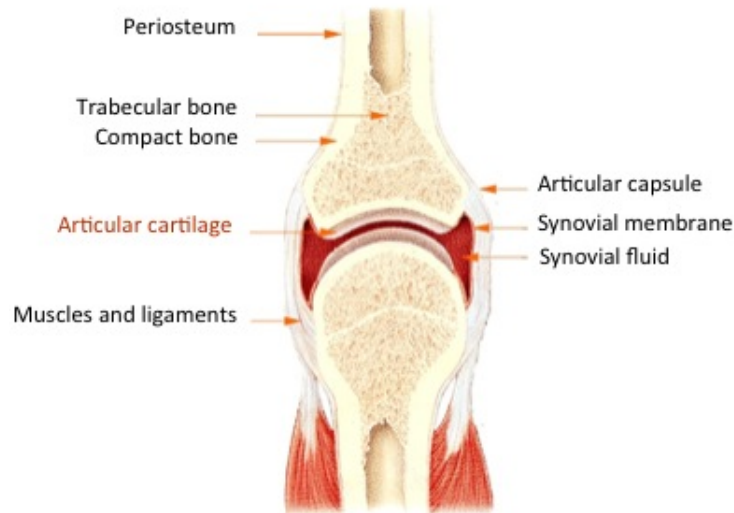


Figure 1.2: Example of a joint and its components (adapted from [8]).

## 1.2 Human joint anatomy

This section will describe the human joint anatomy and the main characteristics of cartilage and bone. As previously mentioned, it is fundamental to know tissue properties both in normal and pathologic conditions to design a scaffold for its regeneration. In this way the scaffold can be developed in order to reproduce the peculiar characteristics of the tissue *in vivo* and to induce the desired response even if in a potentially hostile environment. Therefore, cartilage and bone will be briefly illustrated here, while the etiology and the current treatments of osteochondral defect will be presented in the following section.

The joint is composed by hyaline cartilage and subchondral bone, which have completely different mechanical and morphological features (figure 1.2).

Hyaline cartilage is highly specialized, has a low-friction surface and provides an efficient load distribution [4]. It can be considered a biphasic and

inhomogeneous structure made of a solid phase (15-32%) and a liquid phase (68-85%), which form the extracellular matrix of the tissue [5]. The cellular component, the chondrocytes, is only 5% of cartilage but its fundamental role is to preserve tissue homeostasis, degrading and substituting ECM to maintain tissue integrity and mechanical properties. Mature chondrocytes are rounded, unable to proliferate and completely embedded in ECM. Some of them have cilia in the extracellular environment which can collect mechanical stimuli to modulate tissue composition according to the load applied to the joint [6]. In fact, extracellular matrix composition has a key role to determine the peculiar mechanical properties of hyaline cartilage. Its main component is collagen type II (90-95%): it forms fibrils which give tensile strength to the tissue and entrap other matrix macromolecules. The second constituent of cartilage ECM are proteoglycans (PG), which are characterized by a protein backbone bound to one or more variety of glycosaminoglycans (GAG) (such as hyaluronic acid, chondroitin-sulfate, chondroitin-sulfate). Since they are negatively charged, they are able to retain a huge amount of water that contributes to the viscoelastic behavior of hyaline cartilage. The assemblies of more proteoglycans are called aggrecans (figure 1.3) and their interconnection with collagen molecules prevents PG diffusion during the application of a load [6]. Minor proteins in hyaline cartilage include glycoproteins, fibronectin and anchorin II: their role is to stabilize the ECM and anchor chondrocytes to the surrounding matrix. Finally, cartilage liquid component is formed by water, gas, metabolites, cations which balance the negative charge of GAG molecules. To supply nutrients to chondrocytes, there is a continuous communication between the cartilage liquid phase and the so-called synovial fluid: it covers articular surfaces in physiological conditions and is produced by a specialized tissue (the synovial matrix) which interacts with cartilage forming a complex system to support its metabolic and adaptation processes. Moreover, the synovial matrix seals the articular capsule to prevent liquid leakage during tissue deformation [7].

From a macroscopical point of view, cartilage behaviour during physiological compressive, tensile and shear stresses is strongly anisotropic and non

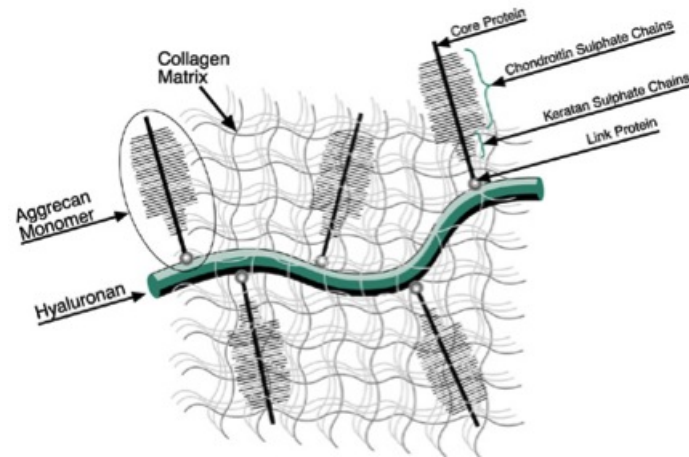


Figure 1.3: Aggrecan structure (adapted from [9]).

linear, because collagen fibers have different orientations throughout the tissue. According to ECM morphology, 4 different zones can be distinguished: a superficial zone (10-20% of total thickness), an intermediate zone (40-60%), a deep zone (30-40%) and a calcified zone at the interface with the subchondral bone (figure 1.4).

The superficial layer contains the highest amount of water and collagen and the lowest quantity of proteoglycans. It comprises 2 zones: the first has no cells but small collagen fibrils, which run parallel to the articular surface and makes this portion resistant to shear stresses due to joint movements; the second is under the previous one and presents flattened chondrocytes, again parallel to the surface.

Collagen concentration decreases in the intermediate zone but there are more PG molecules. Fibrils usually have a higher diameter and a random orientation. Cell morphology also changes and chondrocytes appear more rounded.

In the deep zone there is the greatest amount of proteoglycans and collagen fibrils run perpendicular to the underlying bone surface. Rounded chondrocytes form columnar structures oriented in the same direction and have a strong

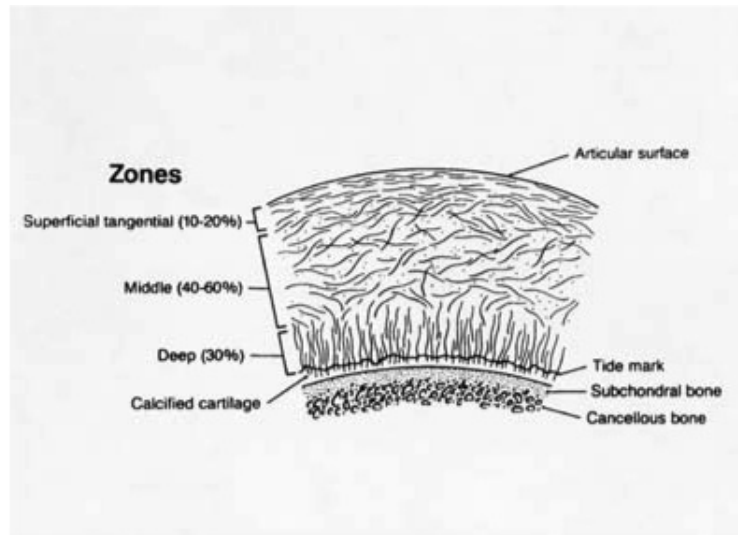


Figure 1.4: Schematic representation of the zonal organization of cartilage (adapted from [10]).

activity of biosynthesis. They can aggregate in complexes of 2-6 cells called isogenous groups.

The calcified zone represents the transition between cartilage and subchondral bone and the fixation zone is completely impermeable. Chondrocytes are smaller than in the other portions of the tissue and have a low metabolic activity [6, 7].

The subchondral bone is a dense and rigid layer of bone tissue between hyaline cartilage and the trabecular bone underneath. Its abundant extracellular matrix is characterized by a protein component and a mineralized component [4]. As in cartilage, the organic part of ECM is formed by collagen fibers, but in this case of type I for 90-95%. They form helical bundles which give rigidity and strength to the tissue. The bundles are then arranged in lamellar tridimensional structures, as shown in figure 1.5. Lamellae are finally distributed around the so-called haversian channels which surround blood vessels and form structures named osteons. An amorphous component made of proteoglycans

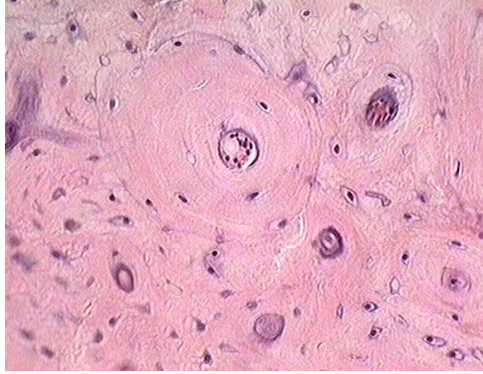


Figure 1.5: Histological section of a compact bone, showing the lamellar organization of osteons [11].

and glycoproteins is dispersed in the fibrous part of ECM: fibronectin, thrombospondin and osteopontin are some elements of this phase and their role is to make cells adhere to the extracellular matrix. Other characteristic proteins of bone tissue are osteocalcin, involved in ECM synthesis, and osteonectin, responsible for the promotion of the mineralization of the tissue.

The peculiar property of bone is in fact its mineralization: minerals are the framework which provides tissue hardness and therefore allows bone to support and sustain the human body. The main bone mineral components are calcium phosphates, especially hydroxyapatite (empirical formula:  $Ca_{10}(PO_4)_6(OH)_2$ ). It forms prism crystals, with a length of 20 nm and a thickness of 2 nm.

Bone cellular component comprises 4 different kinds of cells: osteoblasts, whose role is to synthesize and mineralize new ECM; osteoclasts, which degrade the tissue so that it can be substituted and renewed continuously; osteocytes, which are osteoblasts in a quiescent state surrounded by calcified ECM; finally, osteoblast precursors, i.e. inactive cells but able to differentiate in bone cells [12].

Thanks to cell activity, bone tissue undergoes a continuous renewal in a delicate equilibrium between synthesis and degradation of the extracellular matrix. Its metabolism and regeneration are regulated by several growth factors,

such as Insulin-like Growth Factor (IGF), Fibroblast Growth Factor (FGF) and Bone Morphogenetic Protein (BMP). As in cartilage, bone matrix composition is fundamental to provide the suitable mechanical properties and the ability to adapt to different applied loads. In fact, it was demonstrated that the orientation of collagen fibrils is modified according to the direction of the load to optimize tissue strength.

### 1.3 Osteochondral defect: aetiology and limits of the surgical treatments

Cartilage and bone can degenerate because of pathologies or traumas; if it involves both tissues in the joint, the damage is called osteochondral defect. These lesions are found most frequently in the femoral condyles, capitellum of the elbow, dome of the talus and the dorsal surface of the patella [13, 14]. The main issue related to this problem is the inability of cartilage to self-repair, since it is avascular and aneural and cannot access the normal pathways of wound healing [4].

The origins of an osteochondral degeneration have not been clarified yet. Several factors can contribute to the formation of an osteochondral defect, such as ischemia, genetics, abnormal vasculature and metabolic disorders [15]. The most frequent associated pathology is osteoarthritis (OA), an age-related debilitating and degenerative disease. OA leads to an imbalance in the anabolic and the catabolic activity in cartilage, which determines a decrease of proteoglycan synthesis, the rupture of collagen fibrils and finally tissue necrosis and cell apoptosis. This process changes significantly the biomechanical properties of hyaline cartilage until its degradation and at the end can involve the subchondral bone [5].

As previously mentioned, age is the most frequent cause of osteoarthritis: the ability of chondrocytes to maintain tissue homeostasis decreases with time and therefore the structural and biochemical organization of cartilage ECM undergoes a modification. Also an inflammatory process can lead to an ab-

normal regulation of the activity of cytokines, i.e. signaling molecules used for cellular communications. These substances can stimulate the production of metalloproteinases (MMP), which are enzymes able to degrade collagen and other ECM molecules. However, it is still unknown what can trigger an inflammation in the joint: inappropriate joint loads and/or products of matrix degradation (such as fibronectin fragments) are potential candidates [5, 15].

Traumas are the third cause of osteoarthritis: injuries or excessive mechanical stresses (articular misalignment, muscular weakness, sport) can lead to proteoglycan depletion or the rupture of the collagen network. Thus, OA is induced by a chronic overload determined by joint incongruity and instability: these factors can cause tissue degradation because they increase cell apoptosis, MMP production and oxidative stress [16].

Degenerative joint diseases and osteochondral defect have a strong social and economical impact: for instance, in 2008 they represented the leading cause of chronic disability in the United States, affecting 20% of the adult population and forcing one third of patients to limit their daily activity and undergo surgical intervention; the total cost of osteoarthritis is estimated in 28.6 billion dollars a year and it will rise because aged population is increasing [17]. The situation is particularly problematic because all current treatments are unable to achieve a long-term repair of the joint. In the field of reparative surgery, therapies include arthroscopic debridement, abrasion arthroplasty and microfracture: these techniques stimulate the repair process inducing the release of mesenchymal stem cells from bone marrow into the damage site. However, fibrocartilage is formed with low resilience, reduced stiffness and weak wear resistance, thus it cannot withstand physiological loads in long term [18]. Other options comprise mosaicplasty, which implies the remotion of osteochondral plugs (autografts) from not-bearing sites of the patient and the transplantation of these plugs in the site of injury, and Autologous Chondrocyte Transplantation (ACT), where lesions are filled with pre-cultured chondrocytes extracted from the patient, expanded *in vitro* and confined under a periosteal flap to the damaged site. Both these techniques are affected by

lacking availability and morbidity of donor sites, low integration with the surrounding tissues, difficulty in matching the topology of the graft to the shape of the injured site and the formation of fibrocartilage, as reported above [17, 19].

To overcome these limitations, the application of tissue engineering principles outlined in paragraph 1.1 has shown a great potential, because the morphological, biological, chemical and mechanical properties of the graft necessary to obtain a complete and durable repair of the joint can be tailored *ad hoc* [17, 21]. In the following section, the state of art of osteochondral tissue engineering will be presented, with particular attention to the most recent concepts regarding the restoration of cartilage and the osteochondral interface.

## 1.4 Osteochondral tissue engineering: state of the art

As previously mentioned, a scaffold for Tissue Engineering and the subsequent strategy for tissue restoration should follow the principle of biomimetics. In the case of osteochondral regeneration, this means to design an integrated system able to guide the formation of two tissues with different properties and different needs to achieve a complete functionality. Thus, the complexity increases. Two worlds has to be combined together conjugating the best outcomes for cartilage and bone regeneration, but this is not enough: the system has also to allow their integration among each other and the surrounding environment, inducing the restoration of a physiological interface between these tissues.

Therefore, the main strategies in cartilage and bone Tissue Engineering will be presented in this section and followed by examples about how they have been combined for osteochondral regeneration. Finally, new concepts and recent developments in the restoration of cartilage-to-bone interface will be shown.

### 1.4.1 Cartilage regeneration: materials and strategies

A scaffold for cartilage regeneration should be characterized by a high and interconnected porosity to simulate what happens in the physiological environment, where chondrocytes are suspended and isolated in a dense ECM. The material has to be chosen according to several criteria, such as the type of damage (its extension, for instance), joint conditions after implantation (it may be conjugated with anti-inflammatory drugs), *in vitro* culture method (if mechanical stimulation is provided, scaffold material has to be able to sustain the applied load) [5, 6].

Both natural and synthetic polymers have been proposed for cartilage Tissue Engineering (figure 1.6). Natural materials have many advantages, including a known biocompatibility also because of ligands which can be recognized by cells. However, they may be difficult to find and process, have weak mechanical properties and a too high degradation rate [5, 12]. One of the most common natural polymers used for cartilage regeneration is collagen. A first study was conducted in 1983, where chondrocytes seeded on collagen gels maintained their phenotype and produced GAG after a 6-week culture [22]. Since these first results, collagen have been widely used in cartilage Tissue Engineering, also with stem cells of different origin both *in vivo* and *in vitro* [23, 24, 25]. The main advantage of collagen is that it is part of cartilaginous ECM, thus it is recognized by cellular enzymes and can be degraded and remodeled after implantation. Moreover, it was observed that collagen can stimulate the production of new collagen more than other materials [6].

Another commonly used natural polymer is hyaluronic acid, which is also physiologically present in cartilage. A more detailed discussion about its properties and its recent uses will be reported in paragraph 3.1; however, it is worth to mention one of its main advantages, i.e. its ability to decrease MMP and nitrogen oxide (NO) levels *in vitro* and inhibit cell apoptosis [5]. For this reason, it may have a fundamental role in regulating the inflammatory process associated with osteoarthritis.

Material	Advantages	Disadvantages
<b>Natural polymers</b>		
Collagen	Low antigenicity and good cell-binding properties.	Low biomechanical stiffness and rapid biodegradation. Toxicity of some of the cross-linking agents.
Silk fibroin	Long standing history of use in clinical applications. Slow degradability, versatility in processing, remarkable mechanical strength and thermal stability. Easy chemical decoration, genetically tailorable composition and sequence.	Need of purification. Contamination from residual sericin may cause biocompatibility problems.
Chitosan	Hydrophilic surface promoting cell adhesion, proliferation and differentiation. Good biocompatibility and acceptable host response. Antibacterial activity.	Mechanical weakness and instability. Incapacity to maintain a predefined shape. Impurities affecting material properties.
Hyaluronic acid	No immunogenic properties, ease of chain size manipulation, Interactions with cell-surface receptors. Production through large-scale microbial fermentation.	Water solubility. Its anionic surface does not thermodynamically promote cell attachment and tissue formation.
Alginates	Cross-linking under very mild conditions. Gel injection avoiding an open surgical procedure.	Mechanical weakness, difficult to sterilize and to handle. Impurities affecting material properties.
<b>Synthetic polymers</b>		
Aliphatic polyesters (Polylactid acid, polyglycol acid and their copolymers)	FDA approval for various medical applications. Degradation rate, physical and mechanical properties adjustable by changing the copolymer ratio.	Possible premature fail of scaffold due to bulk hydrolysis. Adverse tissue reactions caused by acidic degradation products. Poor wettability and lack of cellular adhesion and interaction.
Poly( $\epsilon$ -caprolactone) (PCL)	FDA approval for various medical applications.	Slow degradation rate (years). Release of acidic degradation products (slower than short chain saturated aliphatic polyesters). Poor wettability and lack of cell adhesion and interaction.

Figure 1.6: Advantages and disadvantages of natural and synthetic polymers used in cartilage Tissue Engineering (adapted from [20]).

Other natural materials used for scaffolds in cartilage Tissue Engineering comprise agarose, cellulose, chitosan, starch, which have been employed to produce hydrogels, sponges and meshes [26, 27, 28, 29]. Among natural polymers, silk fibroin (SF) has been shown promising results: it has a high biocompatibility and processing can modulate its degradation rate and mechanical properties. Since fibroin was widely used in this work, an exhaustive description of its characteristics and its applications will be reported in paragraph 1.5.

With respect to natural materials, synthetic polymers have a high versatility and a virtually endless availability, can be processed more easily and their chemical and physical properties can be designed *ad hoc* by copolymerization or composite fabrication [5]. However, their biocompatibility has to be carefully tested, with particular attention to the degradation products which may be potentially toxic. The most used artificial polymers are polylactic acid (PLA), polyglycol acid (PGA) and their copolymers, polycaprolactone (PCL), polyurethane, polyethylene glycol (PEG) [5, 29, 30, 31]. They have been often processed to obtain injectable materials such as hydrogels, which may be suitable for cartilage regeneration because of their high water content and their ability to encapsulate cells or incorporate drugs. However, the weak mechanical properties of these scaffolds are still an issue to be solved [5, 32].

### 1.4.2 Bone regeneration: materials and strategies

Bone regeneration requires a scaffold with high mechanical properties, since its structure should be strong enough to sustain weight bearing loads. It can be: osteoconductive, i.e. able to be populated by cells after implantation and substituted by new tissue starting from the surrounding; osteoinductive, if it is also a system to deliver cytokine, such as bone morphogenetic proteins (BMPs), insulin-like growth factors (IGFs), transforming growth factors (TGFs), to induce differentiation of mesenchymal stem cells (MSC) *in loco*; or a combination of these two [12]. Moreover, scaffold degradation rate should be compatible with the natural bone remodeling process [33].

The most important parameters to take into account to design a scaffold for bone Tissue Engineering are porosity and pore diameter distribution. In fact, scaffold morphology has to allow cell migration and help neo-angiogenesis after implantation. *In vivo* vascularization is a fundamental requirement to develop a functional tissue and insufficient blood vessels in bone can lead to a decrease of tissue formation and mass [34]. In addition, studies demonstrated that vascularity supports MSC and osteoblasts during tissue repair and osteogenesis follows angiogenesis in a bone fracture model [35, 36]. To induce neo-angiogenesis after implantation, it has been reported that scaffold porosity should be over 60%, while the minimum pore diameter should be 100  $\mu\text{m}$  to obtain osteogenesis and mineralization. Moreover, microporosity of pore walls ( $< 10 \mu\text{m}$ ) can help cell attachment and differentiation, adsorbance of osteogenic proteins and mechanical stability at the fixation to the natural bone [12].

Nevertheless, even if high porosity and pore diameter are suitable for bone regeneration, they necessarily weaken scaffold mechanical properties and structural integrity. Thus, a compromise is needed [37] and this constraint determines the existence of an upper limit in scaffold mechanical properties. This limit depends, however, on the biomaterial used and the scaffold fabrication method. For instance, scaffolds made of a biomaterial with a high degradation rate cannot be more porous than 90%, otherwise material would rapidly deplete and mechanical stability would be lost before the scaffold was substituted with new formed tissue. Scaffolds of low-degrading biomaterials can have a higher porosity, instead [12].

Several ceramics materials have been proposed for bone Tissue Engineering applications, especially hydroxyapatite and tricalcium phosphate. Specifically, hydroxyapatite is a physiological component of bone extracellular matrix. It has been demonstrated that these materials are osteoconductive, can increase osteointegration and have high mechanical properties [38, 39]. However, scaffolds resulted too brittle with a low degradation rate [12]. Other materials employed for bone Tissue Engineering include PLA, PCL, PCL blends and silk

fibroin. Using polymers, scaffold morphology has been controlled more easily, recreating in some extent the structural organization of the bone [12, 40, 41]. In particular, silk fibroin scaffolds showed to sustain the differentiation of mesenchymal stem cells in osteoblasts *in vitro* and the deposition of hydroxyapatite crystals with a geometry similar to the trabecular bone [42].

### 1.4.3 Osteochondral strategies

All approaches in osteochondral Tissue Engineering can be classified according to scaffold type and cell source. In particular, four strategies can be identified (figure 1.7) [43]:

1. a scaffold for bone regeneration (subchondral component or phase) and no scaffold for cartilage regeneration (no chondral component or phase);
2. two different scaffolds for bone and cartilage regeneration separately cultured and combined at the time of implantation;
3. a single heterogeneous scaffold, with different properties *ad hoc* for the two phases;
4. a single and homogeneous scaffold.

Several cell sources have been used in combination with these scaffolds: a single cell type with chondrogenic ability, two cell types with chondrogenic and osteogenic ability respectively or one cell type able to differentiate in both chondrocytes and osteoblasts. Alternatively, a totally cell-free approach can be considered.

Different biomaterials and cells have been combined to evaluate the best properties of a Tissue Engineering system for osteochondral regeneration and a summary is reported in figure 1.8. Promising results have been obtained *in vitro* and using *in vivo* models, but some issues still remain open. The following paragraph will explain the crucial points regarding what needs to be solved and studied according to the results obtained until today.

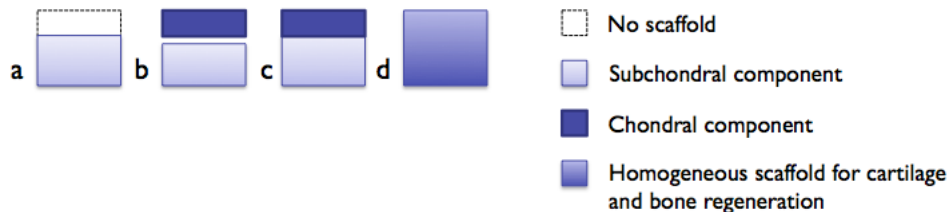


Figure 1.7: Scheme of the scaffold strategies for osteochondral Tissue Engineering: (a) scaffold for bone regeneration, no scaffold as chondral component; (b) different scaffolds for each tissue phase; (c) single but heterogeneous scaffold; (d) homogeneous scaffold.

First, size and shape of an osteochondral construct should be designed taking into account two problems: the integration between patient cartilage and the new tissue of the graft and the eventual incongruities of the contact surfaces. The former is due to the scarce ability of chondrocytes to communicate, because of their low metabolic activity and their isolation in lacunae in the dense ECM of cartilage. Thus, interaction should be minimized, so that cellular dialogue can take place only where it is actually essential. The latter, instead, is related to the avoidance of excessive mechanical stresses because of an increase of local pressure; so the surfaces of the graft and the implantation site should be as complementary as possible. The obvious conclusion from these observations is that an osteochondral construct should have a size developed *ad hoc* for the defect to heal. This represents a limitation for a standardized and systematic application of this approach. Moreover, the size of a defect may also change with time, a complex shape may complicate the fixation process and the costs would rapidly rise [43].

A possible solution to these problems may be the use of injectable materials able to assume a suitable shape *in situ*, but their mechanical properties still need to be improved, as mentioned in paragraph 1.4.1 [5]. Therefore, the best criterium to design the form of an osteochondral graft has not been established,

Scaffolds	Cells	Ref.
OPF with gelatin microparticle hydrogel	Cell-free/marrow mesenchymal stem cells	42
PCL/TCP-PCL scaffold	Cell-free/marrow mesenchymal stromal cells	29
Hyaluronic acid gel sponges	Autologous mesenchymal stromal cells	43
Hyaluronate - collagen type I - fibrin scaffold	Cell-free/autologous chondrocytes	44
Hyaluronic acid - atelocollagen/ $\beta$ -TCP bilayered scaffold	Cell-free/chondrocytes	45
Collagen/hydroxyapatite gradient scaffold	Cell-free/autologous chondrocytes	46
Poly(lactide-co-glycolide)/nano-hydroxyapatite scaffold	Cell-free/marrow mesenchymal stem cells	47
Poly(lactic acid) - coated polyglycolic (PGA) scaffold	Cell-free/autologous marrow mesenchymal stem cells	48
Collagen/ $\beta$ -TCP bilayered scaffold	Cell-free	23
PLA and collagen/hydroxyapatite scaffold	Cell-free/chondrocytes	49
PLA scaffold	Mesenchymal stem cells	50
PGA fibrous scaffold - PLGA/PEG foams	Periosteum-derived cells/articular chondrocytes	51
PCL scaffold	Marrow mesenchymal stem cells/chondrocytes	52

Figure 1.8: Overview of the constructs for osteochondral regeneration studied in the last few years (adapted from [33]).

yet.

The second critical issue still open in osteochondral Tissue Engineering is the choice of a cell source able to promote an efficient regeneration. In particular, the selection of cells for cartilage restoration is the most crucial, since osteoblast progenitors are already present in the subchondral bone and are potentially able to synthesize new tissue if a suitable osteoconductive scaffold is employed. However, even if a pre-seeded subchondral phase is used, choosing cells for cartilage regeneration is still decisive and several possibilities have been explored. A natural choice has been the use of articular chondrocytes, human or animal, but many problems are connected to this option. First, animal models have evident limitations, because human physiology is different and, if the study is *in vivo*, the defect is artificially induced; thus, the pathologic variability due to osteoarthritis, for instance, is not considered. In the case of human chondrocytes, they have to be extracted from healthy sites in the donor and this leads to an additional morbidity that should be avoided. Moreover, cell number is always limited and therefore chondrocytes have to be expanded *in vitro*. It has been demonstrated that during a bidimensional culture, they undergo a downregulation of chondrogenic genes, a decrease in their ability to synthesize ECM and a modification of membrane markers; nevertheless, this de-differentiation may be avoided using specific growth factors during culture, such as transforming growth factor (TGF- $\beta$ ) [5, 43].

Stem cells have shown promising results to overcome some of these constraints and represents one of the most studied cell source for osteochondral regeneration. In particular, bone marrow mesenchymal stem cells (BMSCs) and adipose-derived stem cells (ASCs) have demonstrated great potential in chondrogenic and osteogenic differentiation [33]. Their main advantages include a high availability, the ease of *in vitro* expansion and intrinsic repair capacity [5]; on the other hand, stem cells have a potential instability and careful and specific stimulations are required to induce the expression of a chondral phenotype [43]. However, results have been encouraging and autologous BMSCs transplantation was employed for the repair of full-thickness

articular cartilage defects in patellae of two human patients [55]. Other resources for stem cells include synovial tissue and periosteum: cells derived from synovial membrane can be harvested with minimum complications for the donor and have a high regenerative capacity [56], while in the periosteum progenitor cells are present with a high proliferation rate and differentiation potential [57]. However, more investigations are still needed.

The third unresolved problem in osteochondral regeneration regards the maturation stage of the engineered construct at the time of implantation. It has been demonstrated that if the graft is pre-cultured for some weeks, the ECM in the scaffold allows a significant improvement of mechanical properties and therefore increases the chances of success [43]. This happens because cells can experience an environment close to a physiological situation and regeneration is therefore more effective. However, the weak integration ability of chondrocytes must be considered in the definition of the most appropriate maturation stage. In fact, an implant may fail even if the construct is mature enough to bring the advantages previously mentioned. In this case, the failure would be determined by a lack of integration due to the absence of communication between the newly formed tissue and the damaged cartilage in the joint. Thus, a compromise is needed between mechanical properties and duration of the *in vitro* culture [43]. Moreover, an earlier maturation stage at the time of implantation may even imply a benefit: even if the mechanical properties and biological functions of the engineered graft are insufficient, human body itself may be considered an *ad hoc* bioreactor and provide an optimal stimulation to develop new tissue in a functional way for an effective regeneration. Also in this case, the best compromise has yet to be found [43].

On the basis of the previous considerations, it appears clear how the design of a Tissue Engineered system for osteochondral regeneration is a delicate process and many variables have to be considered and modulated to find an equilibrium able to induce the regeneration of functional tissues. In this point of view, efforts have been made to reproduce the complexity of an osteochondral system, using the biomimetic approach previously described. In particu-

lar, a new concept has been developed recently, i.e. a necessary requirement for a long-term osteochondral regeneration is the restoration of a functional interface between cartilage and bone. Therefore, scaffold properties have to provide a suitable support and appropriate stimulations not only for chondral and subchondral regeneration separately, but also for a reproduction of a physiological interfacial zone between both tissues. This can be achieved by a controlled heterogeneity of scaffold properties to recreate the physiological gradients at the interface [58]. Several strategies have been explored to this purpose [33]. For instance, in a recent study [59], MSCs were incorporated in collagen microspheres and then separately differentiated towards chondrocytes and osteoblasts; then, loaded microspheres were used as building blocks to produce an osteochondral construct. A layer of microspheres with undifferentiated MSCs was inserted in the middle of chondral and subchondral phases and the formation of a calcified interface was observed after 3 weeks of *in vitro* culture, thanks to the interaction of MSCs with the surrounding microenvironment. In another study [60], PLGA scaffolds were loaded with opposing gradients of TGF- $\beta$ 1 and BMP-2 for the differentiation of human umbilical cord MSCs and human bone MSCs towards cartilage and bone phenotypes respectively. Authors showed that gradients of bioactive signals were beneficial in terms of stem cell differentiation.

The previous works are only examples of how gradients in scaffold properties can help the restoration of the functionality of both tissues and their interface. Other approaches include *in vitro* co-culture of chondrocytes and osteoblasts, or undifferentiated/pre-differentiated stem cells with stem cells or osteoblasts. In fact, it has been demonstrated that growth and differentiation of chondrocytes can be enhanced by endogenous signals secreted in a co-culture system with osteoblasts [61, 62, 63]. Also osteogenic differentiation of stem cells can be improved by a co-culture with chondrocytes [64]. A more detailed description of these results will be reported in paragraph 5.1.

In light of the discussion presented here, it is evident how the perfect means for osteochondral regeneration is still far to be found. The principles and in-

struments of Tissue Engineering have the potential to overcome the current limitations, although a deep and complete comprehension of the physiological environment is mandatory. New strategies have been adopted to translate nature complexity into an engineered graft, with particular attention to the integration with the host tissue and to the exploitation of cellular dialogue for an effective regeneration of tissutal functionality. Efforts have been made in this direction and, even if the best characteristics of an osteochondral engineered construct have not been discovered yet, results are promising.

## 1.5 A natural polymer: silk fibroin

As mentioned before, natural polymers have been frequently used for both cartilage and bone Tissue Engineering. Their main advantages include a high biocompatibility thanks to ligands which can be recognized by cells, but on the other hand, their use is limited because of weak mechanical properties and processing difficulties. Among natural materials, silk fibroin has been shown a great potential to overcome these limitations.

The term silk indicates the protein polymers synthesized by epithelial cells in specialized glands of Arachnids and some Lepidoptera. According to their animal origin, silk proteins differ in composition and final configuration, but some general properties can be identified: their primary structure is usually simple and repetitive, while the secondary structure is mostly  $\beta$ -sheet because of the predominance of amino acids with a short lateral chain in hydrophobic domains. These domains allow the formation of a packed tertiary structure thanks to the establishment of hydrogen bonds along protein chains. This assembly gives silk high resistance and resilience, which are needed during the formation of cocoons or spider webs [65]. Indeed, besides a remarkable stability, having impressive mechanical properties is one of the peculiar characteristics of silk, as shown in figure 1.9.

Regenerated silk is obtained after the remotion of the external protein layer which coats the core fibers of silk filaments (degumming process). It

Material	Stiffness (GPa)	Strength (GPa)	Extension to failure (%)
<i>Bombyx mori</i> cocoon silk (w/sericin)	7	0.4 - 0.6	18 - 22
<i>Bombyx mori</i> cocoon silk (degummed)	12-17	0.45 - 0.7	22
<i>Bombyx mori</i> regenerated fibroin electrospun fibers	0.3	0.019	5.8
Kevlar	130	3.6	2.7
Tendon collagen	1.5	0.15	12
PLA	1.2 - 3.0	28 - 50	2 - 6

Figure 1.9: A comparison among the mechanical properties of silk filaments and other common biomaterials (adapted from [67]).

has a high biocompatibility and a tunable proteolytic biodegradation. All silk proteins can be easily processed in an aqueous environment or with organic solvents and also their chemistry can be eventually modified [65, 66]. As previously mentioned, all these properties make silk suitable for the production of a scaffold for Tissue Engineering.

In particular, silk from *Bombyx mori* cocoons has been widely utilized as biomaterial; for instance, silk fibers have been used for sutures in clinical practice for decades. These fibers have a diameter of 10-25  $\mu\text{m}$  and consist of two inner filaments of fibroin coated by a layer of sericin, which acts as a glue and represents 25-30% of the whole fiber (figure 1.10) [66].

### 1.5.1 Silk fibroin structure

A fibroin molecule is made of two protein chains, a light chain (about 26 kDa) and a heavy chain (about 390 kDa) in a ratio 1:1. They are joined by disulfide bonds between two cysteine amino acids (Cys-c20, 20th residue of the heavy chain from the C-terminus, and Cys-172, a residue of the light chain). A glycoprotein called P25 is non-covalently linked to both fibroin and sericin [65].

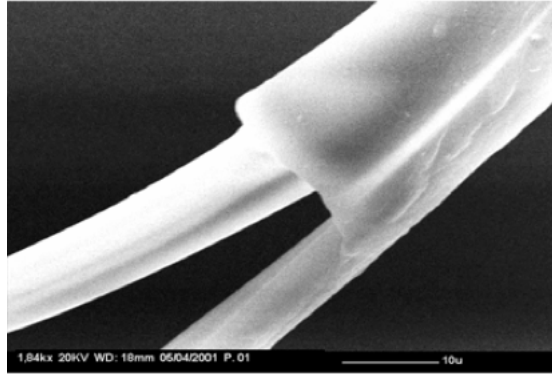


Figure 1.10: Scanning electron micrograph of a partial degummed silk filament.

Amino acid composition of fibroin from *Bombyx mori* consists mainly of glycine G (43%), alanine A (30%) and serine S (12%). The heavy chain is formed by 12 domains which compose the crystalline regions of the silk fiber: they are repetitions of sequences Gly-X, where X can be one of the following amino acids: alanine, serine, valine or threonine. Each domain is about 400 amino acid-long and contains subdomains of esapeptides, such as GAGAGS, GAGAGY, GAGAGA, GAGYGA (where Y stays for tyrosine). They end with tetrapeptides like GAAS or GAGS [65]. As previously indicated, the formation of crystalline structures is due to the short lateral chains of the amino acids in these regions, which allow protein folding in a  $\beta$ -sheet conformation [68]. The less crystalline portions of the heavy chain are called linkers and are 42-44 amino acid-long. They have a non-repetitive sequence of 25 charged residues which are not present in the crystalline region of fibroin and have bigger lateral chains. Therefore, their secondary structure is random coil due to a steric effect [65].

Silk fibroin exists in two different polymorphisms: the glandular state before crystallization (Silk I) and the state which follows its extrusion with the formation of  $\beta$ -sheet secondary structures (Silk II). When fibroin is in a Silk I state, it is water soluble and can be easily crystallized by heat or shear stresses,

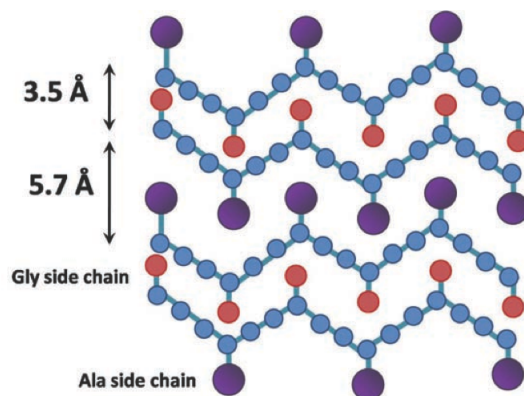


Figure 1.11: Model of silk fibroin polymorphism Silk I [69].

which are indeed employed during the spinning process. Fibroin is in a Silk I state also in the aqueous solution obtained *in vitro* (see paragraph 2.2.1) and in this case crystallization is usually induced by a chemical treatment with methanol or potassium chloride. After crystallization,  $\beta$ -sheet structures are asymmetric: one side is occupied by the hydrogen atoms of glycine residues, while methyl groups of alanines populate the other side (figure 1.11). Strong hydrogen bonds and van der Waals forces form a structure which is thermodynamically stable [65].

After the process of degumming, silk can be isolated in a third polymorphism, Silk III. It can be found at air/water interface, where fibroin molecules assembly in an approximately hexagonal structure with a three-folded helical conformation. In this way, serine residues (hydrophilic) and alanine residues (hydrophobic) are maintained at the opposite sides of the molecules [70].

In an aqueous environment, fibroin structure depends on the reciprocal interaction between its characteristic hydrophilic and hydrophobic blocks. As shown in figure 1.12, fibroin assumes a micellar conformation in order to maintain the hydrophilic regions at the liquid interface and the hydrophobic portion in the internal part.

The interaction among micellae increases with fibroin concentration and

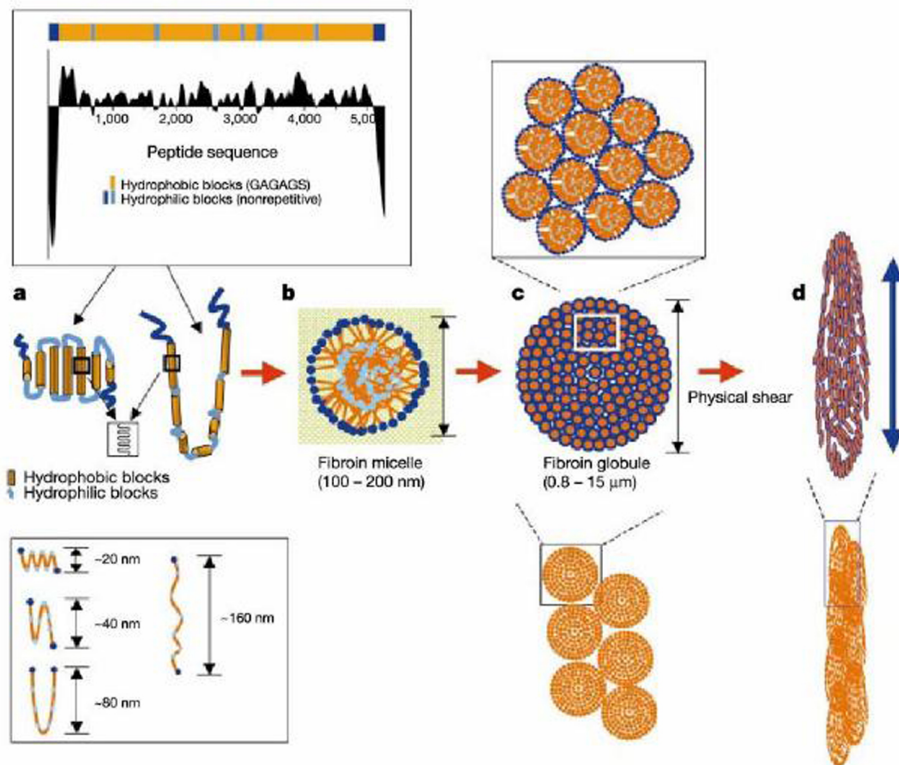


Figure 1.12: Model of fibroin heavy chain structure (a), micellae formation (b), globular aggregation of micellae (c) and shear stress effect (d) [68].



Figure 1.13: Liquid crystalline domains of *Bombyx mori* silk fibroin [71].

bigger and bigger globular structures form until the establishment of a gel state [68]. It has also been observed that a liquid crystalline phase exists when fibroin moves from a solution state to a fiber state. A model describes this phenomenon with the formation of supermolecular elongated structures shown in figure 1.13, composed by 15 micellae arranged in column. This phase promotes the extension and the cooperative alignment of fibroin molecules, which is improved by the shear stresses exerted during spinning [71].

### 1.5.2 Silk fibroin as a multifunctional polymer

Examining the protein structure described in the previous paragraph, silk fibroin can be considered as a responsive polymer whose versatility is based on the self-assembly of nanostructures (hydrophobic and hydrophilic blocks) into molecular conformations which depend on the environment conditions. Thanks to these properties, silk fibroin can be easily modeled and processed controlling specific parameters (pH, temperature, salt concentration and so on).

<b>Fibroin matrix</b>	<b>Application</b>
Fibers	Tendon and ligament tissue engineering
Films	Bone and hepatic tissue engineering Antithrombogenesis Wound dressing
Sponges, hydrogels	Connective tissue regeneration (cartilage and bone)
Non-woven nets	Endothelial and blood vessels

Figure 1.14: Silk fibroin-based matrices for Tissue Engineering and their potential applications (adapted from [65]).

In addition, in the perspective of Tissue Engineering applications, silk fibroin has the nature of a multifunctional polymer. Indeed, silk fibroin possesses active domains in the linkers among hydrophobic blocks, which can be recognized by cell receptors and demonstrated to stimulate cell adhesion and growth [72]. This has been widely exploited in Tissue Engineering applications, as it will be discussed in the following section.

### 1.5.3 Silk fibroin in Tissue Engineering

As previously mentioned, *Bombyx mori* silk fibers are currently the primary resource for silk-based biomaterials. In particular, silk fibroin has a high versatility when a compromise is needed between scaffold mechanical properties and adequate biological response [65]. Films, hydrogels, sponges and non-woven nets with potential applications in Tissue Engineering can be obtained (figure 1.14). After degumming and the preparation of a fibroin aqueous solution, several procedures can be employed to prepare silk-based matrices with different morphologies, as schematically shown in figure 1.15. In this section, a short summary of these scaffolds and their use will be presented, with particular attention to the salt leaching technique employed in this research work.

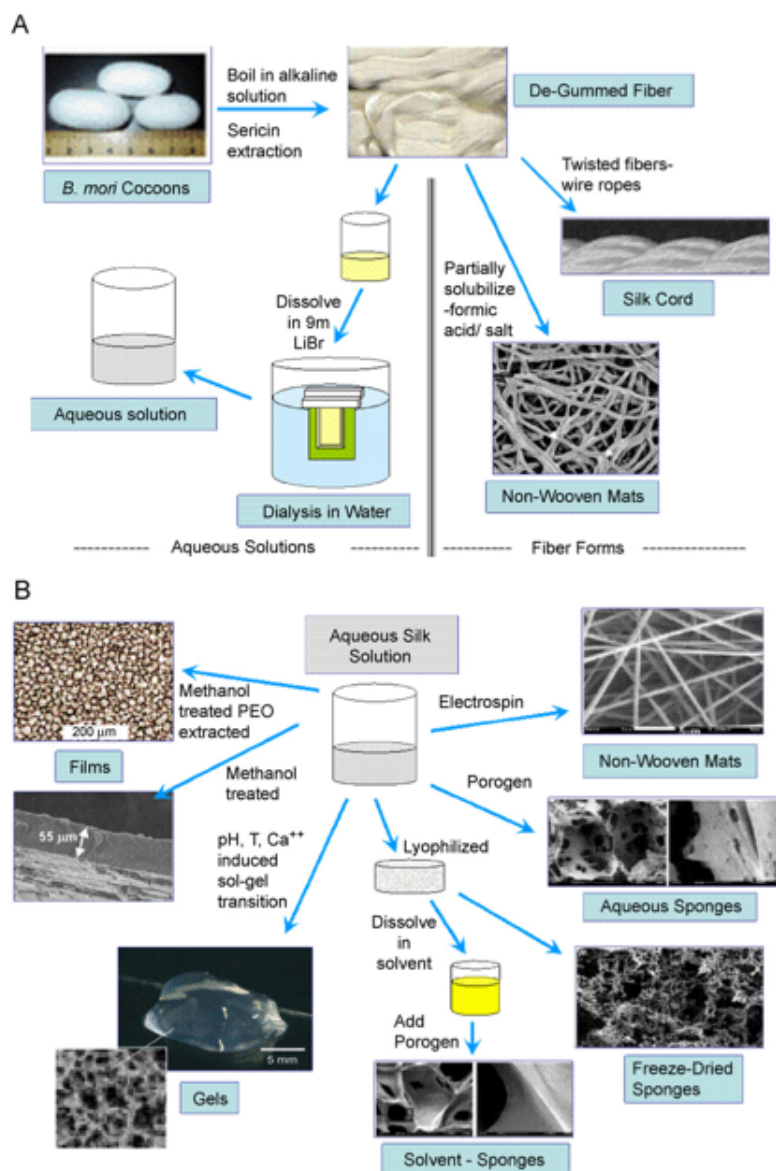


Figure 1.15: Silk fibroin is purified in a boiling alkaline bath (A). Degummed fibers can be processed or dissolved in lithium bromide to obtain an aqueous solution which can be used to prepare nets, sponges, hydrogels, films (B).

Fibroin non-woven nets can be prepared starting from degummed fibers or by electrospinning. In the first case, nets with a fiber diameter of 10-30  $\mu\text{m}$  and an interfibrillar space of 300  $\mu\text{m}$  has been produced and used with several cell types, such as cheratinocytes, fibroblasts and osteoblasts [65]. For instance, they supported adhesion and proliferation of endothelial cells inducing the formation of structures similar to microvascularization after 1 week of culture *in vitro* [73]. Instead, electrospinning allows the production of nets with a fiber diameter in a wide range, from few nanometers to some micron according to the parameters used. Examples include polyethylene oxide PEO/fibroin nets fabricated with a fiber diameter less than 0.8  $\mu\text{m}$  and high mechanical properties and fibroin nets conjugated with BMP-2 to support MSC differentiation into osteoblasts [74].

This versatility is a characteristic of fibroin films, as well. They can be easily obtained by casting of fibroin in water, in organic solvents or mixed with other polymers. For instance, oxygen and water vapor permeability of fibroin films produced from an aqueous solution could be modulated by methanol treatments of different duration, which affected also mechanical properties and degradation rates [65]. Fibroin films were also modified for the *in vitro* culture of osteoblasts with the addition of growth factors [75] or RGD domains for cell adhesion (i.e. sequences of arginine, glycine, aspartic acid) [76].

Fibroin can also be used to produce hydrogels, which have been employed in Tissue Engineering as injectable materials as means to deliver cells, drugs or growth factors (see paragraph 1.4.1). In this case, the main advantage is the possibility to obtain a hydrogel in mild conditions starting from a fibroin aqueous solution. Gelation time can be modulated since it depends on several factors: protein concentration, temperature, amount of  $\text{Ca}^{++}$  ions and pH [65]. Potential applications of fibroin hydrogels are various and comprise bone Tissue Engineering. In fact in a recent study a fibroin gel was used to heal a femoral defect in a rabbit model, leading to new tissue formation and a higher degree of mineralization than a commercially available PLGA product [77].

Fibroin sponges are one of the most used silk-based scaffolds in cartilage

and bone Tissue Engineering, especially because of their high porosity. Several techniques can be employed, such as particulate leaching (with salt or glucose as porogen) and freeze-drying, which may be eventually combined with gas foaming [65, 78]. In particular, salt leaching allows the formation of a more interconnected porosity and pore dimension can be modulated by the diameter of porogen grains. Two procedures have been developed for sponge production: the first is schematically shown in figure 1.16 and implies the dissolution of fibroin in hexafluoro-2-propanol (HFIP). NaCl with a controlled granulometry is added to this solution and after solvent evaporation scaffolds are treated in methanol to induce the formation of  $\beta$ -sheet structures and make fibroin insoluble in water. At this point, salt grains can be removed by several washing steps in distilled water and porosity will reflect the arrangement of the voids left by the porogen. Thanks to this flexible technique, it is also possible to obtain porosity gradients if a suitable NaCl granulometry is used (figure 1.16).

The use of toxic solvents such as HFIP and methanol is however a strong limitation for the production of a scaffold. Nevertheless, fibroin sponges can also be produced using a process completely conducted in an aqueous environment without losing the control on pore dimension and distribution. In addition, the final matrices have a faster degradation rate and surface properties more suitable for cell adhesion [79]. In this case, NaCl is directly added to a fibroin solution at 4-10% w/V in order to obtain an oversaturated solution (fibroin concentration depends on the grain diameter used). Therefore, the surface of NaCl particles dissolves only partially leaving the salt in a solid state. This leads to the gelation of fibroin in 3-5 days and hence to the formation of porous structures stable in an aqueous environment, as schematically shown in figure 1.17. As in the previous case, salt can be removed washing the sponges in distilled water.

The cause of fibroin gelation and the consequent  $\beta$ -sheet formation is an alteration of water solvation forces due to a high concentration of salt ions. In a recent study this mechanism was analyzed comparing fibroin behavior in several highly concentrated aqueous solutions of salts with chlorine ions

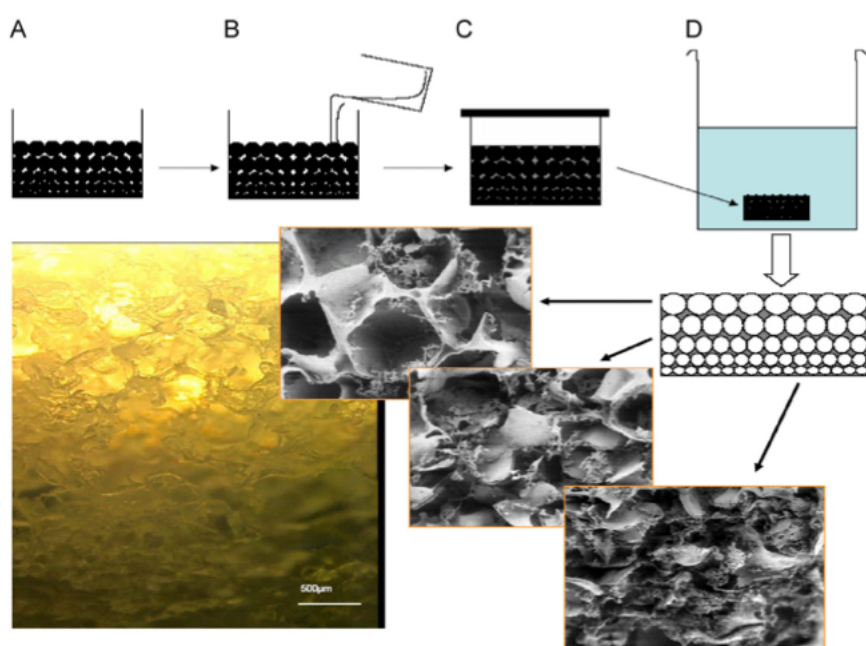


Figure 1.16: Fibroin porous sponges with a porosity gradient induced by a controlled distribution of salt granulometry (A). The solution of fibroin in HFIP diffuses in NaCl crystals (B, C) which are then dissolved by washing in distilled water [65].

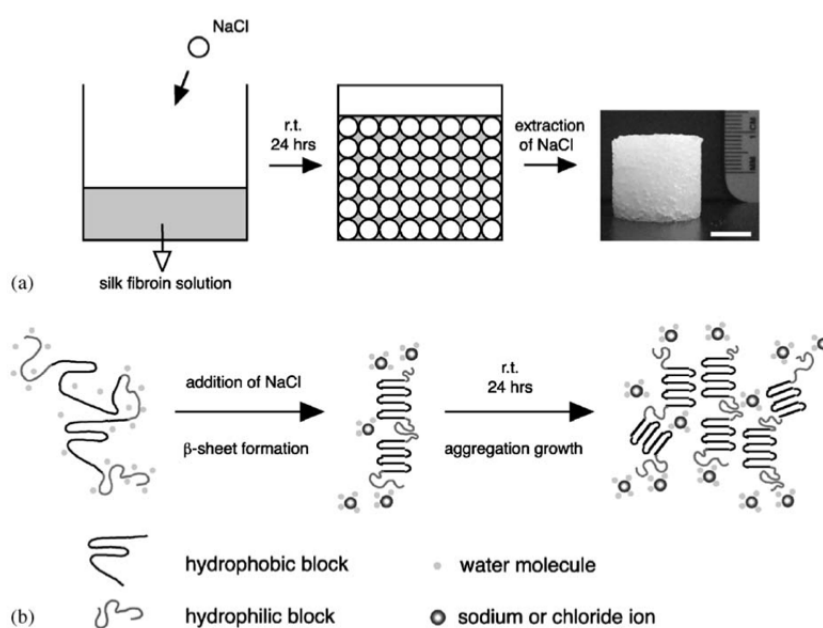


Figure 1.17: Scheme of the salt leaching technique to prepare fibroin sponges from an aqueous solution (a) and of the mechanism underlying the structural modifications of the protein during the process (b) [79].

(until 3 M): NaCl, KCl, CaCl<sub>2</sub> and MgCl<sub>2</sub> [79]. A hydrogel was formed only in NaCl and KCl solutions, while no gelation was observed with CaCl<sub>2</sub> and MgCl<sub>2</sub>. Authors associated these results with the outcomes obtained for the solubility of an uncharged model peptide, acetyltetraglycine ethyl ether, in concentrated saline solutions. They claimed this peptide can reasonably mimic fibroin behavior because of the predominant presence of hydrophobic blocks in the protein molecules [79].

Ions are classified as kosmotropic (“capable of order”) or chaotropic (“capable of disorder”), based on their size and charge, which also determine their behavior in water. Kosmotropic ions are usually small or have a high charge density and contribute to stabilize the interaction among macromolecules and water. This is the case of  $Ca^{++}$  and  $Mg^{++}$ . Instead, chaotropic ions tend to destabilize the structure of macromolecules dissolved in water interfering with the non-covalent bonds (hydrogen bonds and van der Waals forces) which determine the formation of those structures. *Cl* is weakly chaotropic [79].

At low salt concentrations fibroin solution contains enough water molecules to hydrate both the protein surface and the dissolved ions. At higher concentration of salt more and more water molecules are required to hydrate the increasing number of ions. Therefore, water is removed from fibroin surface, the protein-protein interaction becomes stronger than the solute-solvent interaction and the hydrophobic regions of fibroin can interact more easily in correspondence to their apolar residues. This effect is called “salting out”.

In light of the previous considerations, we can conclude that in concentrated solutions of CaCl<sub>2</sub> and MgCl<sub>2</sub> the number of bonds among proteins and kosmotropic ions in solution increases; the subsequent structuring of water molecules around fibroin prevents the hydrophobic interactions which would allow the formation of crystalline  $\beta$ -sheet structures. Instead, in NaCl solutions, ions are able to remove the molecules of water which otherwise would hide the hydrophobic domains of fibroin, promoting chain-chain interactions and the creation of a more stable  $\beta$ -sheet conformation [79].

As previously mentioned, fibroin sponges have been used for both cartilage

and bone Tissue Engineering and combined with several cell sources such as chondrocytes, osteoblasts and stem cells of different origin. For cartilage regeneration, MSCs were cultured on aqueous-derived sponges and after 3 weeks they were embedded in structures similar to lacunae with a spherical morphology. This indication of chondral differentiation was also confirmed by histological and immunohistochemical analyses. Moreover, scaffold roughness, hydrophilicity and pore interconnection allowed an uniform distribution of cells and new extracellular matrix [80]. In another study with MSCs, GAG deposition on silk scaffolds was significantly higher compared to collagen controls when the *in vitro* culture was performed with a serum-free culture medium [81]. The same scaffold was studied with articular chondrocytes and also in this case results were significant in terms of formation of new cartilage tissue. However, authors observed a slower adhesion kinetics and a critical dependence of cell differentiation on seeding density: indeed, only a higher initial cell number determined an up-regulation of cartilage specific genes and a higher deposition of new ECM [82]. In a recent paper, the properties of salt leaching fibroin sponges with two different pore diameter ranges (315-500  $\mu\text{m}$  and 500-1180  $\mu\text{m}$ ) were compared to freeze-dried silk scaffolds and combined with dynamic culture conditions [83]. Rat chondrocytes from the resting zone of costochondral cartilage growth plate were cultured in a static environment or on a rocking platform for 15 days and cell proliferation, cell distribution, chondrogenic gene expression and new ECM deposition were evaluated. It was observed that the fibroin sponge with the highest porosity and pore size significantly improved chondrocyte proliferation and differentiation in terms of their round morphology and gene expression. Moreover, a hydrodynamic environment was beneficial in a way directly dependent on pore diameter with a higher production of cartilage matrix and limited hypertrophic differentiation.

For bone regeneration, salt leaching fibroin sponges were modified with RGD domains and used to culture human mesenchymal stem cells in a medium enriched with osteogenic growth factors. These experimental conditions induced cell differentiation, production of mineralized ECM and up-regulation

of osteoblast markers [84]. In another paper, fibroin sponges with a pore size of 900  $\mu\text{m}$  were seeded with human MSCs and cultured in an osteogenic medium. After 28 days of culture, structures similar to trabecular bone were observed *in vitro* [85].

These studies are only examples of the potential of silk-based sponges in cartilage and bone regeneration. Fibroin porous scaffolds have demonstrated a suitable biocompatibility and the ability to induce new tissue formation both *in vitro* and *in vivo*. Their properties have been also modulated by fibroin processing and this versatility have permitted the design of scaffolds *ad hoc* for these specific Tissue Engineering applications.

#### 1.5.4 Degradation and immunological response

As previously reported in paragraph 1.1, the degradation rate of a biomaterial has to be taken into account to design a scaffold for Tissue Engineering because it has to be compatible with the growth rate of new tissue at the implantation site. According to US Pharmacopeia, a biomaterial is absorbable if it “loses most of its tensile strength within 60 days post-implantation *in vivo*” [66]. Based on this definition, silk fibroin in a fiber form is considered a non-degradable material. However, the debate about fibroin biodegradability is still open: indeed, it depends on several factors and can be modulated *ad hoc* according to its application. Degradation of fibroin is proteolytic and usually mediated by a foreign body response. During degradation less crystalline regions of the protein are broken in peptides which can be phagocytized by cells more easily [66].

Protein structure, scaffold morphology, biological and mechanical conditions at the implantation site are only some of the elements which affect fibroin degradation rate. Several studies have been performed to evaluate the biodegradability of films and fibers. To this purpose, different proteolytic enzymes have been used, including chymotrypsin which is produced by macrophages during an inflammatory response. In these studies it was observed that films degraded faster than fibers if exposed to the same enzymes with a

modification of fibroin molecular weight, an increase of protein crystallinity and a dramatic change in tensile strength [66].

The degradation rate of fibroin porous sponges depends strongly on the production method. Aqueous-derived salt leaching sponges degrades slower if the initial fibroin concentration increases. These sponges, however, degrades faster than HFIP-derived scaffolds with the same pore size. This dissimilarity is due to differences in the surface roughness and the crystallinity grade of the scaffolds [65]. Besides these factors, fibroin scaffold degradation can be also regulated varying porosity, pore dimensions and molecular weight distribution. The latter can be modified with a heat treatment in alkaline conditions, leading to a disruption of ordered structures and a decrease in cross-links. However, there are no exhaustive or systematic studies about how all these variables can influence fibroin degradation rate and therefore, it is difficult to have a clear and complete cognition of the relationship between fibroin structure and biodegradability [65, 66].

Biocompatibility of silk fibroin has been extensively established. It was observed that silk sutures could elicit hypersensitivity in some cases, but it was demonstrated that the major cause of these responses was sericin. Once sericin is removed by degumming, the biological response of fibroin is comparable to all biomaterials [65, 66]. For instance, fibroin films implanted *in vivo* induced a lower inflammatory response than similar scaffolds of collagen and PLA [86]. Moreover, fibroin nets were implanted subcutaneously in rats, leading to a weak foreign body response without the formation of a fibrotic capsule. After six months *in vivo*, a slight up-regulation of inflammation processes without a significant presence of lymphocytes was observed at the site of implantation [87].

## 1.6 Proposed research and objectives

The final objective of this research work is the production and the validation of a scaffold for osteochondral regeneration. In particular, the advanced

concepts of biomimetics were applied to design a multicomponent scaffold to regenerate cartilage, bone and a functional interface between them. We hypothesized that a multiphasic scaffold is more suitable for osteochondral Tissue Engineering because chondral and subchondral phases can be designed separately in order to offer the most favorable environment for cartilage and bone regeneration respectively. We also hypothesized that the restoration of a functional interface can be improved using a nanometric net to separate the two components. The aim of the net is to allow a dialogue among cells between the two phases thanks to a physiological solute flow, while preventing cell migration towards the chondral site. In this way, the interaction between chondrocytes and osteoblasts can be assured; indeed, as previously reported, it can have beneficial effects improving the synthesis of a cartilage ECM with a functional organization [61, 62, 63]. Moreover, besides mechanical stabilization, the role of the osteochondral interface is to prevent vascularization and the subsequent mineralization of the non-calcified cartilage [59]. Hence, the avoidance of blood cells in the cartilage component precluding their migration can help to maintain a physiological environment. Finally, a multicomponent scaffold is more feasible, since it can be assembled at the time of implantation or used only partially according to the existing defect in the joint.

Silk fibroin was chosen as the main material to prepare the multicomponent scaffold, to exploit its biocompatibility and versatility in tissue engineering applications shown in paragraph 1.5. Instead, poly-d,l-lactic acid (PdlLA) was used to fabricate the nanometric net: as previously reported, PdlLA is a biomaterial commonly used in tissue engineering and it can be easily processed by electrospinning, a technique which allowed to obtain a porosity and a pore size suitable for the application, as it will be shown later. Therefore, it was used to prepare and test the assembled scaffold *in vitro*, in order to evaluate the effectiveness of the net in promoting cellular dialogue.

The main issue in osteochondral tissue engineering is the regeneration of cartilage, because of its poor ability to self-repair. Therefore, this research work focused mainly on the design of the chondral phase, since the great po-

tential of silk fibroin for bone regeneration is well-established [41, 42, 43] and it has been demonstrated that an osteoconductive scaffold may be sufficient to induce bone restoration [12]. To this purpose, our starting point was the tissue engineered system tested in [83] in collaboration with Dr. Barbara D. Boyan's laboratory at the Georgia Institute of Technology (Atlanta, US). In this study it was demonstrated that rat chondrocytes isolated from the costochondral growth plate gave the best outcomes in terms of cell distribution, cartilage phenotype maintenance and new ECM deposition, when cultured on a salt leaching fibroin sponge with a porosity greater than 80% and a pore size of 500-1180  $\mu\text{m}$  in combination with hydrodynamic culture conditions. Our aim was to improve both components of this system, i.e. cell source and scaffold. In the first case, we decided to employ adipose-derived stem cells (ASCs) for cartilage regeneration, because of the advantages already mentioned in paragraph 1.4.3. ASCs were cultured on the previous silk sponges trying different combinations of culture conditions: growth or chondrogenic medium, static or dynamic environment. The best combinations were used to pre-culture for 28 days cell/scaffold constructs, which were then implanted in an *in vivo* model of critical size defects in rat xiphoid. Results will be reported in the next chapter.

To improve scaffold properties, we combined silk fibroin with hyaluronic acid (HA). Hyaluronic acid is a physiological element of cartilage extracellular matrix and its use has been recently explored for cartilage regeneration. Indeed, it can help the maintenance of chondral phenotype during *in vitro* culture and improve new ECM deposition [5, 88, 89, 90, 91, 92, 93]. We conjugated silk fibroin and hyaluronic acid to merge their properties and produce sponges by salt leaching, using the same porosity as in the previous study but different concentrations of HA to evaluate how scaffold properties could be modulated. Moreover, genipin (a natural cross-linker extracted from gardenia fruits which also has weak anti-inflammatory properties) was used to cross-link sponges to improve HA retention inside scaffolds and modify the interpenetrated network formed by scaffold components. A more detailed description of the rationale behind these choices and the original contributions of this work will be re-

ported in paragraph 3.1. Silk fibroin/hyaluronic acid sponges were completely characterized in terms of morphology, silk fibroin conformation, water uptake, porosity, cross-linking degree, mechanical properties, wettability and HA distribution in the scaffolds (both in a qualitative and quantitative way). Results are reported in chapter 3. Biological properties were assessed culturing rat chondrocytes from the costochondral growth plate in dynamic conditions, using the optimal parameters found in the previous study [83]. Chondrogenic gene expression, alkaline phosphatase (ALP) activity, GAG deposition and mechanical properties were measured to analyze how cell responses were affected by different HA concentrations and cross-linking.

So two different strategies were adopted to develop the chondral phase of the multicomponent scaffold, improving the results previously obtained in [83]. The nanometric net was produced by electrospinning of poly-d,l-lactid acid/polyethylene glycol (PdlLA/PEG) blends and characterized in terms of morphology and thermal properties. PEG was used to avoid fiber shrinkage in an aqueous environment, which is a frequently reported issue when PdlLA is used in Tissue Engineering applications. Then, the net was assembled to silk fibroin sponges to obtain the upper part of the multicomponent scaffold and the morphology of the resulting construct was assessed.

Subsequently, a co-culture system was designed to verify the ability of the net to ensure the dialogue between chondrocytes and osteoblasts. To this purpose, primary human articular chondrocytes were seeded in silk fibroin sponges with the PdlLA/PEG nanometric net on one side and then put in contact with an underlying layer of osteoblasts, so that the biochemical communications between cells could take place only through the nanometric fibers. Cell proliferation and viability were assessed during 11 days of co-culture, then results were compared to those obtained for silk fibroin sponges without net and similar samples maintained in the same culture conditions but without being exposed to bone cells.

## Chapter 2

# Adipose-derived stem cells and silk fibroin scaffolds for chondral repair

### 2.1 Introduction

This chapter will describe the first strategy explored for cartilage regeneration, that is the combination of 3D porous silk scaffolds and adipose-derived stem cells (ASCs). As previously mentioned, the aim of the following study was to improve the tissue engineered system used in [83], focusing on the cell source in the perspective to employ it in an osteochondral multiphasic scaffold. Therefore, adipose-derived stem cells were used to exploit advantages such as their great potential of self-renewal and the ability of multilineage differentiation, including chondrogenesis [5, 33].

Adipose tissue has been lately considered as an attractive source for adult stem cells, due to their abundance and easy accessibility. Indeed, 1% of adipose cells are mesenchymal stem cells, while only 0.001-0.002% can be found in bone marrow [94]. In addition, even if ASCs have a weaker chondrogenic potential with respect to bone marrow stem cells [95], ASCs have shown to bet-

ter maintain a chondrocyte phenotype rather than undergoing a hypertrophic differentiation improving for cartilage regeneration [96].

The use of silk scaffolds for cartilage tissue engineering has been recently explored in combination with both chondrocytes and stem cells of different origin (paragraph 1.5.3). In particular, several combinations of chemical and/or mechanical stimuli have been employed to induce chondrogenic differentiation in stem cells cultured on silk scaffolds. However, an exhaustive formulation of the culture environment (3D structure, growth factors, dynamic stimulation) has not been found yet and it needs to be modulated according to the biomaterial used, the cell source employed and the final application.

In our previous study [83], it was demonstrated that a hydrodynamic environment can have synergistic beneficial effects on the maintenance of chondrocyte phenotype and the production of new cartilage ECM when combined with highly porous silk scaffolds.

The aim of this work was to examine if and how dynamic stimulations and a proper chondrogenic medium can affect the chondrogenesis of adipose-derived stem cells when cultured on silk scaffolds. In addition, the potential of ASCs/silk scaffold constructs to regenerate cartilage *in vivo* was evaluated in a rat critical size xiphoid defect model. To this purpose, ASCs were cultured combining different conditions: growth and chondrogenic media, static or dynamic environment. Cell viability, proliferation, chondrogenic gene expression, new cartilage ECM deposition were evaluated *in vitro* during a 28-day culture. Then, the best combinations of culture parameters in terms of ASCs chondrogenesis were used to pre-culture ASCs/silk scaffold constructs before implantation in rat xiphoid defects. Neo-cartilage formation was assessed 8 weeks after surgery using  $\mu$ CT and histomorphometric analysis.

## 2.2 Materials and methods

This study was conducted in collaboration with Dr. Barbara D. Boyan's laboratory at the Parker H. Petit Institute of Bioengineering and Bioscience,

Georgia Institute of Technology (Atlanta, US), under approval of the Georgia Institute of Technology Institutional Animal Care and Use Committee. All animals were treated humanely per the guidelines outlined in the Guide for the Care and Use of Laboratory Animals by the National Institutes of Health (US).

### 2.2.1 Scaffold preparation

Silk fibroin 3D porous scaffolds were prepared from silk fibroin solution using salt-leaching techniques as described previously [83]. Briefly, selected Silk *Bombyx mori* cocoons (kindly provided by Cooperativa Socio Lario, Como - Italy) were boiled in two aqueous alkaline baths of  $\text{Na}_2\text{CO}_3$  (Merck, Germany) (1.1 g/l and 0.4 g/l respectively) 1.5 hours each at 98°C in order to remove from the fiber the external sericin coating and obtain fibroin. Degummed silk was then washed several times in distilled water and dried at room temperature. Fibroin was then dissolved in LiBr (Sigma-Aldrich, US) 9.3 M (2 g in 10 ml) for 2 hours at 65°C, the solution was dialyzed against distilled water for 3 days using a Slide-A-Lyzer Dialysis cassette (3500 MWCO, Pierce, US) to remove LiBr, concentrated to a concentration of 7-8% w/V by dialysis against a 25% w/V Polyethylene Glycol (PEG) solution (10000 Da MW, Sigma-Aldrich, US) for 5 hours, and finally filtered to eliminate impurities. To form porous sponges, 4 g of NaCl particles, size 425-1180  $\mu\text{m}$ , (Sigma-Aldrich, US) were added to 2 ml of the SF solutions in a Petri dish of 35 mm diameter. The salt partially dissolved subtracting water to the fibroin so inducing fibroin gelation. After three days at room temperature, gels were washed for 4 days in distilled water to remove salt, then dried.

Before cell seeding, the sponges were rehydrated in distilled water for 2 hours and formed into cylinders (6 mm in diameter and 3 mm in thickness) using a biopsy punch (Miltex, UK). Scaffolds in aqueous suspension were autoclaved at 121°C for 15 min. After cooling to room temperature, the water was removed and SF sponges were incubated overnight with culture media at 37°C, 5%  $\text{CO}_2$ . After conditioning the scaffolds, the bubbles inside of the scaf-

olds were removed by the syringe-vacuum system used in [83]: the scaffolds were transferred into a 20 ml syringe with 5 ml of medium. Vacuum pressure was used for 2 minutes to load media and remove air in the scaffolds. These prewetted silk scaffolds were then blotted dry and ready for seeding.

### 2.2.2 Isolation and culture of adipose-derived stem cells (ASCs)

Adipose-derived stem cells were isolated from inguinal fat pads of the hind legs of Sprague-Dawley rats. In brief, the tissue was pooled and washed three times in Hank's balanced saline solution (HBSS) and digested in 0.25% trypsin at 37°C for 30 minutes. The tissue was then cut into smaller pieces and digested in 9125 units of collagenase IA (Sigma Aldrich, US) and 75 units of dispase (Gibco, Invitrogen, US) for three hours. The upper layer of adipocytes was removed and the cell suspension was filtered through a 40- $\mu$ m cell strainer. The digestion was stopped with MSC growth media (GM) (Lonza, Switzerland). The cells were collected by centrifugation and then plated at 5000 cells/cm<sup>2</sup> in T-175 flasks. Cultures were washed twice with phosphate buffered saline (PBS) and fed with GM containing 10% fetal bovine serum and 1% penicillin-streptomycin at 24 and 48 hours after plating. Primary passage confluent cells were used for seeding on scaffolds.

### 2.2.3 Cell seeding and culture of silk fibroin/ASC constructs

Each scaffold was placed in the center of each well of a 24-well plate containing 200  $\mu$ l of growth media. To seed the scaffolds,  $1 \times 10^6$  P1 ASCs were loaded on the top of the scaffolds through pipette tips. 4 hours after cell seeding, 1.5 ml of growth media was added to each well. 6 hours after cell seeding, samples either remained in a static culture or were subjected to a rotation culture at 50 rpm on an orbital rocker. After 72 hours of culture, the ASCs/silk scaffolds were then transferred to new plates and the media was replaced with either the same growth media as the initial culture or replaced with commercially available chondrogenic media (CM) (Lonza, Switzerland) containing 10 ng/ml

of TGF- $\beta$ 1 (R&D Systems, US). Four experimental groups of scaffolds were obtained: growth media + static culture (GMS), growth media + rotation culture (GMR), chondrogenic media + static culture (CMS), and chondrogenic media + rotation culture (CMR). The ASCs/silk scaffolds were maintained in a humidified, 95% air/5% CO<sub>2</sub> atmosphere at 37°C. Medium was changed every two days for up to 28 days of culture.

#### 2.2.4 Cell seeding efficiency

In order to determine the appropriate time for cell attachment on the scaffolds, seeded scaffolds were maintained under static culture for 6, 12 or 24 hours before rotation culture. At the end of each culture period, unincorporated cell numbers were measured using a Beckman Coulter Cell Counter (Beckman Coulter Inc., US). Cell seeding efficiency was then calculated using the formula:

$$\text{Cell seeding efficiency (\%)} = \left(1 - \frac{\text{unincorporated cell number}}{\text{initial cell seeding number}}\right) \times 100$$

#### 2.2.5 Cell viability

The viability of ASCs in the scaffolds was examined after 28 days of culture by a Live/Dead<sup>®</sup> assay (Invitrogen Corporation, US) as described in literature. Briefly, ASCs/silk scaffolds were washed twice with PBS for 5 minutes, and then incubated with 2  $\mu$ M calcein AM and 4  $\mu$ M EthD-1 in PBS for 30 minutes at room temperature. After removing extra dyes by washing in PBS for 5 minutes, the scaffolds were sliced in half, and the images were taken from both the surface and the center of the scaffolds using Zeiss confocal microscopy with an excitation wavelength of 495 nm and an emission wavelength of 515 nm.

#### 2.2.6 Cell proliferation

Cell proliferation in scaffolds was evaluated on day 1, 7, 14, 21 and 28 after seeding using an alamarBlue<sup>®</sup> assay (AbD Serotec, US) according to the

manufacturer's instructions. Briefly, seeded scaffolds were incubated with 1 ml of 10% alamarBlue<sup>®</sup> reagent in culture medium for 2 hours in humidified, 95% air/5% CO<sub>2</sub> atmosphere at 37°C. At the end of incubation, 100 µl of the supernatant were then transferred to a 96-well plate and fluorescence intensity was determined with a microplate reader (Spectromax Gemini XS, Molecular Devices, US) (excitation/emission: 565 nm/595 nm). Media incubated with unseeded scaffolds were used as controls and their fluorescence value was subtracted from those of cell-seeded scaffolds.

### 2.2.7 Real time PCR analysis

ASCs/silk scaffolds were harvested on day 14 and day 28. Total RNA was isolated from the silk scaffolds using an RNeasy kit<sup>®</sup> (Qiagen Inc., US) and reverse-transcribed into cDNA using Applied Biosystems High-Capacity cDNA Reverse Transcription kit (AB Inc., US) according to the manufacturer's instructions. Realtime PCR was performed to measure the expression of cartilage-related genes including Sox9, collagen 2a1, aggrecan, Comp, collagen 1a1 and collagen 10a1 and normalized to RPS18. The amplification of genes was carried out on an iCycler real-time PCR machine using iQ SYBR Green supermix (both Bio-Rad Laboratories, US) with specific primers as described previously [83].

### 2.2.8 Compressive mechanical properties

Compressive modulus of unseeded and ASCs-seeded silk scaffolds after 28 days of culture was evaluated by a compression test. At harvest, the constructs were washed in PBS for 10 minutes before testing. The compression test was then performed at room temperature on wet scaffolds using an Instron 4502 mechanical tester (Instron, US) equipped with a 25 N cell load in uniaxial ramp condition at a strain rate of 0.1 mm/sec. The Young's modulus was calculated as the slope of the initial linear section of the stress-strain curve.

### 2.2.9 Sulfated glycosaminoglycan production

Culture media from each group were harvested on day 7, 14, 21 and 28 and frozen at -20°C until the measurement of sulfated glycosaminoglycan (GAG) content in the medium. The ASCs/silk scaffolds were harvested after 28 days of culture. After mechanical testing, the scaffolds were digested in 1 ml of Proteinase K solution (Qiagen Inc., US) at 1 mg/ml for 24 hours at 55°C. The GAG content was measured spectrophotometrically at 520 nm following the reaction with dimethylmethylene blue (DMMB) dye (Sigma Aldrich, US) [83]. The DNA content of ASCs/silk scaffolds was quantified by PicoGreen assay (Invitrogen Corporation, US) with lambda DNA as a standard and then used to normalize the GAG content in the scaffolds.

### 2.2.10 Histological analysis

Histological analysis was used to evaluate the *in vitro* chondrogenesis of ASCs after 28 days of culture under various conditions. At harvest, scaffolds were washed in PBS, fixed overnight in 10% formalin and then dehydrated using sequential ethanol series. Finally, the scaffolds were embedded in paraffin and 7- $\mu$ m thick sections were cut using a microtome. After deparaffinization, sections were subjected to hematoxylin and eosin (H&E), safranin-O/fast green or immunofluorescence (IF) staining. Rabbit polyclonal antibodies against rat type I and type II collagen (Abcam, Inc., UA) and aggrecan (Santa Cruz Biotechnology, Inc., US) were used to immuno-label the sections. This was followed by the incubation with secondary antibodies (Alexia 488 goat anti-rabbit IgG) (Invitrogen Corporation, US). After staining, slides were assembled with Fluoro-Gel (Electron Microscopy Sciences, US) and examined under a light microscope for H&E and Safranin-O/fast green staining or under Zeiss confocal microscopy for immunofluorescence staining.

### 2.2.11 *In vivo* implantation and evaluation

A 3-mm diameter, 2-mm deep xiphoid cartilage defect was created in 7-to-8 week-old male athymic RNU rats (200-250 g each) as reported in [97]. Empty scaffolds as well as ASCs/silk scaffold constructs cultured in chondrogenic medium under static or rotation conditions for 28 days were placed in the defect area. Empty defects and defects implanted with autografts were used as negative and positive control respectively. Seven rats were randomly enrolled in each experimental group. Following implantation, a strip of SeptraFilm<sup>®</sup> (Genzyme Corporation, US) was placed over the deep and superficial face of the xiphoid in order to keep the implants in place and avoid potential adhesions. The xiphoid was then internalized back to its anatomical position. Post-operatively, rats were given 0.03 mg/kg of buprenorphine for pain control and housed in single cages with no restrictions on diet or exercise. All animals survived the surgery and no animals died prior to harvest.

Animals were euthanized by CO<sub>2</sub> inhalation 8 weeks after surgery. Xiphoids were harvested by sharp dissection and subjected to contrast-enhanced  $\mu$ CT analysis based on equilibrium partitioning of an ionic contrast agent (EPIC  $\mu$ CT). Samples were scanned in air using a  $\mu$ CT 40 (Scanco Medical, Switzerland) at 45 kVp, 177 mA, 200-m integration time, and a voxel size of 16  $\mu\text{m}^3$  [83]. Color images based on the X-ray attenuation were created in order to visualize the three dimensional distribution of sulfated GAG in the tissue. Low X-ray attenuation (green) corresponded to regions at high proteoglycan concentration, while high X-ray attenuation (yellow) indicated regions at low proteoglycan concentration. Scanco medical software was used for a quantitative measurement of cartilage volumes in the defect area. After  $\mu$ CT evaluation, the xiphoids were washed in PBS and fixed in 10% neutral formalin. Xiphoids were bisected in the sagittal plane, embedded in paraffin, and successive cuts were taken at 100  $\mu\text{m}$  intervals. Representative sections were stained with hematoxylin and eosin (H&E) to evaluate structure and morphology as well as with safranin-O/fast green to evaluate the amount of proteoglycans (red). Slides

were reviewed blindly and scored according to a modified Wakitani grading system, in which the maximum cumulative histology score is 11 and a lower score indicates a repair more similar to native cartilage. Images were taken and analyzed for neo-cartilage formation in the defect area using Image-Pro Plus software (Medium Cybernetics, Inc., US).

### 2.2.12 Statistical analysis

All measurements were collected for  $N = 6$  or  $N = 7$  independent determinations per data point for *in vitro* and *in vivo* experiments, respectively. Data were expressed as mean  $\pm$  standard error and were subjected to two-way or one-way ANOVA with Bonferroni corrections. All statistical analyses were carried out using GraphPad Prism 5.0 (GraphPad Software, Inc., US).  $P < 0.05$  was considered as statistical significance.

## 2.3 Results and discussion

### 2.3.1 Cell loading efficiency, viability and distribution

Starting the rotation culture 6, 12 and 24 hours after seeding resulted in a cell seeding density of  $90\% \pm 2\%$ ,  $91\% \pm 1\%$  and  $91\% \pm 5\%$  respectively. No significant differences were found among these time points. Therefore, 6 hours after seeding was chosen for subsequent experiments in order to achieve a potentially more homogenous cell distribution.

Live/dead assay revealed few detectable dead cells while the majority of cells was alive as stained green after 4 weeks of culture (figure 2.1). Additionally, the distribution of cells throughout the scaffold was similar among all the groups. Cells were found both on and in the porous structures of the sponges, especially close to the surface of the scaffolds with fewer cells in the center of the scaffolds.

The distribution of ASCs was less homogeneous with respect to what was found previously with chondrocytes seeded on the same type of scaffold. At

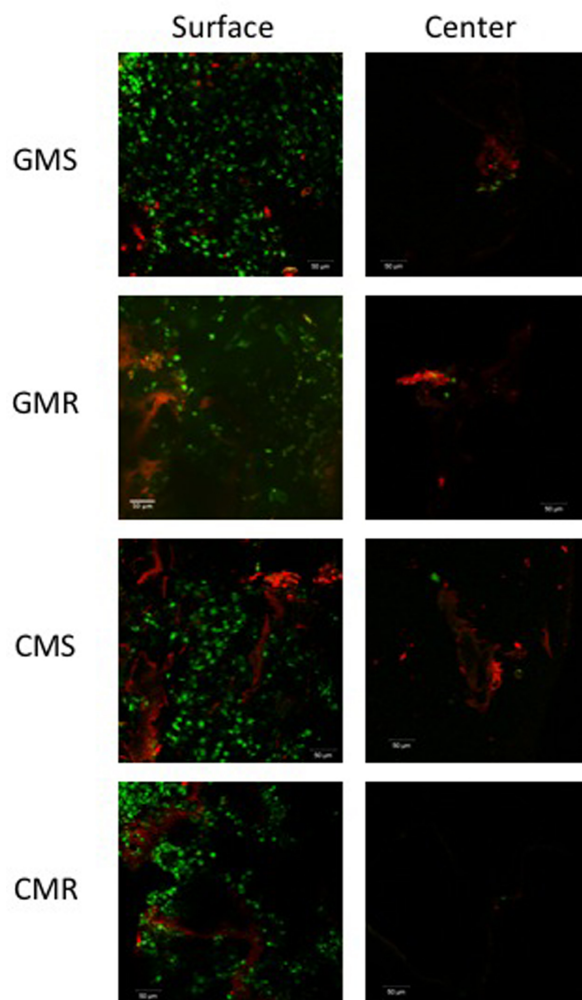


Figure 2.1: Cell viability on silk scaffolds under different culture conditions. ASCs/silk scaffolds after 28 days of culture under various conditions were stained with a Live/Dead<sup>®</sup> kit and then observed with confocal microscopy. GMS: scaffolds cultured in growth medium under static condition; GMR: scaffolds cultured in growth medium under rotation condition; CMS: scaffolds cultured in chondrogenic medium under static condition; CMR: scaffolds cultured in chondrogenic medium under rotation condition. Green staining represents live cells while red staining represents dead cells and stained silk scaffolds. Scale bar = 50  $\mu\text{m}$ .

the same time, a much higher seeding density was achieved with ASCs compared to chondrocytes 24 hours after seeding. These differences indicated that ASCs can attach more strongly and faster to silk fibroin scaffolds. Therefore, an earlier application of rotation culture conditions or the use of a perfusion bioreactor may be beneficial to increase the homogeneity of cell distribution and subsequent cartilage formation in the defect site.

### 2.3.2 Cell proliferation

AlamarBlue<sup>®</sup> assay was employed to monitor cell proliferation during 28 days of culture. In fact, AlamarBlue<sup>®</sup> is reduced in the mitochondria of metabolically active cells, giving a fluorescent molecule which can be detected by a spectrofluorimeter. Since the resulting fluorescence is proportional to the number of viable cells in the sample, proliferation of ASCs could be assessed. As shown in figure 2.2, on day 1, there are no significant differences among the groups. While the number of ASCs in all groups increased during culture, ASCs/silk scaffold constructs cultured in growth medium in rotation conditions exhibited the greatest increase in cell number ( $p < 0.05$ ). Moreover, the increase in cell number reached a plateau between day 21 and day 28. Interestingly, the samples cultured in chondrogenic medium exhibited a slight decrease in cell proliferation between day 7 and day 14, but resumed the increase trend in the following weeks.

### 2.3.3 Chondrogenic differentiation

ASCs/silk scaffolds cultured in chondrogenic medium elicited a statistically significant higher gene expression of chondrogenic markers (Sox9, Col2, Aggrecan and Comp) in comparison to those cultured in growth medium (figure 2.3). In addition, static culture resulted in a relatively higher expression level of Col2, Aggrecan and Comp on day 14 and day 28, while the expression of Sox9 at day 28 is higher in the CMR group than in the CMS group. Furthermore, the expression of Aggrecan and Comp increased at day 28 com-

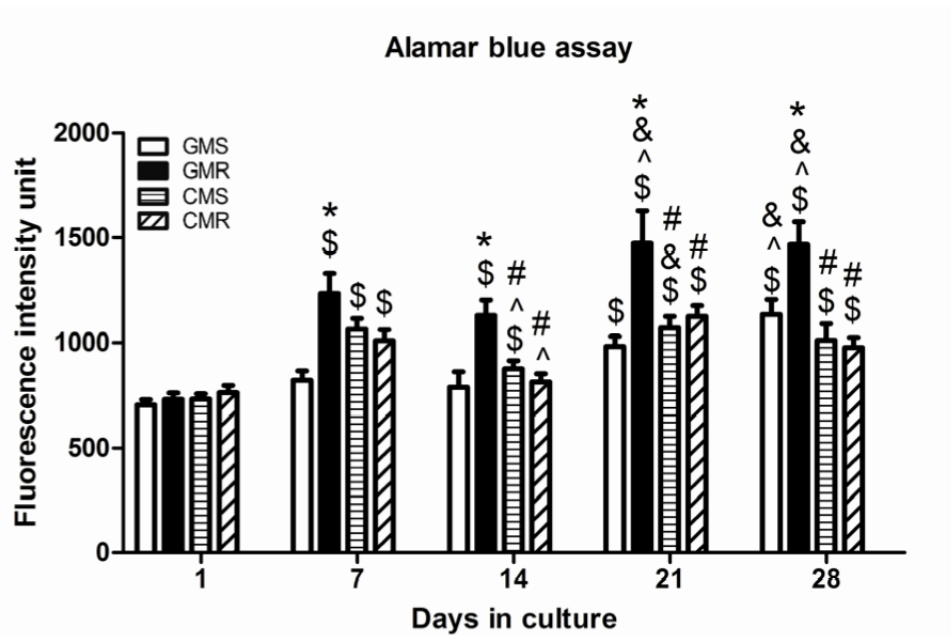


Figure 2.2: Cell proliferation of ASCs on silk scaffolds under different culture conditions. AlamarBlue<sup>®</sup> assay was used to monitor cell proliferation during culture. White bars represent scaffolds cultured in growth medium under static condition (GMS); black bars represent scaffolds cultured in growth medium under rotation condition (GMR); striped bars represent scaffolds cultured in chondrogenic medium under static condition (CMS) and slashed bars represent scaffolds cultured in chondrogenic medium under rotation condition (CMR). Each bar represents the mean and standard error of  $N = 6$  independent cultures. \*  $p < 0.05$  vs. GMS group; #  $p < 0.05$  vs. GMR group; \$  $p < 0.05$  vs. day 1; ^  $p < 0.05$  vs. day 7; &  $p < 0.05$  vs. day 14.

pared to day 14. However, a greater expression of Col1 was also induced by chondrogenic medium compared to growth medium. Moreover, ASCs cultured in chondrogenic medium under static condition showed the highest expression level of hypertrophic gene Col10 at day 14. However, no significant difference in Col10 expression level between different culture media was observed at day 28, while its expression level was higher under rotation culture compared to static culture.

The production of GAG in the medium steadily increased along the culture time (figure 2.4, A). The amount of GAG found in the medium from CMS and CMR groups was more than 10 times higher than from those cultured in growth medium at all time points tested. A similar trend was also observed for the amount of GAG in the scaffolds. Chondrogenic media induced a two-fold GAG production with respect to growth media (figure 2.4, B). Although a slightly lower amount of GAG in the medium was detected under rotation culture compared to static culture at some time points, no significant differences were found at the scaffolds level. This result was also confirmed by safranin-O/fast green staining of scaffold sections (figure 2.5). While the majority of cells in the GMS, GMR and CMR groups was stained green, cells in CMS groups displayed light red staining indicating the presence of GAG in the extracellular matrix. Immunofluorescence staining against collagen type II, aggrecan and collagen type I also demonstrated the production of these molecules in ASCs/silk scaffold constructs under different culture conditions (figure 2.6). Limited staining of collagen type II and aggrecan was observed in the samples cultured in growth medium, whereas widespread staining on cell surfaces as well as in the extracellular matrix was found in those cultured in chondrogenic medium. Furthermore, static culture resulted in stronger staining than rotation culture in the same chondrogenic medium. No significant differences in terms of collagen type I production were observed among all the groups.

According to the presented results, the chondrogenesis of ASCs in this study can be viewed as a two-stage process. An initiation step can be identified in

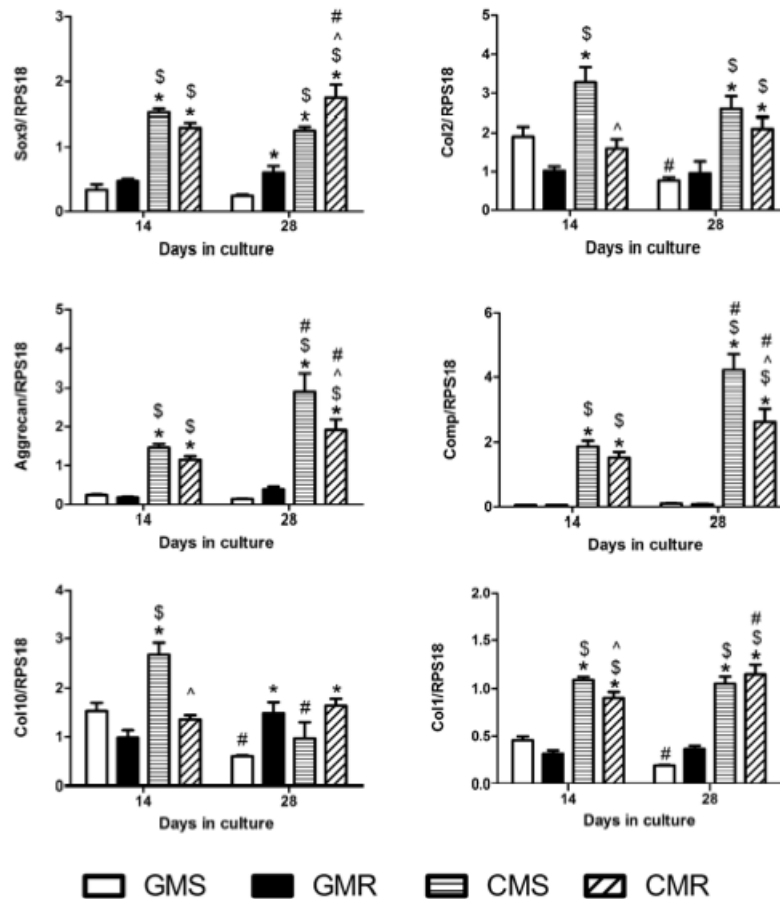


Figure 2.3: Real-time PCR analysis of cartilage-related gene expression in ASCs on silk scaffolds under different culture conditions for 14 days or 28 days. White bars represent scaffolds cultured in growth medium under static condition (GMS); black bars represent scaffolds cultured in growth medium under rotation condition (GMR); striped bars represent scaffolds cultured in chondrogenic medium under static condition (CMS) and slashed bars represent scaffolds cultured in chondrogenic medium under rotation condition (CMR). Each bar represents the mean and standard error of N = 6 independent cultures. \* p < 0.05 vs. GMS group; \$ p < 0.05 vs. GMR group; ^ p < 0.05 vs. CMS group; # p < 0.05 vs. day 14.

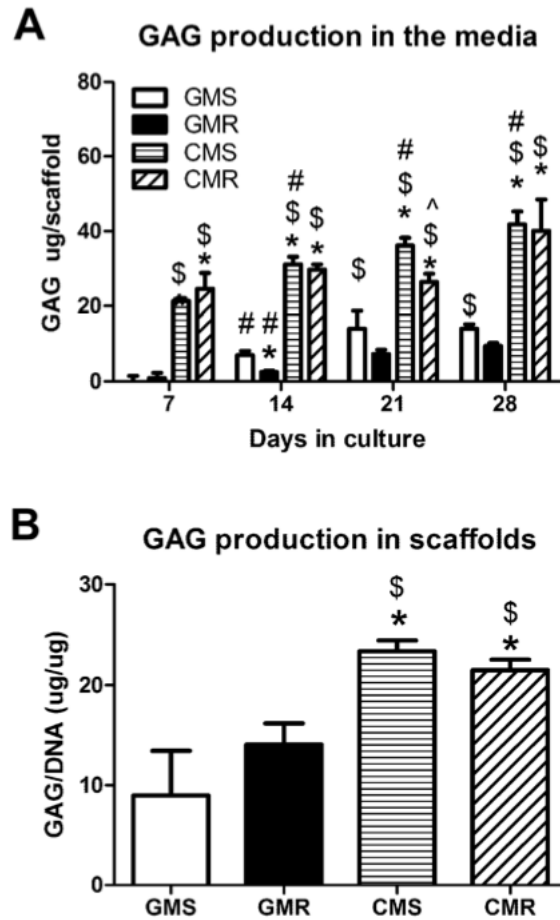


Figure 2.4: Glycosaminoglycan GAG production by ASCs cultured on silk scaffolds in different conditions. The amount of GAG in both medium (A) and scaffolds (B) was measured using DMMB assay and normalized to DNA content of scaffolds. White bars represent scaffolds cultured in growth medium under static condition (GMS); black bars represent scaffolds cultured in growth medium under rotation condition (GMR); striped bars represent scaffolds cultured in chondrogenic medium under static condition (CMS) and slashed bars represent scaffolds cultured in chondrogenic medium under rotation condition (CMR). Each bar represents the mean and standard error of  $N = 6$  independent cultures. \*  $p < 0.05$  vs. GMS group; \$  $p < 0.05$  vs. GMR group; ^  $p < 0.05$  vs. CMS group; #  $p < 0.05$  vs. day 14.

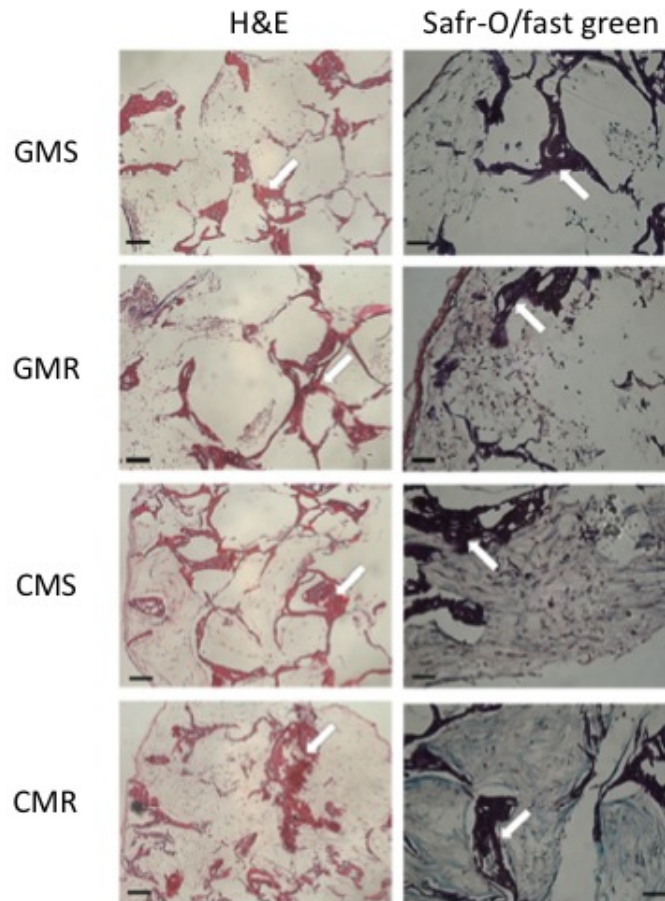


Figure 2.5: Histological analysis of ASCs/silk scaffold constructs under different culture conditions. Scaffolds were harvested after 28 days of culture. After serial histological processing, scaffolds were sectioned into 7  $\mu\text{m}$  slices and subjected to H&E (objective 10x) and safranin-O/fast green staining (objective 20x, red represents glycosaminoglycans) or immunofluorescence staining against collagen type II, aggrecan and collagen type I proteins with propidium iodide counterstaining of nuclei (objective 20x, green represents target proteins and red represents nuclei). White arrows indicate the silk scaffolds.

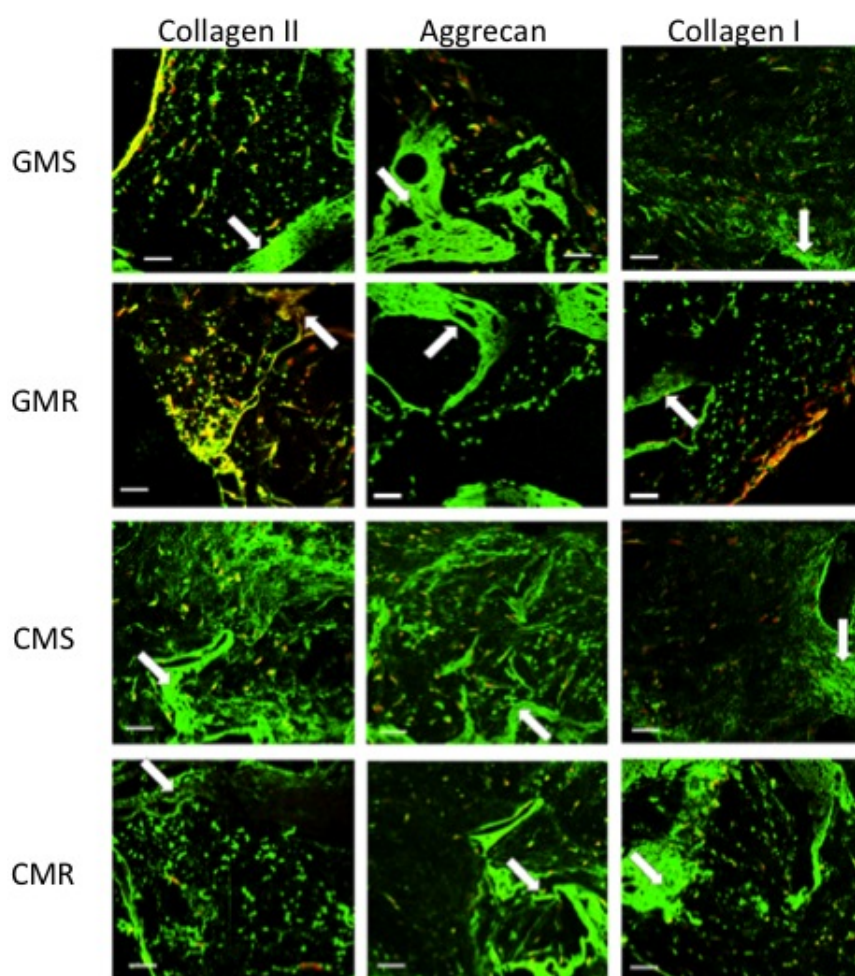


Figure 2.6: Immunofluorescence staining of ASCs/silk scaffold constructs against collagen type II, aggrecan and collagen type I with propidium iodide counterstaining of nuclei (objective 20x, green represents target proteins and red represents nuclei). White arrows indicate the silk scaffolds.

the first 14 days, when ASCs undergo a transitory decrease in cell proliferation and start to express chondrogenic markers when cultured in chondrogenic medium. From day 14 to day 28, an advanced stage of chondrogenesis takes place with a further increase of Comp and aggrecan expression. In addition, ASCs chondrogenesis on silk scaffolds seemed not to go through a hypertrophic differentiation stage, since after 28 days Col10 expression dropped back to a level compatible with that measured for ASCs cultured in growth medium. Thus, this limited hypertrophy can be an advantage in case of cartilage regeneration. It is also important to note that the expression of collagen type I increased when ASCs/silk scaffold constructs were cultured in chondrogenic medium, which may be due to the heterogeneity of this cell source. Sorting of ASCs subpopulation with markers such as CD105 may allow better *in vitro* chondrogenesis and subsequent *in vivo* cartilage regeneration.

ASCs chondrogenesis affected the production of glycosaminoglycans, both in the culture medium and in the scaffolds. A significant improvement in GAG synthesis was observed in the ASCs/silk scaffold constructs cultured with chondrogenic media. However, this increase was higher in combination with static culture conditions, which also improved collagen type II and aggrecan deposition according to immunofluorescence analysis. On the basis of these considerations, static culture induced a superior chondrogenesis *in vitro* when combined with chondrogenic media. This outcome is apparently conflicting with previous results, where a hydrodynamic environment was beneficial for maintaining chondrocyte phenotype and promoting chondrogenesis because of the enhanced transportation of nutrients and metabolic waste and the subsequent mechanical stimulation provided to the system [83, 98, 99, 100]. However, different cell sources have been employed, giving dissimilar results. For instance, a recent study reported that rotational culture induced different responses in porcine chondrocytes and bone marrow MSCs seeded in 2% agarose gels [101]. A more homogeneous tissue was achieved in the constructs seeded with chondrocytes, while rotation conditions significantly limited chondrogenesis in MSCs. On the contrary, the use of a perfusion bioreactor induced a better chondrogenesis in

MSCs derived from human embryonic stem cells cultured on silk scaffolds, as evident by a higher amount of GAG, total collagen and collagen type II with respect to static conditions [102].

These findings suggest that distinct cell sources can respond differently to a hydrodynamic stimulation. In addition, scaffold geometry may affect the responses of cells, which are subjected to different mechanical environments according to scaffold properties, such as porosity and pore size. Finally, various bioreactors can provide different stimulations in terms of intensity, frequency and so on; therefore, cells may be also affected by the kind of stimuli supplied. In our study, fluid volume, rotation speed and stimulation frequency need to be further optimized to obtain beneficial effects on ASC chondrogenesis from the hydrodynamic environment.

Lastly, the appropriate time to start rotation culture has been shown to be critical. A delay in the initiation time of the hydrodynamic stimulation may improve cell response, allowing the formation of a pericellular matrix before rotation and therefore altering the mechanical stimuli experienced by cells. Also this point needs to be further investigated.

#### 2.3.4 Mechanical properties of *in vitro* cultured silk scaffolds

Compressive mechanical tests were performed on unseeded and ASCs/silk scaffolds in wet states after 28 days of culture. As previously mentioned, construct mechanical properties before implantation are indeed crucial to sustain physiological loads and tissue regeneration *in vivo*.

All samples exhibited sponge-like behavior. As shown in figure 3.9, no significant differences were detected among unseeded scaffolds in different culture conditions ( $p > 0.05$ ). Culture of ASCs led to a significant increase of Young's modulus when compared to empty sponges regardless the culture condition. ASCs/silk scaffolds cultured in chondrogenic medium under static condition achieved the significantly highest Young's modulus among all the groups. Furthermore, there are no significant differences between those cultured in growth medium and in chondrogenic medium under rotation culture.

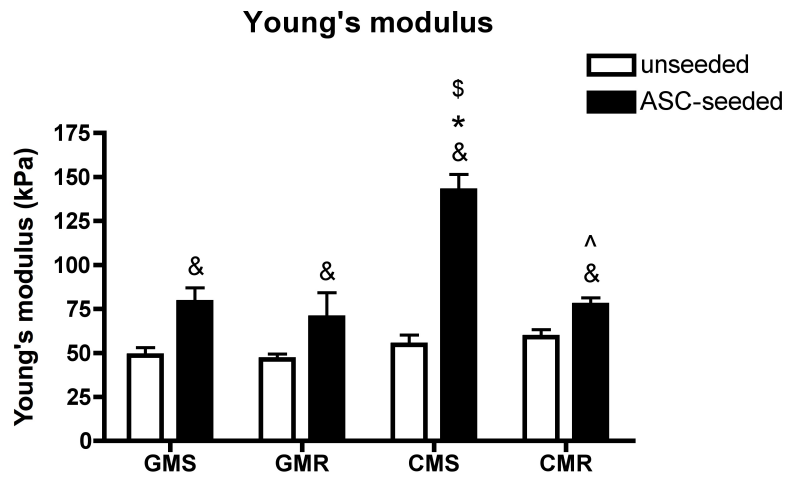


Figure 2.7: Compressive Young's modulus of unseeded and ASCs-seeded silk scaffolds under different culture conditions. The compression test was performed after 28 days of culture in growth medium under static condition (GMS) or rotation condition (GMR) and chondrogenic medium under static condition (CMS) or rotation condition (CMR). &  $p < 0.05$  vs. empty scaffolds; \*  $p < 0.05$  vs. GMS group; \$  $p < 0.05$  vs. GMR group; ^  $p < 0.05$  vs. CMS group.

Compressive moduli of ASCs/silk scaffold constructs increased after 4 weeks of culture because of new ECM deposition. DMMB assay, histological analysis and immunofluorescence indicated a significantly higher amount of GAG and collagen type II in the scaffolds when ASCs were cultured in static conditions with chondrogenic media and this corresponded to the highest increase of Young's modulus.

### 2.3.5 *In vivo* repair of chondral defects

To evaluate their potential for cartilage regeneration *in vivo*, ASCs/silk scaffold constructs were implanted in rat xiphoid defects after 28 days of culture with chondrogenic medium in static or rotation conditions. Empty defects, unseeded silk scaffolds and autografts were used as negative and positive controls, respectively.

No spontaneous neo-cartilage formation was observed in empty defects, as shown in the corresponding EPIC  $\mu$ CT images which exhibited a yellow color in the implantation site (figure 2.8, A). Negative safranin-O staining also confirmed that fibrous tissue filled the defect area (figure 2.8 F, K). Silk scaffolds integrated well in the implantation area with tight binding to the surrounding cartilage (figure 2.8, G, H, I), while fibrous tissue filled the zone between the inserted autografts and the surrounding cartilage (figure 2.8, J). Defects implanted with empty silk scaffolds showed little green staining on a yellow background indicating a very low amount of cartilage formation (figure 2.8, B). No evident positive safranin-O staining was observed (figure 2.8, L). In contrast, a significant amount of green staining was noticed in EPIC  $\mu$ CT images of defects where ASCs/silk scaffold constructs cultured in chondrogenic medium under both static (figure 2.8, C) and rotation conditions (figure 2.8, D) were implanted. Positive safranin-O staining also indicated neo-cartilage formation (figure 2.8, M, N). Autograft implants displayed identical staining and morphology as the surrounding original cartilage tissue except for the area in between, which showed negative Safranin-O staining in correspondence of fibrous tissue (figure 2.8, E, O).

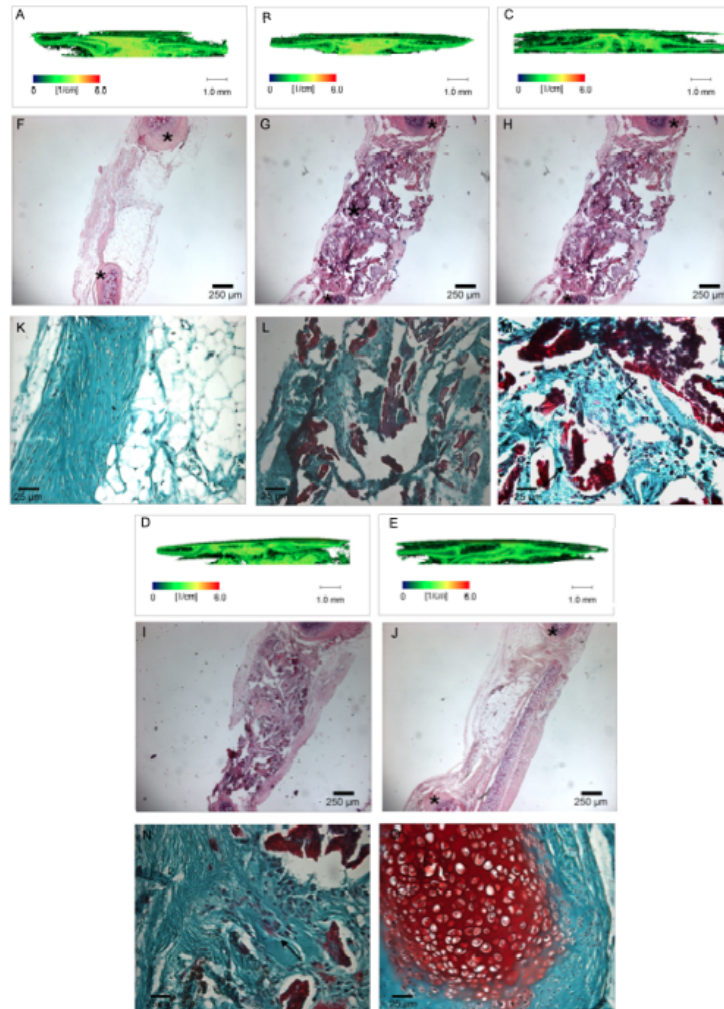


Figure 2.8: EPIC- $\mu$ CT and histological analysis of repaired xiphoids 8 weeks post surgery. The xiphoid samples were first processed for EPIC-  $\mu$ CT scanning. Areas with low proteoglycan content were colored in yellow whereas areas with high proteoglycan content were colored in green in the 3D reconstructed images (A-E, scale bar = 1.0 mm). Then, samples were sectioned and subjected to H&E (F-J, objective 4x) and safranin-O/fast green staining (K-O, objective 40x, red represents areas rich in proteoglycan). Asterisks indicate original cartilage while arrows indicate neo-cartilage.

Quantitative results are shown in figure 2.9.  $\mu$ CT-based quantification of neo-cartilage formation indicated a significantly higher cartilage volume in xiphoid defects where CMS constructs, CMR constructs and autografts were implanted. In addition, no significant differences were observed when unseeded scaffolds were employed with respect to the empty defect control group.

Despite the lower histology score, neo-cartilage volume in CMR group was similar to the volume measured when only silk scaffolds were implanted. Instead, CMS groups showed a significantly higher cartilage volume and a lower histology score compared to empty scaffolds and CMR construct groups, indicating more neo-cartilage formation. The highest neo-cartilage volume was observed in the positive control group. Autografts also had the lowest cumulative histology score ( $0.5 \pm 0.1$ ), indicating that the new tissue was similar to original cartilage.

In this study, the better outcomes *in vitro* in terms of ASCs chondrogenesis, new ECM deposition and mechanical property improvement were obtained when chondrogenic media and static culture conditions were employed. Similar results were assessed *in vivo*: with the exception of the positive controls, CMS groups induced the greatest formation of new cartilage, corresponding to the lowest histological score. However, it has to be noticed that safranin-O staining of both *in vitro* and *in vivo* constructs was much weaker and less homogeneous than in the case of native cartilage. This indicates a relative immature stage of the new chondral tissue. It has been shown that an excellent chondrogenesis of MSCs can be achieved after 8-12 weeks of *in vitro* culture [103]; furthermore, a higher quality of new cartilage has been obtained after 12 weeks of *in vivo* implantation of MSCs/3D scaffolds [104]. Therefore, in our study, neo-cartilage maturity may be improved prolonging the *in vitro* culture and/or the *in vivo* implantation.

In addition, it has been demonstrated that the differentiation ability of MSCs is dependent on cell seeding density [94]. Our results revealed a limited proliferation of ASCs when cultured in chondrogenic medium, causing a relatively low cell density in the silk scaffolds. Hence, an increase of the initial

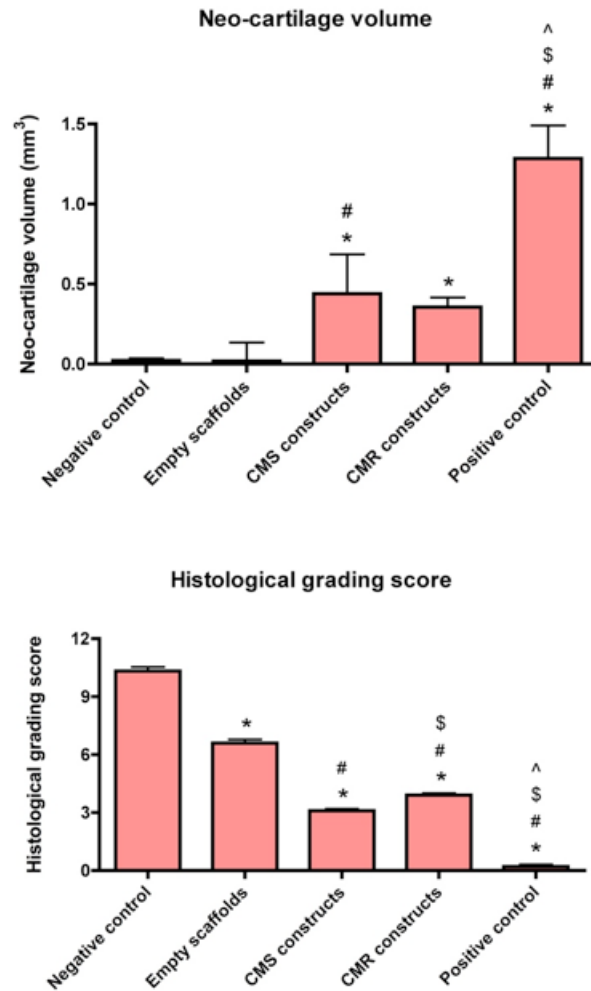


Figure 2.9: Histomorphometric evaluation of neo-cartilage formation in the defect areas by EPIC- $\mu$ CT and histological analyses of various ASCs/silk scaffold constructs 8 weeks after implantation in rat xiphoid cartilage defects. Empty scaffolds and ASCs-seeded silk scaffolds were pre-cultured for 28 days in chondrogenic medium under static condition (CMS) or rotation condition (CMR). \*  $p < 0.05$  vs. negative control; #  $p < 0.05$  vs. empty scaffolds; \$  $p < 0.05$  vs. CMS constructs and ^  $p < 0.05$  vs. CMR constructs.

seeding density of ASCs may be an advantage to improve neo-formed cartilage properties. Finally, the formulation of the chondrogenic medium may be refined, for instance including BMP-6 to enhance ASCs differentiation [105].

## 2.4 Conclusions

In this study, the potential of combining 3D silk scaffolds and adipose-derived stem cells for cartilage tissue engineering was evaluated, in the perspective to employ this system in a multicomponent scaffold for osteochondral regeneration. Results demonstrated that highly porous silk fibroin sponges produced by salt leaching can support chondrogenesis of ASCs. The highest levels of chondrogenic gene expression, GAG and collagen type II production and increase of compressive Young's modulus were achieved when constructs were cultured for 28 days in chondrogenic medium and in static conditions. ASCs/silk scaffolds also supported *in vivo* neo-cartilage formation in rat critical size xiphoid defects after 8 weeks. Also in this case, the best outcomes in terms of new tissue volume and quality were obtained when static conditions and chondrogenic medium were employed during pre-culture.

Nevertheless, further experiments are needed to improve the homogeneity of neo-cartilage *in vivo*, for instance refining the formulation of chondrogenic media, prolonging pre-culture duration, increasing ASCs seeding density and optimizing hydrodynamic stimulations. However, this study established that adipose-derived stem cells can be potentially used with silk fibroin scaffolds for cartilage tissue engineering.



## Chapter 3

# Silk fibroin/hyaluronic acid 3D matrices for cartilage tissue engineering

### 3.1 Introduction

This chapter concerns the modification of silk fibroin sponges fabricated by salt leaching to improve scaffold characteristics for cartilage repair. To this purpose, hyaluronic acid (HA) was conjugated to silk fibroin (SF), in order to exploit its properties for chondral regeneration, as briefly mentioned in the previous paragraphs.

Hyaluronic acid is a natural polysaccharide physiologically present in cartilage ECM. It consists of disaccharide subunits of glucuronic acid and N-acetylglucosamine and its molecular weight varies from  $10^6$  to  $10^7$  Dalton, depending on the tissue source. HA has several distinct molecular functions during tissue formation or remodeling: it contributes to tissue homeostasis and biomechanics, gives structural integrity to extracellular and pericellular matrix and influences cell behavior through the interaction with specific surface receptors [106]. In particular, hyaluronic acid can provide a hydrated,

fluid pericellular matrix which facilitates cell mitosis and allows cell invasion through the ECM. In this way, other matrix components can assemble near cell membrane and growth factors can be presented to cells without interference from the structured fibrous ECM found in fully differentiated tissues. In case of cartilage, besides these functions, hyaluronic acid directly contributes to the structural and mechanical properties of the tissue, as described in paragraph 1.2 [106]. In fact, the ability of HA to retain a large amount of water gives cartilage its peculiar biomechanical properties and viscoelasticity.

HA has two mechanisms of tethering to cells: first, through its specific receptor, CD44; second, thanks to the transmembrane interaction of “nascent” HA molecules with the enzyme hyaluronan synthase during the process of extrusion (figure 3.1). In particular, HA synthesis by cells has a peak during mitosis, because hyaluronic acid can help cell detachment from its substratum, which is also a necessary step during migration. When cell - hyaluronic acid interaction involves CD44 receptors, it usually causes the rearrangement of cytoskeletal elements, especially during cell proliferation, motility and invasion. Finally, another hyaluronan-binding protein is RHAMM, whose interaction with HA starts a signaling pathway for the initiation of locomotion [106].

Hyaluronic acid has an important role also during embryonic development, in particular during limb formation. In fact, the differentiation of condensed limb mesoderm to cartilage is accompanied by an extensive formation of HA-enriched pericellular matrices, with a concentration of proteoglycans that is much higher than in the matrices surrounding mesodermal cells before cartilage formation [106].

The process of angiogenesis is also affected by hyaluronic acid, but HA effect depends on its molecular weight. High molecular weight HA has been shown to have anti-angiogenetic properties, while short fragments of hyaluronic acid (4-25 disaccharide units) increased the proliferation, migration and sprout formation of endothelial cells in several *in vivo* studies [107, 108, 109].

In cartilage tissue engineering applications, hyaluronan has been shown to modulate chondrocyte behavior preserving their phenotype, which is one of

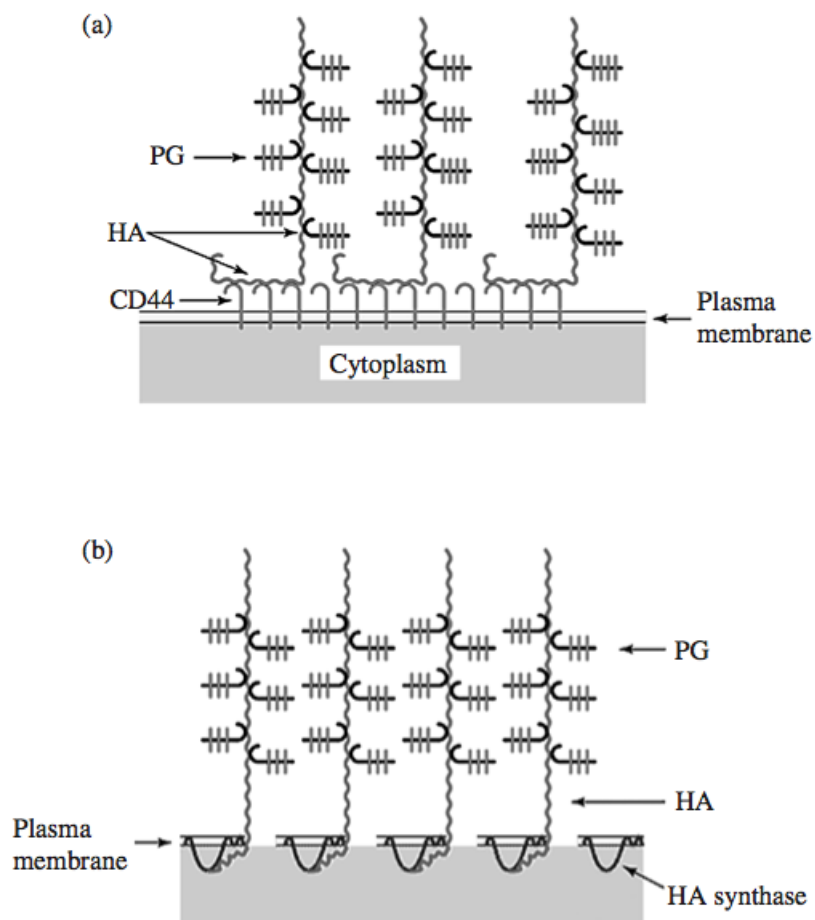


Figure 3.1: Models of HA-dependent pericellular matrix. Hyaluronan is tethered to cell surface by multivalent interactions with CD44 (a) or by a transmembrane retention of hyaluronan synthase on the cytoplasmic side of cells (b) [106].

the main issues in culturing cartilage cells (paragraph 1.4.3) [88]. It has been combined with chitosan [89, 90], PdlLA [88] and collagen [91, 92], determining an increase of the production of cartilaginous extracellular matrix and chondrogenesis.

The use of silk fibroin and hyaluronic acid blends has been recently explored in tissue engineering showing great potential. SF/HA freeze-dried sponges were prepared and cross-linked with EDC for *in vitro* culture of neural cells, which maintained their phenotype after 5 days of culture [110]. SF/HA scaffolds produced by freeze-drying were also employed for MSC culture, leading to a higher deposition of collagen I and III with respect to a pure fibroin scaffold [93, 111]. Other applications include SF/HA hydrogels produced by ultrasonication [112] and cardiac patches synthesized starting from microparticles of silk fibroin/hyaluronan and cross-linked by genipin, a natural cross-linking agent for biopolymers containing amine groups [113]. Genipin is extracted from the Gardenia fruit and reacts with different kinetics with both primary and secondary amines, present on silk fibroin and hyaluronic acid respectively. Moreover, it is considered to be biocompatible and possesses weak anti-inflammatory properties [114, 115]. Genipin has been successfully used to cross-link silk fibroin [116], chitosan-fibroin [27] and collagen type II-chitosan-hyaluronic acid [117].

In our study silk fibroin/hyaluronic acid scaffolds at different HA content were produced for the first time by using the salt leaching technique to obtain a more interconnected and controlled porosity with respect to freeze-drying. High molecular weight hyaluronic acid was used (2 MDa), to avoid any potential damaging angiogenetic stimulation *in vivo*. The process has been conducted in an aqueous environment and to avoid a significant loss of HA, silk fibroin and hyaluronic acid were cross-linked by genipin. Then, a systematic study was performed to assess how scaffold properties can be modulated by HA addition and cross-linking. The stability of the system and hyaluronan distribution in the sponges were also evaluated in a qualitative and a quantitative way. To these purposes, SF/HA scaffolds were characterized in terms

of morphology, silk fibroin conformation, water content, porosity, cross-linking degree and mechanical properties. Wettability properties were also evaluated on films produced by casting the same aqueous solution used for sponge preparation. Films were used as a bidimensional model system to better understand silk fibroin/hyaluronic acid interaction and how it is modified by cross-linking without the additional complexity of the salt leaching process and the 3D structure. To evaluate HA content and distribution in the scaffolds with and without cross-linking, hyaluronic acid was conjugated to a fluoresceinamine and the scaffolds were then observed with a confocal laser microscope.

## 3.2 Materials and methods

### 3.2.1 Scaffold production

Silk fibroin/hyaluronic acid sponges were produced using the salt leaching technique previously described. A 7-8% w/V fibroin solution was obtained as indicated in the paragraph 2.2.1, then NaCl with a grain diameter range of 425-1180  $\mu\text{m}$  was added to this solution to induce protein gelation according to the previous protocol. SF/HA scaffolds were prepared in the same way, dissolving in the silk fibroin solution 1, 2 and 5% by wt. of HA referred to the total protein weight (sample codes: HA1, HA2, HA5). Cross-linked SF and SF/HA materials were prepared by adding 0.5% by wt. of genipin (sample codes: SFgen and HA1gen, HA2gen, HA5gen) to the above solutions. From the same solutions without salt and with or without genipin, SF/HA films were also casted. In this case, 7 ml of each aqueous solution were poured in a 60 mm Petri dish kept under a hood at room temperature till solvent evaporation. The resulting films were stabilized in water vapor for 24 hours and finally dried at room temperature.

## 3.2.2 Scaffold characterization

### 3.2.2.1 Environmental Scanning Electron Microscopy

The morphology of the unmodified and cross-linked SF/HA sponges was evaluated using an ESEM (Environmental Scanning Electron Microscope) XL 30 (Fei Company). Sponges were completely dried at room temperature and images were collected in low vacuum mode (from 0.6 to 0.8 Torr) with a voltage range between 10 kV and 14 kV.

### 3.2.2.2 Fourier Transform Infrared Spectroscopy

Silk fibroin structure in the SF/HA sponges and films was evaluated by FTIR - ATR (Fourier Transform InfraRed – Attenuate Total Reflectance, Spectrum One Perkin Elmer, US). Spectra were collected from 4000  $\text{cm}^{-1}$  to 600  $\text{cm}^{-1}$  as the mean of 16 scans.

### 3.2.2.3 Porosity

The open porosity of the SF/HA sponges was quantitatively evaluated using the principle of liquid displacement. Hexane (n-Hexane, Sigma Aldrich, US) was used because it fills the pores of the submerged fibroin/hyaluronic acid scaffolds without swelling. Each scaffold was immersed in a known volume of hexane,  $V_1$ , in a graduate cylinder for 10 minutes, and the volume  $V_2$  of the hexane with the sponge was measured. The sponge was then removed and the residual volume of hexane  $V_3$  was registered.

The porosity was calculated from the following equation:

$$\varepsilon(\%) = \frac{V_1 - V_3}{V_2 - V_3} \times 100$$

### 3.2.2.4 Cross-linking degree

The degree of cross-linking of the SF/HA materials was evaluated using 2 different methods. The first method used the reaction with ninhydrin of the

free amino groups (both primary and secondary) remained after cross-linking of the blend materials. That reaction occurs with the production of purple products whose amount detected by a spectrophotometer at 570 nm can be related to the amount of the reacted groups [118]. Sponges of SF/HA or pure fibroin, with or without cross-linking with genipin, were frozen at  $-20^{\circ}\text{C}$  and lyophilized for 24 hours. 15 mg of each sample were incubated in 5 ml of 0.35% w/V ninhydrin (Sigma Aldrich, US) in ethanol (96%, Sigma Aldrich, US) for 1 hour at  $90^{\circ}\text{C}$  under mild stirring. 5 ml of this solution without sample were also incubated in the same conditions as a blank. After cooling at room temperature in a cold water bath, absorbance at 570 nm was measured using a microplate reader (Multiskan EX, Thermo Scientific, US) and normalized by subtracting the absorbance of the blank at the same wavelength. For films, 30 mg of material were incubated in 3 ml of ninhydrin solution at 0.35% w/V in ethanol (96%, Sigma-Aldrich, US) for 1 hour at  $90^{\circ}\text{C}$  under mild stirring. Also in this case, 3 ml of ninhydrin solution were incubated in the same conditions as a blank. Cross-linking degree CD was calculated as follows:

$$CD(\%) = \frac{NH_{without} - NH_{with}}{NH_{without}} \times 100$$

where  $NH_{without}$  and  $NH_{with}$  are the amounts of free amino groups in the uncross-linked sponge and the free amino groups in the sponge cross-linked with genipin, respectively. Glycine (Sigma Aldrich, US) was used to set up a calibration curve using known concentrations as standards to correlate absorbance at 570 nm to the number of free amino groups that participate in the reaction. In the second method, the molecular weight of the chains between two cross-linking points,  $M_c$ , was determined by applying the rubber-elasticity theory for hydrogels [119, 120, 121]. According to theory,  $M_c$  can be determined testing hydrogels in a tensile configuration in the range of small deformations (less than 1%), known the density and the swelling degree of the materials. The used model will be discussed in paragraph 3.3.3. Densities were measured with a hydrostatic balance and hexane (n-Hexane, Sigma Aldrich, US) as liq-

uid according to Archimedes' principle. Tensile properties were measured as reported in paragraph 3.2.2.7.

### 3.2.2.5 Water content

For water content, the weight of each sponge was measured in the dry state ( $M_{dry}$ ) after lyophilization. The scaffolds were then soaked drop by drop with Milli-Q water, allowing the water to be slowly absorbed and thus avoiding the formation of air bubbles inside the porous structure. The sponges were considered completely wet when their weight did not change after the addition of a drop and the removal of the water in excess. Their weight was measured ( $M_{wet}$ ) and the weight percentage of the absorbed water referred to the total weight of the wet scaffold was calculated as:

$$W(\%) = \frac{M_{wet} - M_{dry}}{M_{wet}} \times 100$$

### 3.2.2.6 Wettability properties

Wettability of the silk fibroin/hyaluronic acid materials was evaluated by measuring air-water contact angles on films prepared by solvent casting as described above. Sessile drop measurements were performed using a self-developed goniometer. A 3  $\mu$ l drop of MilliQ grade water was gently deposited on the sample and immediately acquired by a digital camera to avoid adsorption. The resulting image was successively analyzed using imageJ 1.43 software and the contact angle was calculated applying spherical approximation. Each value was obtained as the mean of 20 measures carried out on each film.

### 3.2.2.7 Mechanical properties

The compressive mechanical properties of the SF/HA and the pure fibroin sponges with or without cross-linking were measured using a Bose universal testing machine model ElectroForce3200, equipped with a 225 N load cell. Tests were performed on wet discs with a diameter of 12 mm and a variable

height between 3 mm and 4 mm, depending on the sample. Elastic moduli were calculated according to ASTM D 1621-04a, under displacement control in uniaxial ramp condition at a strain rate of 1.2 mm/min at room temperature (50% Relative Humidity, RH). Wet SF/HA and pure fibroin films produced by solvent casting were tested under tension by using a universal testing machine Instron 4502 at 0.5 mm/min of elongation rate in environmental conditions (23°C, 50% RH). Samples had a length of 50 mm and a width of 5 mm with a variable thickness from 0.2 mm to 0.4 mm, depending on the cast film. Elastic moduli were calculated according to ISO 527-1/2:1993.

### 3.2.2.8 Hyaluronic acid mapping and quantification

Fluoresceinamine was conjugated to hyaluronan (fHA) using a method modified by de Belder and Wik [122] and Hua et al. [124], which employed an Ugi reaction for the synthesis. The fluoresceinamine can bind to the carboxyl group of the D-glucuronic acid in the disaccharide units, letting the secondary amine in the N-acetyl-D-glucosamine be still potentially able to bind to genipin in the cross-linking reaction. 50 mg of hyaluronan were dissolved overnight in 40 ml of distilled water and then mixed with 15 ml of dimethyl sulfoxide (DMSO, Sigma Aldrich, US). 25 mg of fluoresceinamine isomer I (Sigma Aldrich, US) were dissolved in a solution of 5 ml of DMSO, 25  $\mu$ l of acetaldehyde (Sigma Aldrich, US) and 25  $\mu$ l of cyclohexyl isocyanide (Sigma Aldrich, US) and then added to the solution with HA. The reaction was performed at room temperature for 5 hours under mild stirring. The resulting solution was then dialyzed against distilled water to separate free fluoresceinamine molecules and other reagents using a Slide-A-Lyzer dialysis cassette (2000 Da MWCO, Pierce, US). Finally, the fHA solution was dried in a rotavap at 40°C to obtain a powder, which was further freeze-dried to remove completely the remaining water. SF/HA sponges (with and without cross-linking) were produced using the fHA powder following the same protocol explained above. The scaffolds were then observed with a confocal laser microscope (Nikon Eclipse Ti-E). The scaffolds with fluorescent HA were also used to quantify HA content: sponges

were cut in 6-mm disks, weighted and digested in a solution of Proteinase K (Qiagen, US) at 1 mg/ml in PBE buffer (10mM EDTA in PBS) for 48 hours at 55°C. The fluorescence of the resulting solutions was quantified using a spectrofluorimeter (Tecan Infinite M200 Pro) using an excitation wavelength of 494 nm and collecting the emission at 521 nm. To correlate fluorescence to the amount of HA in the samples, a calibration curve was set up using solutions of fHA at known concentrations.

### 3.2.2.9 Statistical analysis

Water uptake, porosity, cross-linking degree and mechanical properties were measured on  $N = 3$  samples. All results were expressed as the mean  $\pm$  standard error of the mean and analyzed using a statistical software (GraphPad Prism 5.0, GraphPad Software). To determine the statistical significance of differences among the results before and after cross-linking or at different hyaluronic acid contents, two-way or one-way ANOVA test was performed (if the interaction term was significant). Equality of variances was verified before applying the tests. Significance was assigned at p-values less than 0.05.

## 3.3 Results and discussion

### 3.3.1 Environmental Scanning Electron Microscopy

The micrographs of sponges are shown in figure 3.2. All morphologies were characterized by a high and interconnected porosity with a pore diameter ranging from about 100  $\mu\text{m}$  up to about 500  $\mu\text{m}$ , in a size range that is considered to be optimal for bone or cartilage tissue engineering [125]. The surface of the sponges showed small fibrillar structures and microporosity, which may improve cellular adhesion and solute flow inside the scaffold [12]. At all concentrations of hyaluronic acid, there were no significant differences between the structures of the unmodified and the cross-linked sponges.

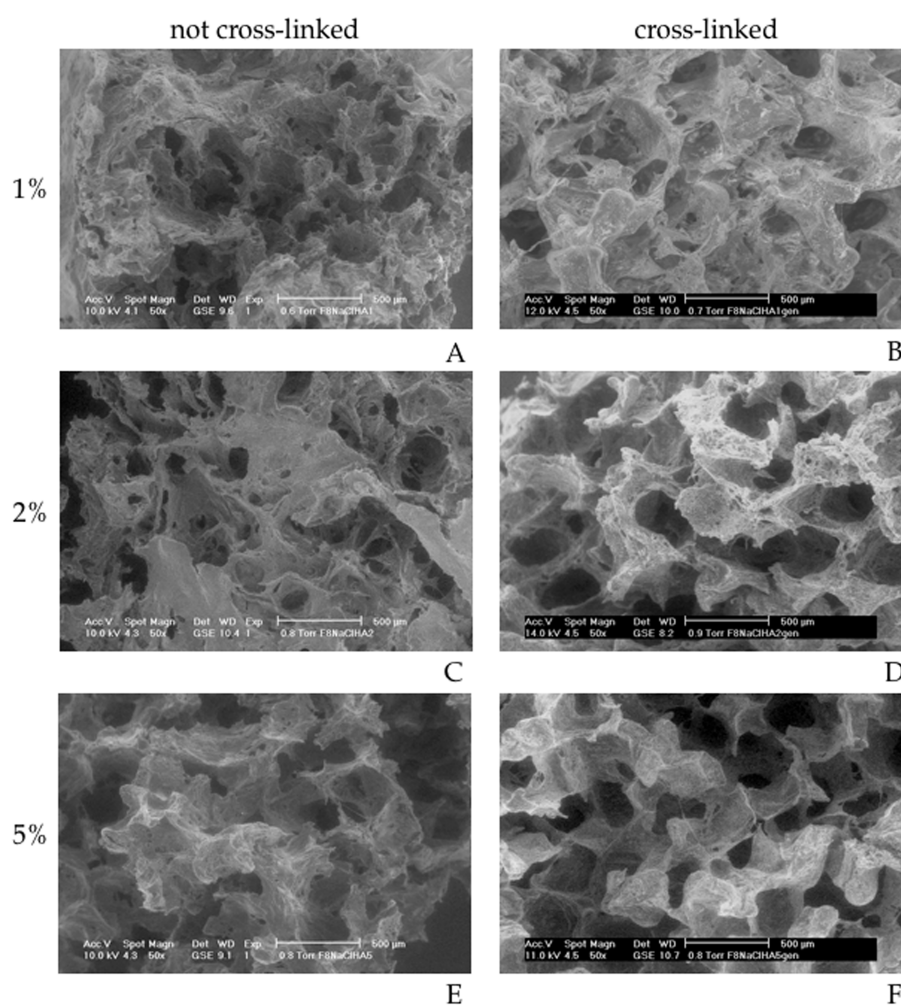


Figure 3.2: ESEM images of the SF/HA sponges with 1%  $w_{\text{HA}}/w_{\text{SF}}$ , 2%  $w_{\text{HA}}/w_{\text{SF}}$  and 5%  $w_{\text{HA}}/w_{\text{SF}}$ , before (A, C, E) and after (B, D, F) cross-linking respectively. Images were collected in low vacuum (from 0.6 to 0.8 Torr) with a voltage range between 10 kV and 14 kV.

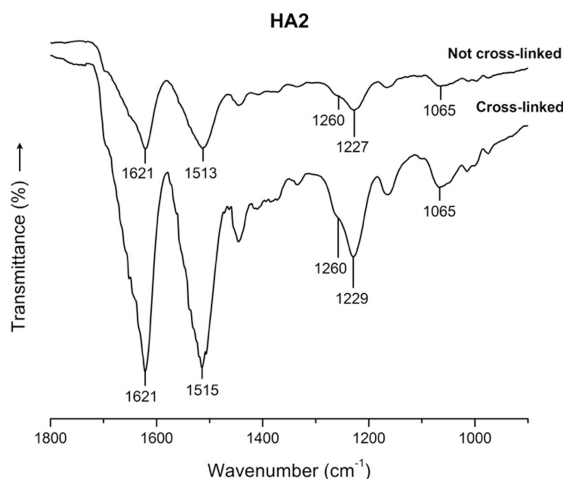


Figure 3.3: IR spectra of the silk fibroin/hyaluronic acid sponges at 2% w<sub>HA</sub>/w<sub>SF</sub>, with and without cross-linking by genipin.

### 3.3.2 Fourier Transform Infrared Spectroscopy

FTIR was used to evaluate the structure of silk fibroin in SF/HA and pure silk fibroin sponges. The collected spectra exhibited no significant differences among sponges; in figure 3.4, the spectrum of the HA2 sample is shown as example.

In all scaffolds, the primary and the secondary amide peaks were at 1621-1622  $\text{cm}^{-1}$  and 1513-1515  $\text{cm}^{-1}$  respectively, and the tertiary amide peak was present as a shoulder at 1258-1260  $\text{cm}^{-1}$ . This indicated the formation of stable  $\beta$ -sheet structures in the silk fibroin molecules [126]. The broadness of the peak at about 1060-1070  $\text{cm}^{-1}$  (range varied from 1063 to 1067  $\text{cm}^{-1}$  among different spectra) indicated however that random coil structures were still present in the protein. Moreover, there were no significant differences in the spectra with or without the cross-linking. This may be due to the predominance of the NaCl contribution to the silk fibroin stabilization when compared to the effect of hyaluronic acid and genipin.

At the concentrations used for sponge preparation, silk fibroin bands hid all

the main infrared bands of the hyaluronic acid [127] (free carboxylic, COOH: 1736  $\text{cm}^{-1}$ , 1230  $\text{cm}^{-1}$ ; carboxylate, COO: 1610  $\text{cm}^{-1}$ , 1410  $\text{cm}^{-1}$ ; monosubstituted amide: 1648  $\text{cm}^{-1}$ , 1560  $\text{cm}^{-1}$ , 1315  $\text{cm}^{-1}$ ; associated methyl group: 1375  $\text{cm}^{-1}$ ; C-O stretching and C-O-H bending: 1000-1200  $\text{cm}^{-1}$ ). Therefore, FTIR measurements were incapable of detecting the presence of the water soluble hyaluronic acid in the blends after washing, neither the effectiveness of the cross-linking reaction.

IR spectra were also collected for the SF/HA films with and without cross-linking. Measurements were performed after casting, after stabilization in water vapor for the uncross-linked materials and after washing in distilled water for 3 days, in order to assess the effect of the single steps of preparation on the structure of fibroin. Wavenumbers of the primary, secondary and tertiary amides and the peak around 1050-1080  $\text{cm}^{-1}$  are reported in figure 3.4. Pure silk fibroin film after casting showed both  $\beta$ -sheet and  $\alpha$ -helix/random structures: the primary amide at 1635  $\text{cm}^{-1}$  and the peak at 1056  $\text{cm}^{-1}$  were in fact due to the  $\alpha$ -helix/random conformation of SF, while the secondary amide at 1515  $\text{cm}^{-1}$  and the presence of the tertiary amide at 1259  $\text{cm}^{-1}$  indicated  $\beta$ -sheet structures. Stabilization in water vapor induced the shift of the primary amide and the 1050-1080  $\text{cm}^{-1}$  peak towards wavenumbers corresponding to stable crystalline structures (1620  $\text{cm}^{-1}$  and 1070  $\text{cm}^{-1}$  respectively). However, the broad shape of the latter peak indicated the persistency of random coil conformation.

An analogous spectrum was collected for the cross-linked silk fibroin film after casting and washing did not significantly change peak wavenumbers: the wavenumbers of primary and secondary amides, the presence of the tertiary amide and the position and shape of the peak at about 1070  $\text{cm}^{-1}$  indicated the formation of stable crystalline structures after casting with some residual random coil. This means that the cross-linker caused the formation of crystalline structures and stabilization of fibroin, as previously reported in literature [128]. In all the spectra of the films with hyaluronic acid regardless cross-linking,  $\beta$ -sheet crystalline structures were detected before stabilization

		Amide I		Amide II		Amide III		1050-1080	
		no CL	CL	no CL	CL	no CL	CL	no CL	CL
SF	after casting	1635	1620	1515	1515	1259	1259	1056	1068
	stabilized	1620	-	1518	-	1259	-	1070	-
	after washing	1624	1619	1515	1514	1258	1259	1067	1067
HA1	after casting	1620	1619	1514	1515	1260	1260	1069	1068
	stabilized	1621	-	1514	-	1258	-	1063	-
	after washing	1620	1619	1514	1514	1259	1259	1062	1066
HA2	after casting	1620	1620	1515	1515	1260	1260	1067	1068
	stabilized	1619	-	1513	-	1260	-	1064	-
	after washing	1620	1619	1514	1514	1260	1259	1065	1066
HA5	after casting	1619	1620	1514	1515	1258	1259	1065	1070
	stabilized	1620	-	1514	-	1259	-	1066	-
	after washing	1620	1618	1514	1513	1260	1260	1065	1065

Figure 3.4: Wavenumbers ( $\text{cm}^{-1}$ ) of the characteristic IR peaks of silk fibroin (amide I, amide II, amide III and 1050-1080  $\text{cm}^{-1}$  peak) measured for the SF/HA films with and without cross-linking by genipin (CL and no CL respectively): spectra were collected after casting, after stabilization in water vapor (for unmodified materials) and after washing in distilled water for 3 days.

(amide I at 1618-1620  $\text{cm}^{-1}$ , amide II at 1513-1515  $\text{cm}^{-1}$ , amide III at 1258-1260  $\text{cm}^{-1}$ , peak around 1070  $\text{cm}^{-1}$ ). In the unmodified materials, there is an effect of the interaction among silk fibroin and hyaluronic acid molecules, which have been known as an inducer of crystallization of the protein through a mechanism previously reported in literature [93]. This process may involve the effect of the carboxylic group of the HA, which is capable to induce silk fibroin crystallization and/or the removal of water molecules from silk fibroin; in this case, HA acts similarly to sericin during the natural spinning of the silk [68]. Stabilization and washing did not determine any changes in the infrared spectra of the SF/HA films.

FTIR spectra showed that in both SF/HA sponges and films silk fibroin has a  $\beta$ -sheet crystalline conformation with some residual random coil structures. In the absence of NaCl, hyaluronic acid and genipin are both able to induce fibroin stabilization in the films produced by solvent casting.

### 3.3.3 Cross-linking degree

To evaluate the cross-linking degree of the SF/HA and pure fibroin materials, two different strategies were explored: first, the ninhydrin test was used to evaluate the percentage of amino groups involved in the cross-linking reaction during sponge preparation; secondly, the molecular weight  $M_c$  between two cross-links was calculated for the SF/HA films using the rubber elasticity theory, in order to estimate the molecular arrangement in the material to a first approximation. We decided to perform this analysis on SF/HA films instead of sponges, because materials need to be tested in a tensile configuration; moreover, the porosity of the sponges increases the complexity of the system and therefore the results would be dependent also on the structure of the scaffolds. Films were also tested with ninhydrin to confirm the results obtained for  $M_c$ , compare them with the sponges and therefore assess the influence of different preparations on the cross-linking process. According to the rubber elasticity theory [119, 120, 121], effective cross-link density  $\nu_e$  and the molar mass between cross-links  $M_c$  can be obtained from the following equations:

Density (Kg/dm <sup>3</sup> )	SF	HA1	HA2	HA5
Not cross-linked	1.40 ± 0.04	1.33 ± 0.06	1.38 ± 0.03	1.32 ± 0.01
Cross-linked	1.41 ± 0.03	1.37 ± 0.02	1.35 ± 0.01	1.35 ± 0.04

Figure 3.5: Density of pure fibroin and SF/HA films with 1%  $w_{HA}/w_{SF}$ , 2%  $w_{HA}/w_{SF}$  and 5%  $w_{HA}/w_{SF}$  before and after cross-linking by genipin.

$$\nu_e = \frac{E\phi_2^{-1/3}}{3RT}$$

and

$$M_c = \frac{\rho}{\nu_e}$$

where  $E$  is the Young's modulus measured in a tensile configuration,  $R$  is the gas constant ( $8.1344 \text{ J} \cdot \text{K}^{-1} \cdot \text{mol}^{-1}$ ),  $T$  is the temperature in Kelvin and  $\rho$  is the density of the material.  $\Phi_2$  is the volume fraction of polymer in the film, defined as:

$$\phi_2 = \frac{M_{dry}/\rho}{M_{dry}/\rho + (M_{wet} - M_{dry})/\rho_{H_2O}}$$

where  $M_{dry}$  and  $M_{wet}$  are respectively the weight of each film in dry state and after 24 hours in distilled water.  $\rho_{H_2O}$  is the density of water at the measurement temperature. Results are shown in figure 3.6 (A): to simplify,  $1/M_c$  is plotted, since it is directly proportional to the material cross-linking degree.

A significant decrease of  $1/M_c$  could be observed in the material with 5% of hyaluronic acid: at higher hyaluronic acid content, the HA molecules may prevent the formation of bonds among silk fibroin chains and this led to an increment of the molecular weight between the cross-links. This is compatible

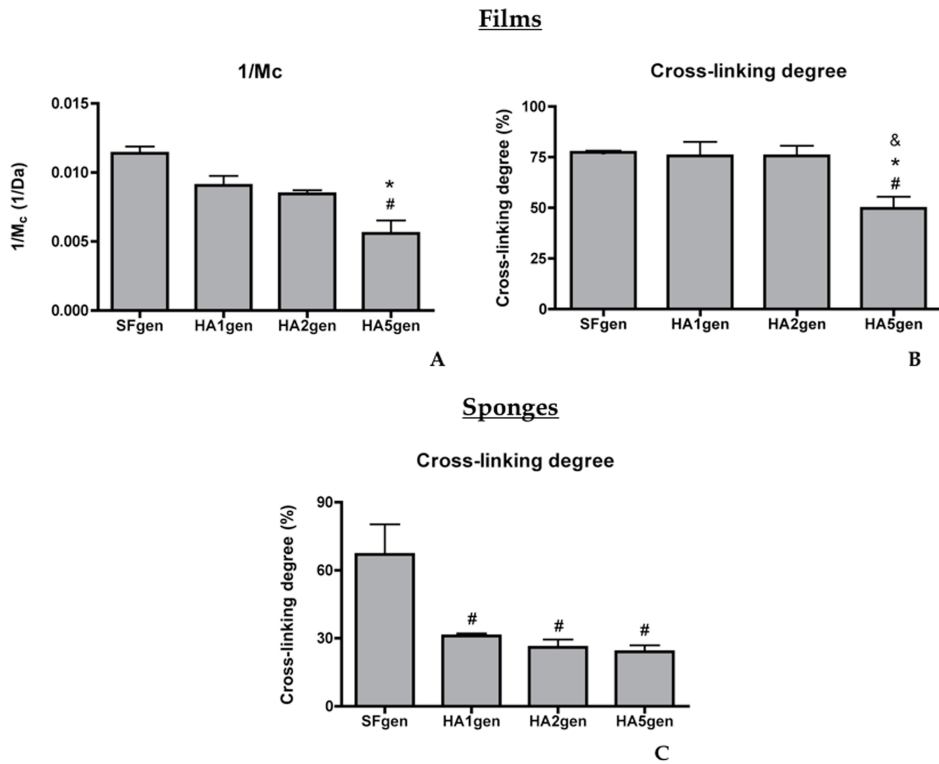


Figure 3.6: Cross-linking degree of SF/HA and pure fibroin films defined as  $1/M_c$ , where  $M_c$  is the molecular weight of the polymer between cross-links calculated from the rubber-elasticity theory applied for hydrogels in the range of small deformations (A). Cross-linking degree defined as the percentage of amino groups which participated in the cross-linking reaction measured on the SF/HA films (B) and sponges (C) with the ninhydrin test. #  $p < 0.05$  vs control w/o hyaluronic acid, \*  $p < 0.05$  vs HA1gen, &  $p < 0.05$  vs HA2gen.

with the results obtained for the cross-linking degree measured on the SF/HA films using the ninhydrin test and reported in figure 3.6 (B). In the material with 5%  $w_{\text{HA}}/w_{\text{SF}}$ , there was a significant decrease in the number of amino groups involved in the cross-linking reaction when compared to the pure fibroin film and the films at lower hyaluronic acid content. This corresponded to fewer cross-linking points and therefore bigger polymer chains among cross-links.

Results of the ninhydrin test on the SF/HA sponges are reported in figure 3.6 (C): the degree of cross-linking was significantly lower (about 50%) in the scaffolds with hyaluronic acid with no differences related to the HA content. In this case, the effect of hyaluronic acid on the cross-linking was important also at lower concentrations: this may be due to the different kinetics of fibroin stabilization, which was not only induced by the cross-linker, but also by the salting-out effect exploited for sponge preparation. In fact, during film casting, stabilization takes place because of the cross-linking reaction and so the kinetics of both reactions are the same; instead, during sponge production, the gelation of silk fibroin starts immediately after the addition of the salt and before the reaction of genipin, which is much slower. Therefore, the formation of  $\beta$ -sheet structures before cross-linking may decrease the availability of reaction sites, which are hidden not only by hyaluronic acid molecules, but also in the crystalline structures. As a consequence, the degree of cross-linking in the SF/HA sponges was about 50-60% less than in the corresponding SF/HA films. It may be expected that the differences among the cross-linking degrees measured with the ninhydrin test corresponded to similar variations of  $M_c$  also in the SF/HA sponges, even if it could not be verified experimentally because of technical difficulties in performing tensile tests on sponges and obtaining reliable results. This hypothesis is supported by the great accordance of the results obtained for the SF/HA films, which showed similar trends in both the measurements: a decrease of about 50% in  $1/M_c$  in the film HA5gen corresponded indeed to a decrease of about 40% in the cross-linking degree measured with the ninhydrin test.

Porosity (%)	SF	HA1	HA2	HA5
Not cross-linked	89 ± 3	89 ± 3	87 ± 4	87 ± 3
Cross-linked	80 ± 1 <sup>§</sup>	86 ± 4	83 ± 3	85 ± 7

Figure 3.7: Porosity of the uncross-linked and cross-linked SF/HA and pure fibroin sponges with 1% w<sub>HA</sub>/w<sub>SF</sub>, 2% w<sub>HA</sub>/w<sub>SF</sub> and 5% w<sub>HA</sub>/w<sub>SF</sub>. § p < 0.05 vs corresponding uncross-linked material.

### 3.3.4 Porosity

The porosity of a scaffold for cartilage tissue engineering is a key property to obtain a physiological cell 3D distribution for a functional organization of the new ECM produced by cells and effective supply of nutrients and waste removal during the *in vitro* culture. The porosity of the SF/HA and pure fibroin sponges was measured by the method of liquid displacement and the results are reported in figure 3.7.

There were no statistical differences in the porosity among the SF/HA sponges at different hyaluronic acid contents or before and after cross-linking. Instead, cross-linking determined a significant decrease in the porosity of the pure fibroin sponges. This may be due to the higher cross-linking degree of the SF sponges with respect to the scaffolds with hyaluronic acid, which can make the pores smaller. For each sponge, porosity is high and over 80%. Porosity greater than 70% is recommended for a scaffold for cartilage regeneration to allow an ECM distribution similar to the physiological tissue [6].

### 3.3.5 Wettability properties

The influence of the addition of hyaluronic acid and the cross-linking by genipin on the wettability properties of the silk fibroin/hyaluronic acid materials was evaluated measuring air-water static contact angle on the SF/HA and pure fibroin films prepared by solvent casting. Results are summarized in figure 3.8 (A).

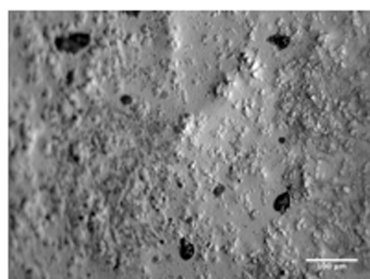
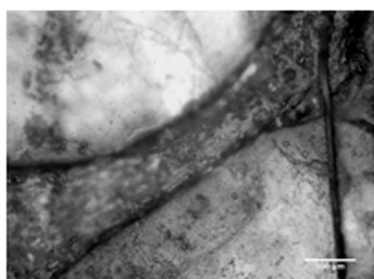
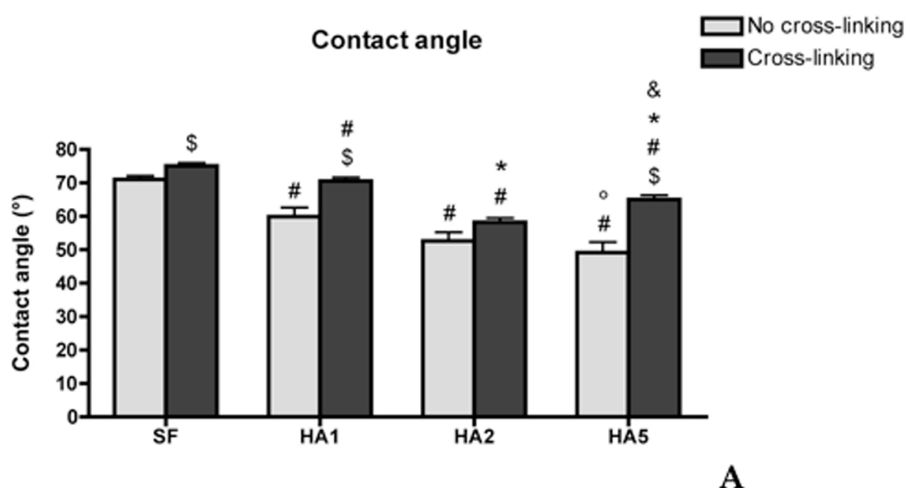


Figure 3.8: Contact angle (A) measured by a static sessile drop method on cross-linked and uncross-linked films obtained by solvent casting from the aqueous pure fibroin SF or SF/HA solutions at 1%  $w_{HA}/w_{SF}$ , 2%  $w_{HA}/w_{SF}$  and 5%  $w_{HA}/w_{SF}$  with or without genipin. Optical images of the surface of the films at 5%  $w_{HA}/w_{SF}$  before (B) and after (C) cross-linking. \$  $p < 0.05$  vs corresponding uncross-linked material, #  $p < 0.05$  vs corresponding control, °  $p < 0.05$  vs HA1, %  $p < 0.05$  vs HA2, \*  $p < 0.05$  vs HA1gen, &  $p < 0.05$  vs HA2gen.

In the unmodified materials, there was a significant decrease of contact angle increasing the concentration of hyaluronic acid. This increase in material hydrophilicity was caused by the higher hydrophilicity of hyaluronic acid with respect to silk fibroin molecules, which have large hydrophobic regions in correspondence to  $\beta$ -sheet structures. The addition of hyaluronic acid caused a decrease of the static contact angle also in the cross-linked materials, but in this case it was not proportional to the HA content. Moreover, at all hyaluronic acid concentrations, the cross-linked film had a significantly higher contact angle respect to the corresponding unmodified material.

This can be explained observing the optical images of the surface of the SF/HA films: in figure 3.8 the images of the film at 5%  $w_{\text{HA}}/w_{\text{SF}}$  without or with genipin (B and C respectively) are shown as example. In the uncross-linked material, a phase separation between hyaluronic acid and silk fibroin occurred, while the cross-linking process made the surface more homogeneous. This reduced the contribution of hyaluronic acid to the increment of hydrophilicity: its behavior was mediated by fibroin hydrophobicity, since the two components were more interspersed. The higher dispersion of the contact angle measurements for the SF/HA films without genipin is also an indication of the phase separation that occurred in the uncross-linked materials. Indeed, standard deviations are about doubled when compared to the standard deviations obtained from the cross-linked films, indicating a lower homogeneity of the material. Interestingly, hyaluronic acid appears to act again as sericin during the silk spinning process: as reported in [68], sericin is much more hydrophilic than fibroin and this leads to the segregation of silk fibroin molecules in the glands of *Bombyx mori* before spinning. This may happen also in the silk fibroin/hyaluronic acid materials where hyaluronan can cause fibroin separation because of its hydrophilicity, unless genipin prevents this phenomenon creating cross-linking points among molecules. In confirmation of this hypothesis, a phase separation also occurred when silk fibroin was blended with the hydrophilic polyethylene oxide to produce films by solvent casting [123].

### 3.3.6 Water content and mechanical properties

Water content and Young's modulus were measured for pure fibroin and SF/HA materials, both films and sponges. Results are reported in figure 3.9 and 3.10 respectively.

Uncross-linked SF/HA films showed no differences in the tensile Young's modulus when compared to the pure SF film and regardless the initial content of hyaluronic acid. The cross-linking reaction determined a significant increase of rigidity in all materials but the HA5gen film. Moreover, the Young's modulus of the cross-linked film with 5%  $w_{\text{HA}}/w_{\text{SF}}$  was significantly lower than the moduli of the cross-linked films at different HA content. Results are consistent with the previous findings about  $M_c$ : at higher hyaluronic acid content, the cross-linking degree is lower and therefore the material is less rigid.

Water content measurements for the uncross-linked films showed a significant increase in the material with 5%  $w_{\text{HA}}/w_{\text{SF}}$ , due to its higher hydrophilicity shown by the contact angle measurements. In the cross-linked materials, there were no significant differences among the water contents of the SF/HA films and the pure SF control material. This may be due to the lower decrease of static contact angle in the SF/HA cross-linked films than in the unmodified films; this was determined by the prevention of the separation between silk fibroin and HA, as shown above. In the SF/HA sponges, the addition of hyaluronic acid induced a significant decrease of water content either with or without cross-linking by genipin. In particular, in the cross-linked materials the reduction was greater at higher HA content.

In general, a decrease in water content of a sponge can be induced by an increase of material rigidity, a decrease of material hydrophilicity and a decrease of the porosity of the sponge structure. Since the porosity of our scaffolds is more than 80%, porosity can be considered the most affecting property to determine the water uptake of the scaffolds. Moreover, water can be entrapped in pores or absorbed by pore walls; in the first case, a decrease in pore volume due to HA addition could determine water uptake results, but no changes in

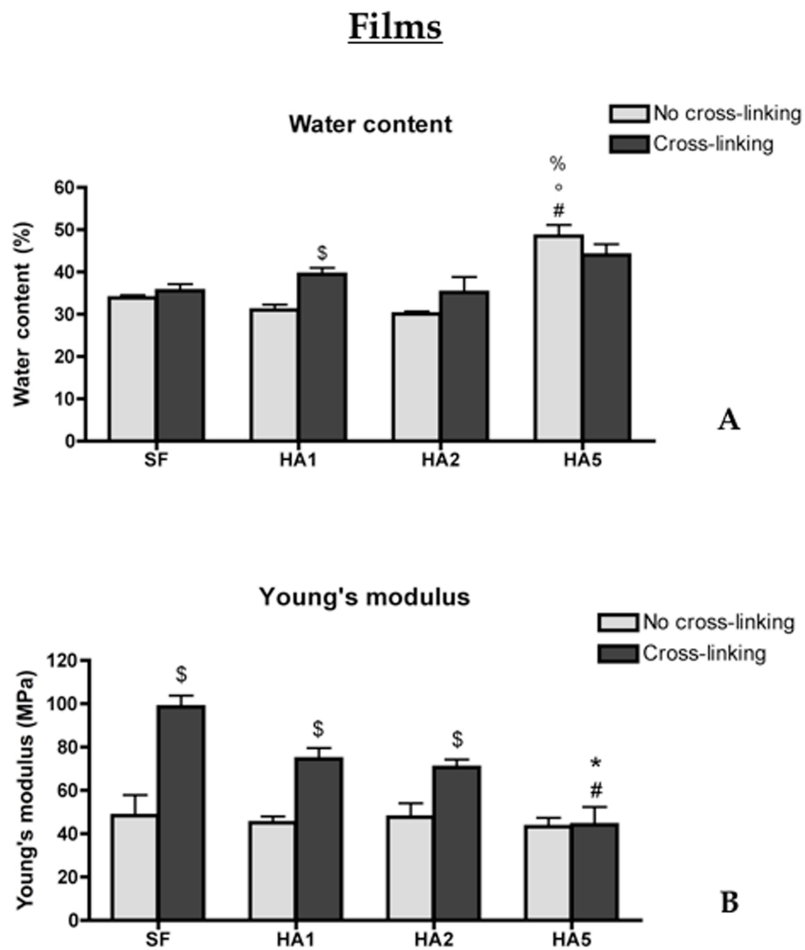


Figure 3.9: Water content (A) and Young's moduli (B) of the uncross-linked and cross-linked SF/HA films with 1%  $w_{\text{HA}}/w_{\text{SF}}$ , 2%  $w_{\text{HA}}/w_{\text{SF}}$  and 5%  $w_{\text{HA}}/w_{\text{SF}}$  compared to the materials without hyaluronic acid (SF). \$  $p < 0.05$  vs corresponding uncross-linked material, #  $p < 0.05$  vs corresponding control, °  $p < 0.05$  vs HA1, %  $p < 0.05$  vs HA2, \*  $p < 0.05$  vs HA1gen, &  $p < 0.05$  vs HA2gen.

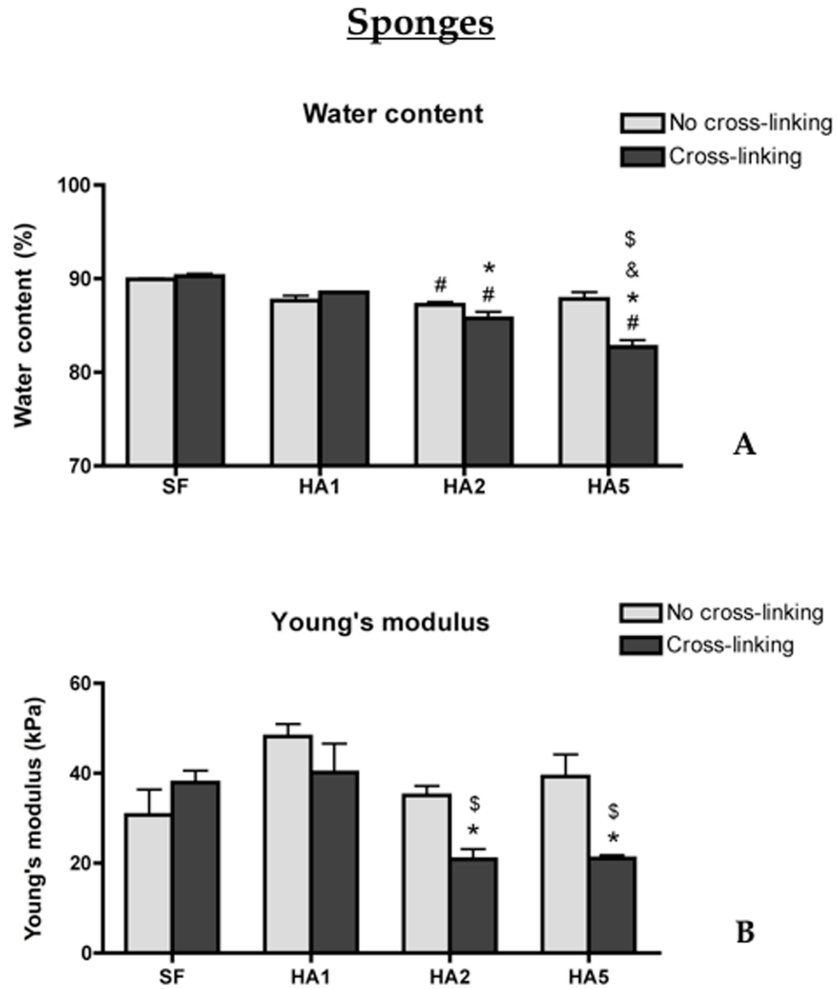


Figure 3.10: Water content (A) and Young's moduli (B) of the uncross-linked and cross-linked SF/HA sponges with 1%  $w_{HA}/w_{SF}$ , 2%  $w_{HA}/w_{SF}$  and 5%  $w_{HA}/w_{SF}$  compared to the materials without hyaluronic acid (SF). \$  $p < 0.05$  vs corresponding uncross-linked material, #  $p < 0.05$  vs corresponding control, °  $p < 0.05$  vs HA1, %  $p < 0.05$  vs HA2, \*  $p < 0.05$  vs HA1gen, &  $p < 0.05$  vs HA2gen.

porosity were detected in SF/HA sponges using hexane porosimetry; it has to be noticed that, however, porosity was measured on a dry sample. When soaked in water, the sponge can swell and expand and therefore pore volume increases; this increment may be lower after hyaluronic acid addition, because pore walls may be unable to expand as much as in the case of a pure silk fibroin sponge. This lack of expansion may be determined by several factors, such as different microporosity of the pore wall (due to partial HA remotion, for instance – see paragraph 3.3.7) or local inhomogeneity of the material; moreover, the higher crystallinity of silk fibroin caused by the presence of HA molecules could also explain this phenomenon.

Mechanical properties were also influenced by scaffold porosity: compressive Young's moduli of unmodified SF/HA sponges showed no significant differences regardless hyaluronic acid content and when compared to the pure SF control scaffold. In the cross-linked sponges with 2% and 5%  $w_{\text{HA}}/w_{\text{SF}}$ , cross-linking determined a significant decrease of the elastic modulus, which was also significantly lower than the modulus of the cross-linked pure fibroin sponge. That means that the contribution of porosity in the wet state at higher concentration of HA was more important than the increase of rigidity induced by the cross-linking reaction, which moreover involved about 30% of the amino groups in the scaffolds.

### 3.3.7 Hyaluronic acid mapping and quantification

To qualitatively evaluate the hyaluronic acid distribution in the scaffolds, fluorescein-hyaluronan was used to prepare SF/HA sponges, which were observed with a confocal laser microscope. The same sponges were digested in a Proteinase K solution to dissolve fibroin and induce the release of the fluorescent HA present in the scaffolds. The resulting fluorescence was measured to evaluate the percentage of fHA with respect to the total weight of fibroin. Results are shown in figure 3.11.

Images showed that a remarkable amount of hyaluronic acid was present in each sponge with or without the cross-linking by genipin. In the cross-linked

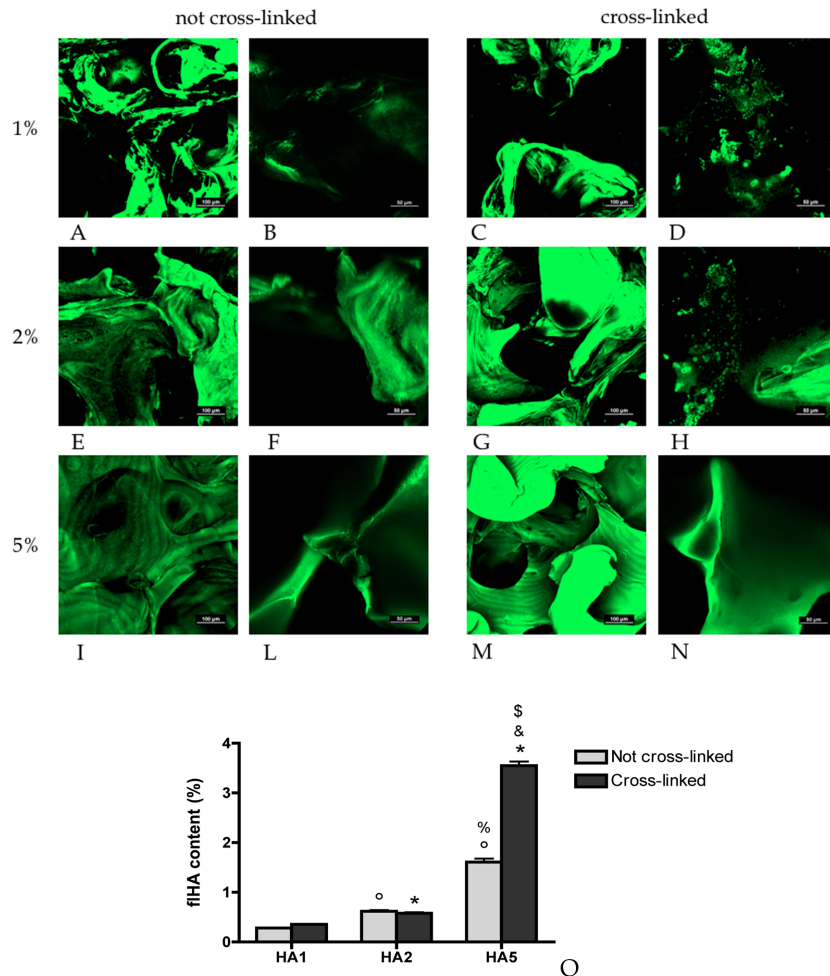


Figure 3.11: Confocal images of the SF/HA sponges produced with fluorescent hyaluronan with 1%  $w_{\text{HA}}/w_{\text{SF}}$  not cross-linked (A, B) and cross-linked (C, D), 2%  $w_{\text{HA}}/w_{\text{SF}}$  not cross-linked (E, F) and cross-linked (G, H) and 5%  $w_{\text{HA}}/w_{\text{SF}}$  not cross-linked (I, L) and cross-linked (M, N). For each scaffold, the first image is the result of a stuck in the range of 300-400  $\mu\text{m}$ ; the second image shows a detail of the surface of the pores. In O, the percentage of fluorescent hyaluronic acid in the SF/HA sponges with respect to the total weight of fibroin is reported.

sponges at lower HA contents, a dot-like distribution of HA could be noticed: small islands of hyaluronic acid became visible on the pore walls, indicating the formation of a more interpenetrating network, as confirmed by optical images and contact angle measurements. At 5%  $w_{\text{HA}}/w_{\text{SF}}$  fluorescence is instead more uniform. This may be due to the increase of the fluorescent signal caused by the higher HA concentration in the sponge: the instrument may lose the ability of resolving each island, which may also become bigger.

Quantitatively speaking, an incorporation efficiency of about 30% was observed for all materials at 1% and 2%  $w_{\text{HA}}/w_{\text{SF}}$  and uncross-linked sponges at 5%  $w_{\text{HA}}/w_{\text{SF}}$ . This may suggest that there is a molecular interaction between fibroin and hyaluronic acid, as reported in M. Garcia-Fuentes et al. [93], which prevented the release of the water-soluble HA during the NaCl removal in the scaffold production. This interaction may therefore entrap the hyaluronan molecules inside the silk fibroin matrix. The cross-linking significantly improved HA retention only at the highest initial concentration of 5%  $w_{\text{HA}}/w_{\text{SF}}$ , leading to an efficiency of about 70%. This may happen because, as previously mentioned, cross-linking degree is independent of hyaluronic content. Thus, only at higher HA content hyaluronic acid molecule aggregates may be large enough to be entrapped in the cross-linked mesh. In addition, at higher concentrations it is more likely that hyaluronic acid participates in the cross-linking reaction with genipin, improving its retention.

### 3.4 Conclusions

In this study, blends of silk fibroin and hyaluronic acid were used to produce 3D scaffolds combining their promising properties for cartilage tissue engineering, such as versatility, biocompatibility and the reported ability of hyaluronic acid to help the maintenance of the chondral phenotype. Different matrices were produced using the salt leaching technique to obtain sponges with a high interconnected porosity as required for a scaffold to regenerate cartilage. Several HA concentrations and cross-linking with genipin were employed to

evaluate how scaffold properties could be modulated.

Hyaluronan was successfully added in the fibroin sponges, with different distributions in the unmodified and in the cross-linked materials: in fact, the highly hydrophilic HA showed to act as sericin during the spinning process, causing fibroin segregation and  $\beta$ -sheet formation during scaffold making. SF separation is instead prevented by the cross-linking process, which determined the formation of a more interconnected network between the two material components. The presence of hyaluronic acid also affected silk fibroin crystallinity and when combined to NaCl, had a synergistic effect to decrease the cross-linking degree of the scaffolds when compared to the pure fibroin cross-linked sponge. Water uptake and mechanical properties were mostly modulated by scaffold porosity and additional factors such as microporosity of the pore wall, local different crystallinity of silk fibroin and inhomogeneity of the material.

Biological properties of the SF/HA sponges were also evaluated to understand how cellular response is influenced by different scaffold properties, that is HA content and cross-linking. Results will be presented in the following chapter.

## Chapter 4

# Modulation of chondrocyte response on silk fibroin/hyaluronic acid scaffolds

### 4.1 Introduction

The previous chapter described one of the two strategies explored to produce the chondral phase of a multicomponent scaffold for osteochondral tissue engineering, i.e. the conjugation of silk fibroin and hyaluronic acid. Our aim was to combine the ability of HA to improve the maintenance of chondrocyte phenotype and new ECM deposition *in vitro*, to the excellent biocompatibility and versatility of silk fibroin for cartilage tissue engineering applications (paragraph 3.1).

As mentioned before, one of the main objectives of this research work was to improve both components of the best tissue engineered system for cartilage regeneration tested in [83], i.e. cells (chondrocytes) and scaffold (pure SF salt-leached sponges). Therefore, after the assessment of the chondrogenic potential of adipose-derived stem cells on SF scaffolds both *in vitro* and *in vivo* (chapter 2), we modified the silk fibroin scaffold with the addition of HA.

Different HA concentrations and cross-linking with genipin were combined to the salt leaching technique to modulate scaffold characteristics, such as HA content and distribution, silk fibroin crystallinity, wettability and mechanical properties. SF/HA scaffolds at 1%, 2% and 5%  $w_{\text{HA}}/w_{\text{SF}}$  with or without cross-linking were systematically characterized and results were reported in chapter 3.

The evaluation of the biological properties of SF/HA scaffolds will be presented in this chapter. First, the effect of hyaluronic acid dissolved in media on primary rat chondrocytes cultured on pure SF scaffolds was evaluated using the best culture parameters developed in [83], to verify if and how HA can affect the chondrogenic phenotype of cartilage cells. Then, chondrocytes were cultured *in vitro* on SF/HA scaffolds, in order to assess how scaffold properties could modulate cell responses in terms of cartilage cell phenotype enhancement and new ECM deposition, with respect to the pure fibroin sponges or when a HA-enriched medium was used. To this purpose, cell seeding efficiency, proliferation, sulfated GAG deposition and compressive mechanical properties were measured during two weeks of culture. The phenotype of chondrocytes was analyzed in terms of chondrogenic gene expression and alkaline phosphatase (ALP) activity, as a further indication of cell hypertrophy. The stability of SF/HA scaffolds in culture medium was also assessed, quantifying the loss of hyaluronic acid in two weeks to evaluate eventual modifications of the environment (both scaffold material and culture medium) experienced by cells.

Finally, it has to be mentioned that the use of chondrocytes to characterize SF/HA scaffold biological properties was a necessary step to verify the potential of SF/HA scaffolds for cartilage regeneration and the best material parameters to induce a significative improvement. In the future, the scaffold which elicited the best responses in chondrocytes in terms of phenotype enhancement and higher ECM deposition will be selected and employed with ASCs to evaluate if the addition of HA could enhance chondrogenesis on SF-based scaffolds.

## 4.2 Materials and methods

This study was conducted in collaboration with Dr. Barbara D. Boyan's laboratory at the Parker H. Petit Institute of Bioengineering and Bioscience, Georgia Institute of Technology (Atlanta, US).

### 4.2.1 Scaffold preparation

Silk fibroin/hyaluronic acid sponges were prepared according to the protocol reported in paragraph 3.2.1, starting from SF/HA aqueous solutions at 7-8% w/V of silk fibroin, 1%  $w_{HA}/w_{SF}$ , 2%  $w_{HA}/w_{SF}$  and 5%  $w_{HA}/w_{SF}$ , with and without cross-linking with genipin at 0.5% w/V (sample codes: HA1, HA2, HA5, HA1gen, HA2gen, HA5gen). Both unmodified and cross-linked pure fibroin sponges were used as controls (sample codes: SF, SFgen). SF sponges were also used to culture chondrocytes with hyaluronic acid dissolved in media.

Before seeding, sponges were soaked in water for 2 hours and cut into disks (6-mm diameter, 2-3-mm thickness) using a biopsy punch (Miltex, UK). Scaffolds in aqueous suspension were autoclaved at 121°C for 15 minutes for sterilization, then cooled down to room temperature and incubated overnight in culture media at 37°C, 5% CO<sub>2</sub>. Air bubbles inside sponges were removed using the vacuum system described previously (paragraph 2.2.1). After blotting dry, scaffolds were ready for seeding.

### 4.2.2 Hyaluronic acid loss of SF/HA scaffolds in culture medium

To evaluate the eventual loss of hyaluronic acid from the SF/HA scaffolds during culture, sponges were prepared using fluorescent HA as reported in paragraph 3.2.2.8. 6-mm disks of each sponge at all HA concentrations and with or without cross-linking were placed in 1 ml of culture medium at 37°C on a shaking platform. Sodium azide at 0.1% w/V was added to prevent contaminations. 150 µl of medium was removed and replaced with fresh medium on day 1 to 7, 10 and 14 and used to measure fluorescence with the spectrofluorimeter Tecan Infinite M200 Pro (excitation: 494 nm, emission: 521 nm). To

correlate fluorescence to the amount of hyaluronic acid, a calibration curve was set up using standard solutions of fluorescent HA at known concentrations in culture medium. Cumulative release was calculated using a correction to take into account sample dilution after the addition of fresh media. Total HA in the scaffolds was measured according to the protocol reported in paragraph 3.2.2.8 and then used to normalize the differential release.

### 4.2.3 Isolation and culture of resting zone chondrocytes

Chondrocytes were isolated from the resting zone of costochondral hyaline-like cartilage growth plate of 125 g Sprague-Dawley rats [129, 130]. After isolation, these cells can retain their *in vivo* phenotype through four passages in culture. Briefly, rib cages were removed from 8 animals and placed in DMEM. The resting zone cartilage was separated, cut and incubated overnight in DMEM with 10% FBS, 50  $\mu\text{g}/\text{ml}$  sodium ascorbate and 3% penicillin–streptomycin–fungizone in 5%  $\text{CO}_2$  at 37°C. After medium was replaced by two washes with HBSS, tissues were incubated in 1% trypsin for 1 hour and 0.02% collagenase for 3 hours. Cells were collected by filtration and subsequent centrifugation at 500 g for 10 minutes, then resuspended in DMEM.

Resting zone chondrocytes (RCs) were plated at a density of 25000 cells/ $\text{cm}^2$  and cultured in DMEM with 10% FBS, 1% penicillin–streptomycin–fungizone and 50  $\mu\text{g}/\text{ml}$  sodium ascorbate in 5%  $\text{CO}_2$  at 37°C. Third passage confluent cells were harvested for seeding on pure SF and SF/HA sponges.

### 4.2.4 Cell seeding and culture of scaffold/chondrocyte constructs

Scaffolds were placed in the center of each well in a 24-well plate with 200  $\mu\text{l}$  of culture medium to keep moisture during the following incubation. For seeding, 20  $\mu\text{l}$  with  $1 \times 10^6$  RCs at passage 4 were loaded in the sponges through pipetting. 4 hours after cell inoculation, 1.5 ml of medium were added to each well. 24 hours after seeding, samples were moved on a rocking platform at 15

rpm, as previously described in [83]. Media were changed every 48 hours until harvest. When cells were cultured on pure SF scaffolds with HA dissolved in media, solutions at 0, 0.1, 0.25, 0.5, 1 and 2  $\mu\text{g}/\text{ml}$  of HA were employed during culture.

#### 4.2.5 Cell seeding efficiency

To evaluate the number of cells effectively loaded in the SF/HA scaffolds, sponges were harvested 24 hours after seeding and washed in PBS. The constructs were then frozen at  $-20^{\circ}\text{C}$  for 1 day and lyophilized overnight. Subsequently, scaffolds were digested in a Proteinase K solution (Qiagen, US) at 1 mg/ml in PBE buffer (10 mM EDTA in PBS) at  $55^{\circ}\text{C}$  for 48 hours. DNA content was quantified using PicoGreen assay (Invitrogen corporation, US) according to manufacturer's instructions with lambda DNA as a standard. The number of cells on each scaffold was obtained assuming 7.7 pg DNA per cell [131]; then, cell seeding efficiency was calculated using the following formula:

$$\text{Cell seeding efficiency (\%)} = \frac{\text{incorporated cell number}}{\text{initial cell seeding number}} \times 100$$

#### 4.2.6 Cell proliferation

The proliferation of chondrocytes on pure SF and SF/HA scaffolds was assessed on day 1, 7 and 14 after seeding using an alamarBlue<sup>®</sup> assay (AbD Serotec, US) as described previously (paragraph 2.2.6).

#### 4.2.7 Real time PCR analysis

After 14 days of culture, chondrocyte/scaffold constructs were harvested, washed in PBS and subjected to RNA isolation as illustrated in paragraph 2.2.7. RNA was reverse-transcribed into cDNA for the subsequent real time PCR analysis to measure the expression of Sox9, collagen 2a1, aggrecan, Comp, collagen 1a1, collagen 10a1 and ALP. RPS18 was used for normalization. To

this purpose, specific primers were employed, as mentioned earlier (paragraph 2.2.7).

#### 4.2.8 Alkaline phosphatase activity

As an indication of chondrocyte hypertrophy, cellular alkaline phosphatase-specific activity (E.C. 3.1.3.1) was evaluated. On day 14 after seeding, scaffolds were washed in PBS and store at -20°C in 0.05% Triton-X in PBS until measurement. Before the assay, samples were thawed, sonicated for a few seconds to cause cell membrane disruption and the resulting solutions were employed for the test. ALP activity was assessed from the release of p-nitrophenol from p-nitrophenylphosphate as described in [132]. Values were normalized to the protein content of scaffold/chondrocyte constructs, which was measured using a colorimetric detection at 570 nm of cuprous cations in a biuret reaction (BCA Protein Assay Kit, Pierce Biotechnology, US).

#### 4.2.9 Compressive mechanical properties

Compressive Young's modulus of scaffold/RCS constructs was measured after 14 days of culture. Empty scaffolds maintained in the same culture conditions were used as negative control. After washing in PBS for 10 minutes, compression tests were performed as described in paragraph 2.2.8 using a 25 N load cell in uniaxial ramp condition at a strain rate of 0.1 mm/sec.

#### 4.2.10 Sulfated glycosaminoglycan production

Scaffold/RCS constructs were harvested after 14 days of culture and subjected to mechanical testing. Then, after samples were digested in a Proteinase K solution at 1 mg/ml in PBE buffer, GAG content was measured using DMMB dye and normalized to DNA amount, as described in paragraph 2.2.9.

#### 4.2.11 Statistical analysis

All biological tests were performed on  $N = 6$  samples at each time point, while HA release analysis was carried out on  $N = 3$  specimens. Data were expressed as mean  $\pm$  standard error of the mean and analyzed using GraphPad Prism 5.0 (GraphPad Software). To determine the statistical significance of differences among the results before and after cross-linking or at different hyaluronic acid contents, two-way or one-way ANOVA test was performed after the equality of variances was assessed. Significance was assigned at p-values  $< 0.05$ .

### 4.3 Results and discussion

#### 4.3.1 Hyaluronic acid loss from SF/HA scaffolds in culture medium

The loss of hyaluronic acid from SF/HA sponges in culture medium was evaluated for two weeks, in order to assess eventual modifications of the materials and the environment experienced by chondrocytes during culture. Results are reported in figure 4.1: in (a), the cumulative release of hyaluronic acid is shown as the percentage of HA with respect to total HA in each scaffold, measured as reported in paragraph 3.2.2.8; in (b) and (c) instead, the differential release is presented after normalization to scaffold weight, starting from day 1 and day 2 respectively.

Cross-linked and unmodified materials showed different kinetics of HA loss in culture medium. Samples without genipin lost a significant amount of hyaluronic acid only on day 1, the more, the higher the initial HA content; moreover, in the cumulative loss perspective, uncross-linked sponges presented a constant trend over time after the first day. Cross-linked SF/HA materials, instead, exhibited a delayed loss of HA until day 4; for the scaffolds at 2% and 5%  $w_{\text{HA}}/w_{\text{SF}}$ , a significant amount of hyaluronic acid in culture medium was lost at each time point: on the first day, HA loss was 0.5 and 1.3  $\mu\text{g}$  of HA

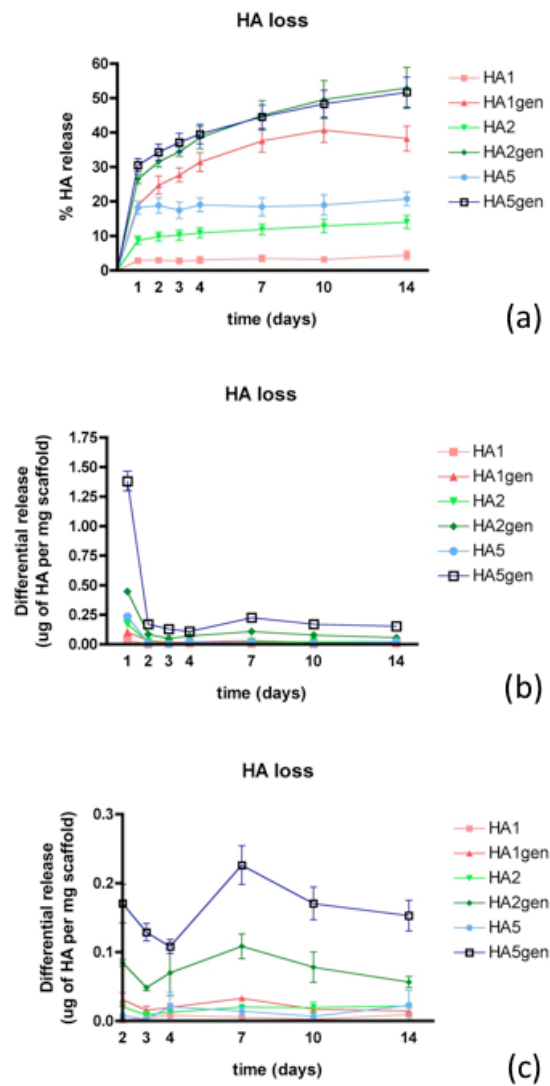


Figure 4.1: Hyaluronic acid loss from SF/HA scaffolds in culture medium. (a) shows the cumulative release of hyaluronic acid as the percentage of HA with respect to total HA in each scaffold. In (b) and (c), the differential release is reported after normalization to scaffold weight, starting from day 1 and day 2 respectively.

per mg of scaffold, respectively; after day 1, hyaluronic acid was released in culture medium in the range of 0.1-0.2  $\mu\text{g}$  of HA per mg of scaffold. It has to be noticed that for these two samples the increase of HA concentration from day 4 to day 7 is due to the longer time elapsed between measurements, while the decrease from day 7 indicated a slowdown in the release process.

On the basis of these considerations, we can observe that cross-linking with genipin induced a longer retention of hyaluronic acid inside SF/HA scaffolds, slowing the release process. This means that during the washing steps of scaffold preparation, hyaluronic acid is lost more easily by the uncross-linked sponges, where HA is entrapped thanks to the only interaction with SF (paragraph 3.3.7). On the contrary, the more interconnected networks of cross-linked SF/HA materials determined a more efficient retention of HA inside scaffolds, which made its loss slower. In addition, the higher amount of HA in the scaffold, the higher HA is lost in culture media.

When chondrocytes were cultured on SF/HA scaffolds, media were changed every two days. Therefore, only in the case of cross-linked sponges at higher HA content, cells could experience the presence of HA in culture medium for two weeks in an approximate concentration range of 0.5 - 1  $\mu\text{g}/\text{ml}$ , calculated from the average weight of SF/HA scaffolds during culture and the volume of media used. Instead, unmodified materials did not change during culture after day 1 and no hyaluronic acid was dissolved in medium.

#### **4.3.2 Effect of HA-enriched medium on chondrocyte/SF constructs**

Rat chondrocytes were cultured on pure SF scaffolds in a HA-enriched culture medium for two weeks to evaluate how hyaluronic acid can affect cartilage cell response. The aim of this experiment was to assess if and how HA can modulate chondrocyte behavior when dissolved in media, then to compare these results with those obtained using SF/HA sponges, also in light of the results about HA loss during culture. To this purpose, chondrocyte/SF scaffold constructs were cultured with 0, 0.1, 0.25, 0.5, 1 and 2  $\mu\text{g}/\text{ml}$  of HA; chondrogenic

gene expression, sulfated GAG content and Young's modulus were evaluated after 14 days of culture on a rocking platform.

Results from real time PCR analysis are shown in figure 4.2. It is evident that hyaluronic acid determined a significant dose-dependent increase of the expression of Sox9, collagen type II and collagen type X; on the contrary, its effect was limited on Comp and aggrecan expressions. 1  $\mu\text{g/ml}$  of HA elicited the best response in terms of chondrogenic expression enhancement with also a significant decrease in collagen type I expression, while a concentration of 2  $\mu\text{g/ml}$  caused a drop back to the values of expression obtained without hyaluronic acid dissolved in media.

The highest HA concentration determined also a significant decrease in DNA content on chondrocyte/SF constructs, indicating a possible toxicity to cells. Besides at 2  $\mu\text{g/ml}$ , hyaluronic acid had no effect on GAG deposition on scaffolds and did not cause an improvement of chondrocyte/SF construct compressive mechanical properties at all concentrations (figure 4.3 and figure 4.4, respectively). However, the increase of GAG/DNA ratio when 2  $\mu\text{g/ml}$  of HA was used, was probably determined by a loss of DNA from SF scaffolds, due to cell death.

This preliminary study about the effect of HA on chondrocytes cultured on SF scaffolds showed that hyaluronic acid mainly affected chondrogenic gene expression, causing a dose-dependent increase of selected genes, such as collagen type II and Sox9, accompanied by an increase of collagen type X expression but also a significant decrease in collagen type I expression, typical markers of chondrocyte hypertrophy and dedifferentiation, respectively. Therefore, hyaluronic acid can effectively modulate the expression of chondrocytes, enhancing chondrogenic expression at appropriate concentrations. However, further investigations may be necessary to better describe HA effect on chondrocyte expression, for instance analyzing additional hypertrophic markers, such as ALP and Runx2, or prolonging the culture time.

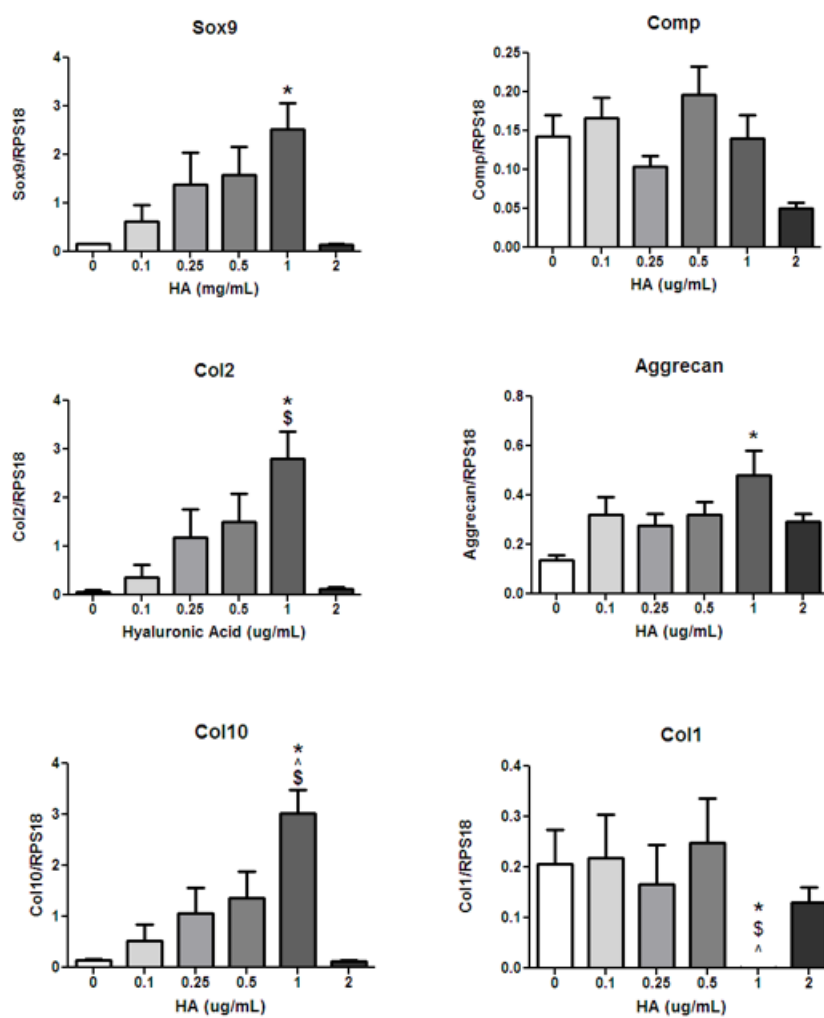


Figure 4.2: Chondrogenic gene expression of chondrocytes cultured for two weeks on pure SF scaffolds with HA-enriched media at different HA concentrations. \*  $p < 0.05$  vs 0  $\mu\text{g/ml}$  of HA, \$  $p < 0.05$  vs 0.1  $\mu\text{g/ml}$  of HA, ^  $p < 0.05$  vs 0.25  $\mu\text{g/ml}$  of HA.

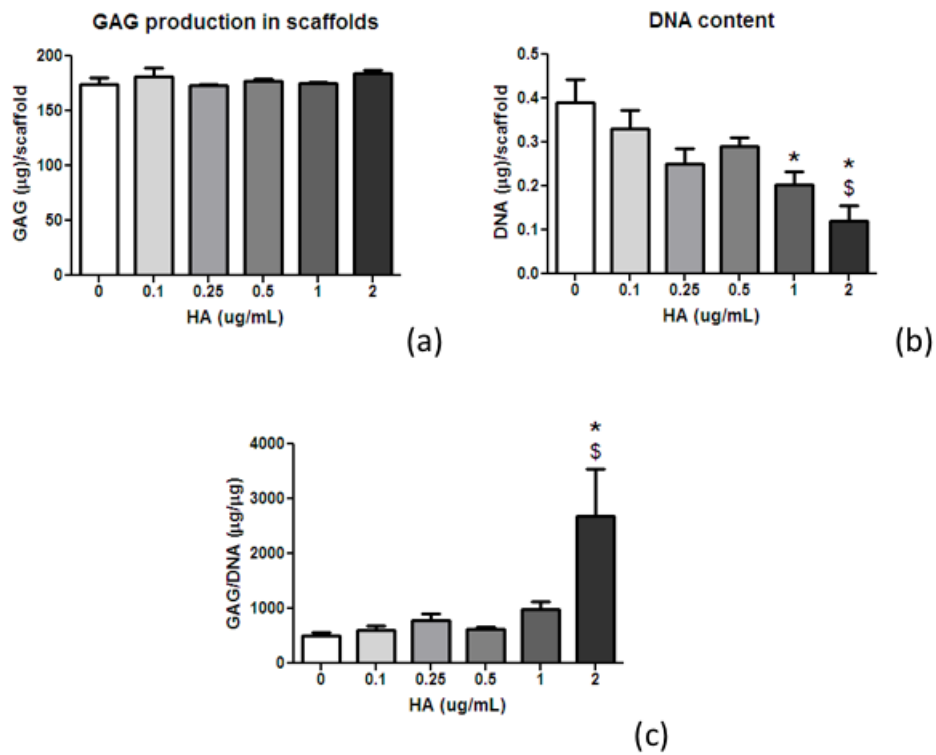


Figure 4.3: GAG and DNA content (a and b, respectively) of chondrocyte/SF constructs cultured for two weeks with medium at different HA concentrations. In (c), the GAG/DNA ratio is presented. \*  $p < 0.05$  vs 0  $\mu\text{g/mL}$  of HA, \$  $p < 0.05$  vs 0.1  $\mu\text{g/mL}$  of HA.

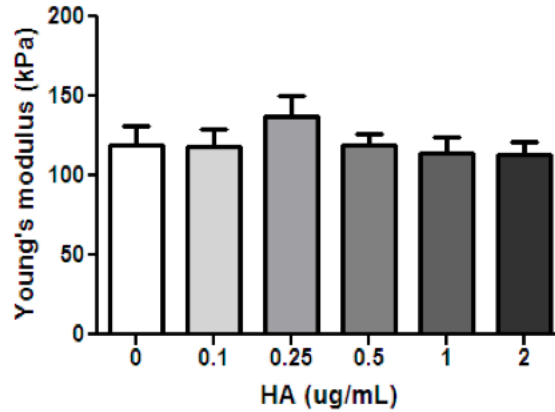


Figure 4.4: Compressive Young's modulus of chondrocyte/SF constructs cultured for two weeks with HA-enriched medium at different HA concentrations.

### 4.3.3 Cell seeding efficiency and proliferation

Cell seeding efficiency was evaluated measuring the number of chondrocytes effectively loaded on SF/HA scaffolds after 24 hours and results were compared with respect to pure SF sponges (figure 4.5). A significantly higher amount of chondrocytes was loaded on cross-linked materials regardless HA content and on the unmodified sponge at 5%  $w_{HA}/w_{SF}$ . This may indicate a better attachment of chondrocytes at higher content of HA; moreover, the more uniform distribution of hyaluronic acid in the SF/HA scaffolds with genipin (paragraph 3.3.5) may enhance this effect also at lower HA concentrations.

Cell proliferation was monitored on SF/HA and pure SF scaffolds with and without cross-linking on day 1, 7 and 14 of culture. Results are shown in figure 4.6, where fluorescence is proportional to the number of viable cells on the samples. Chondrocytes proliferated significantly during two weeks on all SF/HA and pure SF scaffolds. Even if, on day 1, cell proliferation was significantly lower on the cross-linked materials at 2% and 5%  $w_{HA}/w_{SF}$  with respect to control without HA, no big differences were noticed after two weeks

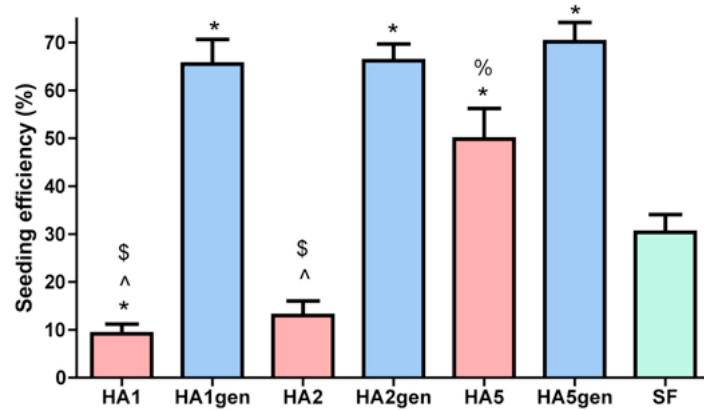


Figure 4.5: Seeding efficiency of chondrocytes on SF/HA sponges with and without cross-linking with genipin, expressed as the percentage of cells effectively loaded on scaffolds 24 hours after seeding. Pure SF sponges were used as negative control. \*  $p < 0.05$  vs SF, ^  $p < 0.05$  vs corresponding cross-linked sponge, \$  $p < 0.05$  vs HA5, %  $p < 0.05$  vs HA5gen.

of culture. This indicated that all SF/HA materials were able to sustain chondrocyte growth *in vitro*.

#### 4.3.4 Chondrogenic phenotype analysis

The phenotype of chondrocytes was analyzed after 14 days of culture on pure SF and SF/HA scaffolds, to evaluate how it was affected by the presence of hyaluronic acid in the sponges and the cross-linking. To this purpose, the expression of typical chondrogenic genes was measured and, as an additional information about chondrocyte hypertrophy, alkaline phosphatase activity was assessed. The results of real time PCR measurements are shown in figure 4.7 and 4.8; data are presented after normalization to pure SF materials with or without cross-linking, used as a control.

Hyaluronic acid did not influence the expression of Sox9 and collagen type I, regardless HA concentration or cross-linking with genipin. Scaffolds at 1%

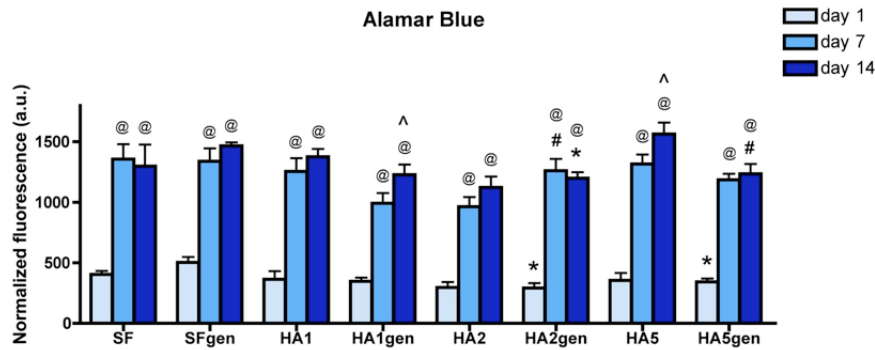


Figure 4.6: Proliferation of chondrocytes on SF/HA and pure SF scaffolds with and without cross-linking with genipin on day 1, 7 and 14 of culture. Fluorescence is proportional to the number of viable cells on the samples. @  $p < 0.05$  vs day 1, ^  $p < 0.05$  vs day 7, \*  $p < 0.05$  vs control w/o HA, #  $p < 0.05$  vs corresponding sponge w/o cross-linking.

$w_{HA}/w_{SF}$  had a slightly negative influence on chondrocyte phenotype, inducing an increase of ALP expression in case of uncross-linked materials and a decrease of collagen type II, aggrecan and Comp expression when genipin was added. Unmodified 2%  $w_{HA}/w_{SF}$  sponges did not affect gene expression when compared to pure SF materials, while cross-linking with genipin induced a decrease in the ratio of collagen type II/collagen type I, which is a typical index for chondrocyte differentiation; in addition, ALP expression was increased when chondrocytes were cultured on cross-linked HA2 scaffolds. The best outcomes in terms of chondrocyte phenotype enhancement were obtained with SF/HA scaffolds at 5%  $w_{HA}/w_{SF}$ , both with and without cross-linking. For the unmodified materials, an increase of collagen type II and aggrecan expression was observed, even if accompanied by a higher expression of collagen type X which was not statistically significant, though. The combination of the highest HA content and cross-linking with genipin determined the highest increase of collagen type II expression, which led to the greatest collagen II/collagen I

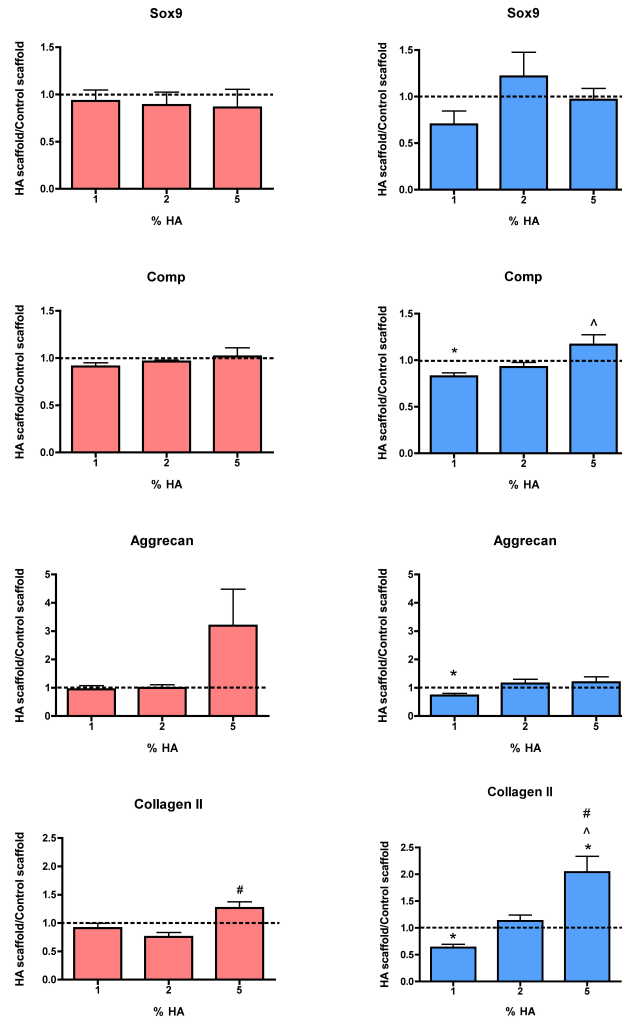


Figure 4.7: Chondrogenic gene expression of chondrocytes on SF/HA scaffolds after 14 days of culture on a rocking platform (red: uncross-linked SF/HA scaffolds; blue: cross-linked SF/HA scaffolds). Data are presented after normalization to the expression obtained after culture on pure SF materials, used as a control. \*  $p < 0.05$  vs control w/o HA, ^  $p < 0.05$  vs HA1, #  $p < 0.05$  vs HA2.

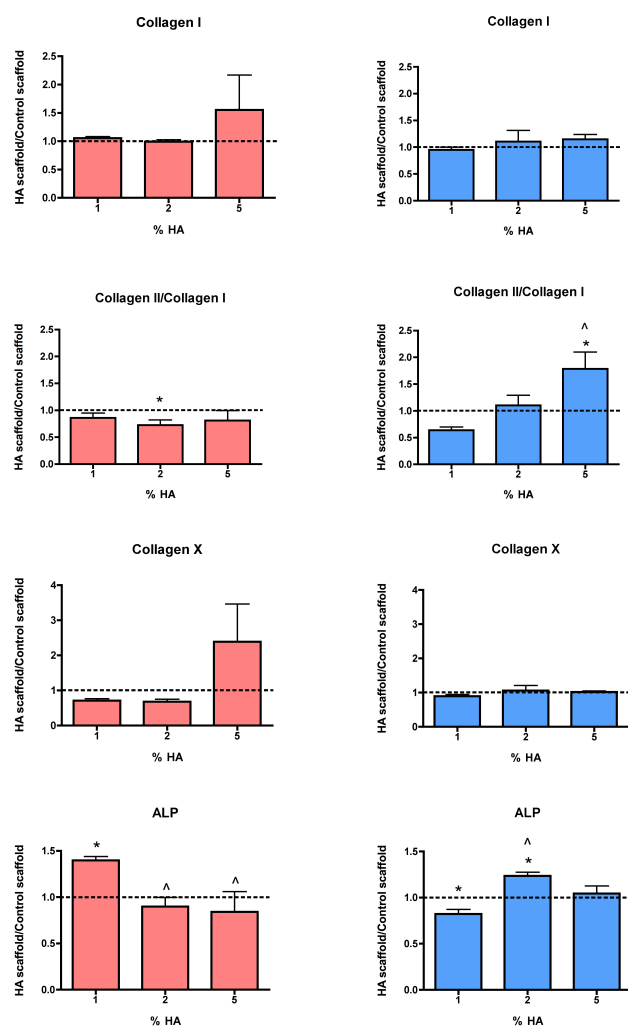


Figure 4.8: Chondrogenic gene expression of chondrocytes on SF/HA scaffolds after 14 days of culture on a rocking platform (red: uncross-linked SF/HA scaffolds; blue: cross-linked SF/HA scaffolds). Data are presented after normalization to the expression obtained after culture on pure SF materials, used as a control. \*  $p < 0.05$  vs control w/o HA, ^  $p < 0.05$  vs HA1, #  $p < 0.05$  vs HA2.

ratio. This reflected the beneficial effects of the highest amount of hyaluronic acid in contact with cells, both on the scaffolds and in the culture medium, being also in agreement with the previous results obtained when HA was dissolved in media. It has to be noticed, however, that cross-linking with genipin induced an increase of ALP activity when 2% and 5%  $w_{\text{HA}}/w_{\text{SF}}$  scaffolds were used to culture chondrocytes (figure 4.9).

In light of the results presented here, chondrogenic gene expression was enhanced when chondrocytes were cultured on SF/HA scaffolds at 5%  $w_{\text{HA}}/w_{\text{SF}}$ . Cross-linked sponges determined different responses by chondrocytes with respect to unmodified materials, in terms of ALP activity and the expression of collagen type II, collagen type X and aggrecan. Interestingly, a recent study [133] showed that genipin dissolved in culture medium at a concentration of 0.01% could influence articular chondrocyte gene expression, increasing collagen type II expression and decreasing Comp expression. However, no other genes were analyzed and it is difficult to estimate the real amount of genipin effectively employed for cross-linking, since it is added in excess to SF/HA solutions and then washed away after fibroin gelation. Therefore, supplemental investigations are needed to evaluate what determined different responses on cross-linked materials. In addition, results may indicate a potential influence of HA distribution or presence in culture medium on cell behavior, which needs to be further studied.

#### 4.3.5 GAG production and mechanical properties of chondrocyte/scaffold constructs

The content of GAG in the SF/HA scaffolds was measured after 14 days of culture with chondrocytes, to evaluate the deposition of new cartilage ECM. Results were normalized to the DNA content of the chondrocyte/scaffold constructs and are presented in figure 4.11 after normalization to the GAG/DNA ratio obtained from pure SF materials with or without cross-linking, used as a control.

An increase of GAG deposition was observed in all cross-linked SF/HA

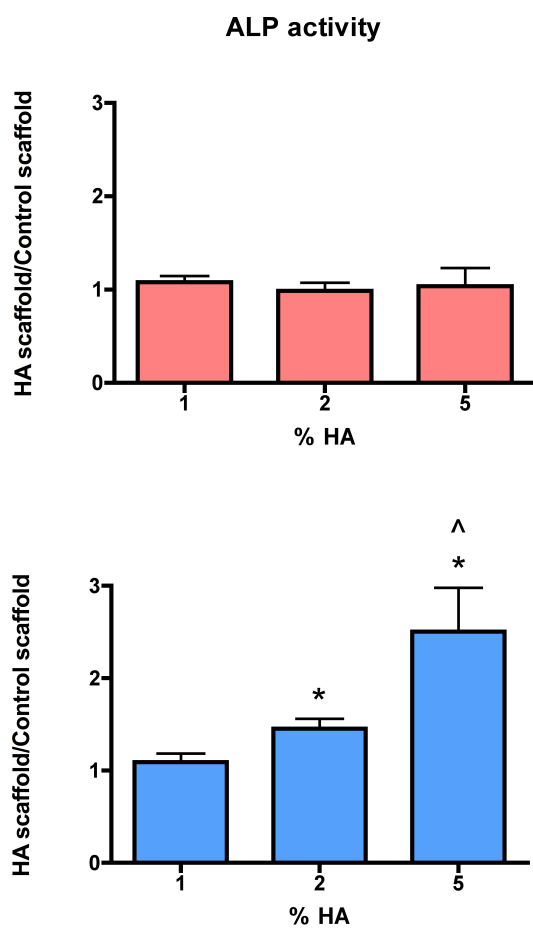


Figure 4.9: Alkaline phosphatase activity measured on chondrocyte/scaffold constructs after 14 days of culture (red: uncross-linked SF/HA scaffolds; blue: cross-linked SF/HA scaffolds). Data are presented after normalization to the ALP activity obtained from chondrocytes cultured on pure SF materials, used as a control. \*  $p < 0.05$  vs control w/o HA, ^  $p < 0.05$  vs HA1.

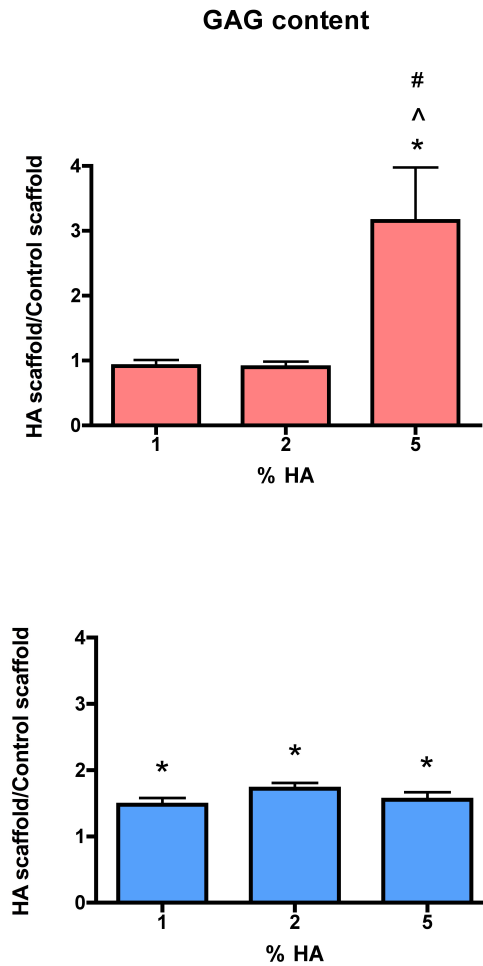


Figure 4.10: GAG/DNA ratio measured on SF/HA scaffolds after 14 days of culture with chondrocytes (red: uncross-linked SF/HA scaffolds; blue: cross-linked SF/HA scaffolds). Data are presented after normalization to the GAG/DNA ratio obtained from chondrocytes cultured on pure SF materials, used as a control. \*  $p < 0.05$  vs control w/o HA, ^  $p < 0.05$  vs HA1, #  $p < 0.05$  vs HA2.

sponges with respect to pure SF material, regardless the concentration of hyaluronic acid. Instead, unmodified SF/HA scaffolds at 5%  $w_{\text{HA}}/w_{\text{SF}}$  induced the greatest production of GAG (3 times higher than negative control), in agreement with the results obtained for chondrocyte gene expression. This corresponded also to the highest increase of compressive Young's modulus of SF/HA scaffolds after two weeks of culture, as shown in figure 4.11. Here, the ratios between the Young's moduli before and after culture are presented for all pure SF and SF/HA scaffolds. In figure 4.12, the correspondent absolute values for cultured scaffolds are reported. A slight decrease of compressive mechanical properties in the case of cross-linked SF/HA sponges at 1%  $w_{\text{HA}}/w_{\text{SF}}$  was also observed, suggesting that GAG deposition may not be sufficient to cause an improvement of Young's modulus for the scaffolds at this HA concentration.

## 4.4 Conclusions

In this study, the biological properties of silk fibroin/hyaluronic acid scaffolds were evaluated: rat chondrocytes were cultured for two weeks on SF/HA sponges at 1%, 2% and 5%  $w_{\text{HA}}/w_{\text{SF}}$  with and without cross-linking with genipin under dynamic culture conditions, as previously reported in [83]. Cell response in terms of enhancement of chondrogenic phenotype and new ECM deposition was assessed and compared to pure unmodified and cross-linked SF materials. In addition, cartilage cells were cultured on silk fibroin scaffolds in HA-enriched media at different concentrations, to study the effect of free HA on chondrocytes and compare the results to those obtained when HA was immobilized on the scaffolds. This experiment was performed also to take into account the loss of hyaluronic acid that cross-linked SF/HA sponges experienced during 14 days in culture medium and to evaluate its effect on cartilage cells. In fact, cross-linking with genipin changed significantly the kinetics of HA loss in culture medium and, in the case of cross-linked sponges, a significant amount of HA (0.5 - 1  $\mu\text{g}/\text{ml}$ ) was released in media during culture.

Results demonstrated that scaffolds with the highest amount of hyaluronic

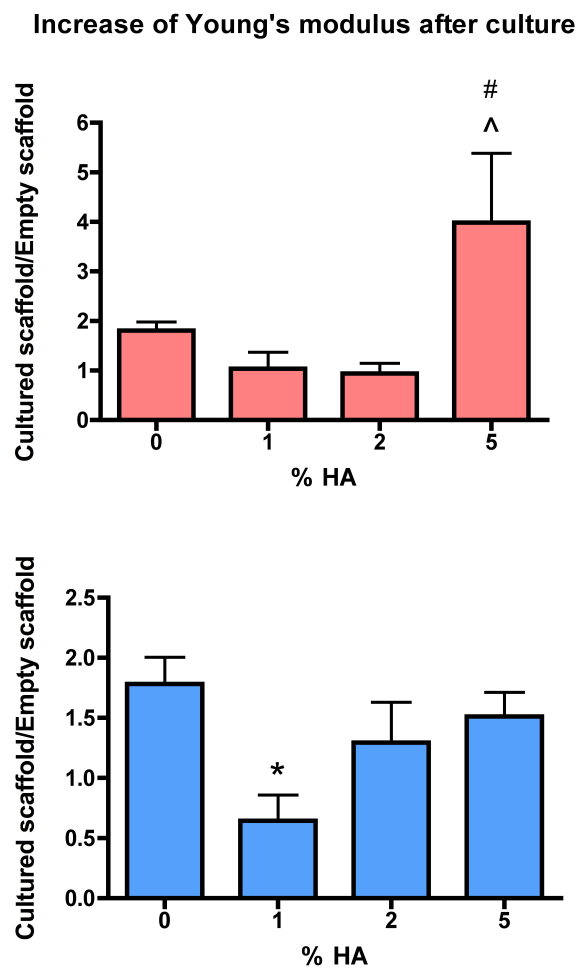


Figure 4.11: Ratios between compressive Young's moduli of pure SF and SF/HA scaffolds measured before and after 14 days of culture with chondrocytes (red: uncross-linked SF/HA scaffolds; blue: cross-linked SF/HA scaffolds). \*  $p < 0.05$  vs control w/o HA, ^  $p < 0.05$  vs HA1, #  $p < 0.05$  vs HA2.

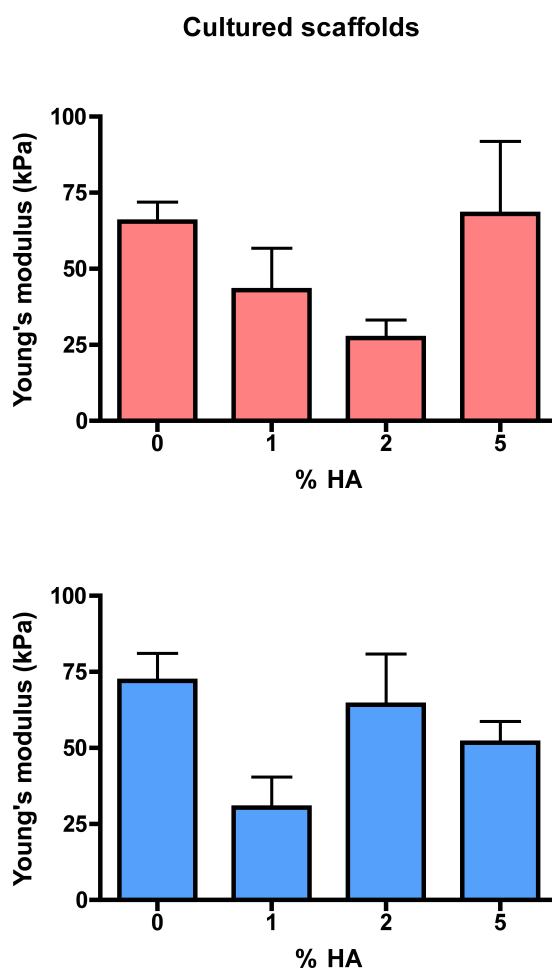


Figure 4.12: Compressive Young's moduli of pure SF and SF/HA scaffolds measured after two weeks of culture with chondrocytes (red: uncross-linked SF/HA scaffolds; blue: cross-linked SF/HA scaffolds). \*  $p < 0.05$  vs control w/o HA, ^  $p < 0.05$  vs HA1, #  $p < 0.05$  vs HA2.

acid both with and without genipin elicited the best responses in chondrocytes: unmodified sponges at 5%  $w_{\text{HA}}/w_{\text{SF}}$  induced the greatest deposition of sulfated GAG, which also caused the best improvement of compressive mechanical properties when compared to pure SF and SF/HA scaffolds at lower concentrations of HA; instead, cross-linked SF/HA sponges at 5%  $w_{\text{HA}}/w_{\text{SF}}$  determined the highest collagen type II expression and collagen type II/collagen type I ratio, indicating an enhancement of chondrocyte phenotype. Interestingly, these findings were in agreement to the results obtained when chondrocytes were cultured on pure SF scaffolds in media at different hyaluronic acid concentrations.

Therefore, we can hypothesize that the loss of HA from cross-linked sponges at 5%  $w_{\text{HA}}/w_{\text{SF}}$  may play a role in determining chondrocyte responses. However, further investigations are needed to describe the mechanisms underlying the different outcomes caused by cross-linking: for instance, chondrocytes may experience the different distribution of HA on the scaffolds and/or genipin may influence gene expression, as recently reported in literature. Thus, a more detailed study needs to be performed, analyzing the response of chondrocytes when cultured in an environment with genipin dissolved in medium. Moreover, prolonging culture times may give us additional information, in terms of cell response after the loss of HA eventually stops in cross-linked scaffolds at 5%  $w_{\text{HA}}/w_{\text{SF}}$ .

Finally, as previously mentioned, the scaffolds at 5%  $w_{\text{HA}}/w_{\text{SF}}$  will be also used in combination with adipose-derived stem cells, to evaluate their potential in improving chondrogenesis both *in vitro* and *in vivo*.

## Chapter 5

# Use of a nanometric net for the osteochondral interface regeneration: production, characterization and preliminary biological evaluation

### 5.1 Introduction

When a scaffold for osteochondral defect regeneration is designed, two main issues need to be addressed: first, the poor ability of cartilage to self-repair and the related difficulties in inducing the restoration of such a highly specialized tissue, both *in vitro* and *in vivo*; secondly, the achievement of a complete functionality of the interface between the subchondral and the chondral phases. In this perspective, scaffold properties have to be carefully tailored considering

the complexity of the osteochondral system which needs to be restored. The biomimetic approach has to be followed, aiming to reproduce the specific heterogeneity of the physiological environment. In light of these considerations, a scaffold for osteochondral regeneration needs not only to induce and sustain bone and cartilage repair, but also stimulate the establishment of a functional interfacial zone.

To these purposes, the physiological complexity has to be translated in a controlled heterogeneity of scaffold properties; several strategies have been recently adopted [33, 60, 61] and have already been described in paragraph 1.4.3. In this research work, we hypothesized that the restoration of the osteochondral interface can be achieved using a nanometric net to separate the chondral and subchondral phases of a multicomponent scaffold. In this way, besides mechanical stabilization, the beneficial dialogue among cells in bone and cartilage tissues can be ensured through the solute flow, allowed by the high porosity of the net. On the other hand, cell migration can be prevented by an appropriate pore diameter range, in order to avoid the unnatural presence of blood cells on the chondral side which may induce vascularization and subsequent mineralization of cartilage [59].

To produce a nanometric net with suitable properties, the electrospinning technique was employed, because it allows to fabricate scaffolds with a tunable fiber diameter and a limited dimension of pores. Poly-d,l-lactic acid (PdlLA) was used, since it is a well-known biocompatible polymer currently utilized for both cartilage and bone tissue engineering (paragraphs 1.4.1 and 1.4.3) and it is easy to process with electrospinning. Therefore, it was chosen to preliminarily evaluate the use of a nanometric net in a multicomponent scaffold for osteochondral regeneration.

Recently, an issue has been reported in literature regarding the use of PdlLA electrospun nets for tissue engineering applications, that is the dimensional shrinkage of PdlLA fibers when exposed to an aqueous environment. This phenomenon occurs because water molecules penetrate the material and act as a plasticizer; as a consequence, the mobility of polymer chains increases

and the residual internal stresses induced by the electrospinning process are relaxed, leading to a dramatic dimensional change of PdlLA fibers. In a recent study, PdlLA/polyethylene glycol (PEG) blends were used to produce electrospun nets which exhibited a significantly reduced shrinkage in water. According to author's explanations, PEG formed crystalline regions in the fiber matrix, determining a limitation of chain mobility, an increase of material rigidity and therefore a little dimensional reduction [137].

On the basis of these considerations, PdlLA/PEG blends were employed also in this study to produce electrospun nets, which were then characterized in terms of morphology and thermal properties. Infrared spectra were also collected and compared to those measured for PdlLA nets. Subsequently, PdlLA/PEG nets were assembled to a silk fibroin sponge produced by salt leaching to obtain the upper part of the multicomponent scaffold for osteochondral regeneration and the morphology of the combined scaffold was assessed.

To evaluate the biological properties of the assembled scaffold, a co-culture system was designed to verify the ability of the net to ensure the communication between chondrocytes and osteoblasts. From a general point of view, interactions among cells are fundamental for the development and homeostasis of tissues, which usually comprise several cell types. Their communications govern tissue remodeling, which occurs thanks to reciprocal signals between cells and extracellular matrix. Cellular interactions can take place via a variety of signaling pathways (figure 5.1), including endocrine signaling (via blood stream), synaptic signaling (via innervation), paracrine or autocrine signaling (when signals are released by a cells and bind to membrane receptors of other cells), juxtacrine signaling (when signals are exposed on the membrane of a cell to bind to other cells) or gap junctions (where a direct signal exchange occurs) [134].

In the case of cartilage, the cellular interactions of chondrocytes depend on their location in the tissue: in the superficial zone, chondrocytes interact mainly with synovial cells and factors in the synovial fluid; in the central regions of cartilage, interactions usually occur between chondrocytes and ECM;

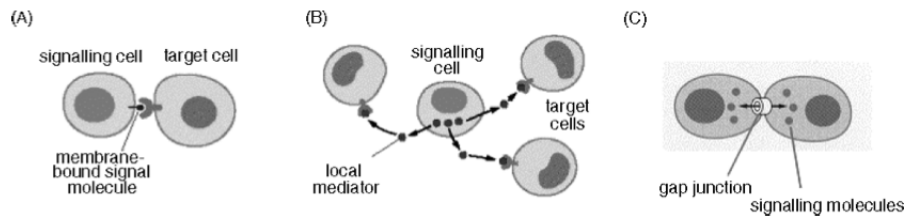


Figure 5.1: Mechanisms of intercellular signaling: (A) juxtacrine, (B) paracrine and (C) gap junctions [134].

in the calcified zone, instead, chondrocytes communicate with osteoblasts from the subchondral bone [134].

Several systems for the co-culture of chondrocytes and osteoblasts have been recently developed to reproduce these communication mechanisms *in vitro* and improve cartilage tissue regeneration. These studies demonstrated that the growth and differentiation of chondrocytes can be enhanced by endogenous signals secreted in a co-culture system with osteoblasts [61, 62, 63], while maintaining the specific phenotypes of both cells [134]. However, different co-culture methods led to conflicting results: for instance in [61], more extensive matrix deposition was observed when chondrocytes and osteoblasts were cultured simultaneously on PLGA/bioactive glass scaffolds, while in [62], chondrocytes deposited more GAG when cultured alone in a micromass than when co-cultured with a layer of osteoblasts. This suggests that the best co-culture parameters to maintain chondrocyte phenotype and improve new ECM deposition have not been found, yet.

Nevertheless, reciprocal interactions between chondrocytes and osteoblasts through their co-culture *in vitro* have proved to be a promising tool to guide and support cartilage regeneration. Co-culture systems have the potential not only to supply chondrocytes with appropriate growth factors, but also to provide them with a physiological distribution and kinetics, since they are released by osteoblasts as it happens in normal tissues [134]. In addition, they can be considered as a model system for the beneficial effects which cellular

communications can provide after *in vivo* implantation.

In this study, primary human articular chondrocytes were seeded in silk fibroin sponges with the PdlLA/PEG nanometric net on one side. The resulting constructs were placed in a commercial Transwell system (Corning, US) in order to allow biochemical communications with the compartment underneath only through the side covered with the net. After 3 days, chondrocytes were put in contact with an underlying monolayer of osteoblasts and cells were co-cultured for 11 days. The proliferation of both cell types was monitored during culture and at harvest, chondrocyte viability was assessed, as a preliminary evaluation of the validity of the co-culture system and cartilage cell response. Results were compared to those obtained for SF sponges without net and similar samples maintained in the same culture conditions but without any exposure to osteoblasts.

## 5.2 Materials and methods

### 5.2.1 Scaffold production

Poly-D,L-lactid acid PdlLA Resomer R207S (Boehringer-Ingelheim, Germany) was dissolved in  $\text{CHCl}_3$  at a concentration of 11% w/w. Polyethylene glycol (4000 Da, Fluka, US) was added at 10% in weight with respect to the PdlLA weight. Nanometric nets of PdlLA and PdlLA/PEG blends were produced by electrospinning, using a home-made apparatus composed of a Gamma High Voltage Research ES30P-10W power supply (Gamma High Voltage Research Inc., US), a single syringe pump (Pump 11 Plus - Harvard Apparatus, Crisel Instrument, Italy), and a flat aluminum collector to produce flat sheets. A 5-ml syringe filled with PdlLA or PdlLA/PEG solution was fitted with a stainless-steel 18G blunt-ended needle connected to 25 cm flexible PTFE tubing. Polymer fibers were collected at a working distance of 22 cm applying a voltage of 26 kV.

To obtain SF scaffolds with a nanometric net on one side (sample code:

SFnet), PdlLA/PEG nets were cut and placed on the bottom of a 35-mm Petri dish; then, 2 ml of silk fibroin aqueous solution (prepared as reported in paragraph 2.2.1) were poured into it. 4 g of NaCl with a grain diameter range of 425-1180  $\mu\text{m}$  were added to induce fibroin gelation as in the previous studies and the formation of  $\beta$ -sheet stable structures induced the attachment of the net to the bottom side of the silk fibroin sponge. SF sponges w/o net produced with the same salt leaching technique was used as a control in the following co-culture experiment.

## 5.2.2 Scaffold characterization

### 5.2.2.1 Scanning electron microscopy

The morphology of PdlLA/PEG electrospun nets was evaluated using a scanning electron microscope FEG SEM Zeiss Supra 40. Samples were gold sputtered to make them conductive and then observed with a voltage range of 3 to 5 kV.

### 5.2.2.2 Fourier Transform Infrared Spectroscopy

Infrared spectra of PdlLA, PdlLA nets and PdlLA/PEG nets at 10% and 30% of PEG (with respect to total PdlLA weight) were measured in FTIR-ATR mode (Fourier Transform Infrared - Attenuate Total Reflectance) using a Perkin Elmer Spectrum One (Perkin Elmer, US). Spectra were collected from 4000  $\text{cm}^{-1}$  to 600  $\text{cm}^{-1}$  as the mean of 16 scans.

### 5.2.2.3 Differential scanning calorimetry

Thermal properties of PdlLA and PdlLA/PEG electrospun nets were evaluated by differential scanning calorimetry using a Mettler DSC 30 calorimeter (Mettler Toledo, US) and 160- $\mu\text{l}$  aluminum pans. Two subsequent scans were performed from  $-50^{\circ}\text{C}$  to  $150^{\circ}\text{C}$  or from  $-20^{\circ}\text{C}$  to  $160^{\circ}\text{C}$  with a heating speed of  $10^{\circ}\text{C}/\text{min}$ .

### 5.2.3 Co-culture of human articular chondrocytes and osteoblasts

Human articular chondrocytes were purchased from PromoCell GmbH (Germany), plated at a density of 13000 cells/cm<sup>2</sup> in T75 flasks and cultured at 37°C and 5% CO<sub>2</sub> in high-glucose DMEM with 10% fetal bovine serum, 1% non-essential amino acids, 50 µg/ml of ascorbic acid and 1% penicillin-streptomycine-fungizone. Third passage confluent cells were used for seeding on SF and SFnet scaffolds.

Human osteosarcoma MG63 cells were plated at a density of 13000 cells/cm<sup>2</sup> in T75 flasks and cultured at 37°C and 5% CO<sub>2</sub> in high-glucose MEM with 10% fetal bovine serum, 1% non-essential amino acids, 2mM L-glutamine, 100 mM sodium pyruvate and 1% penicillin-streptomycine-fungizone. Confluent cells were trypsinized and employed in the following experiment.

#### 5.2.3.1 Cell seeding and co-culture of chondrocyte/scaffold constructs and osteoblasts

SF and SFnet scaffolds were soaked in distilled water for 2 hours and then cut into 6-mm discs, as previously described. Then, the sponges were incubated in 70% ethanol at 4°C overnight for sterilization and washed 3 times in sterile distilled water. Finally, SF and SFnet samples were pre-conditioned for 2 hours at 37°C and 5% CO<sub>2</sub> in co-culture medium, that is high-glucose DMEM with 10% fetal bovine serum, 1% non-essential amino acids, 50 µg/ml of ascorbic acid and 1% penicillin-streptomycine-fungizone [61]. Scaffolds were placed in the center of each well of a 24-well plate containing 200 µl of co-culture media. Third passage  $4 \times 10^5$  articular chondrocytes were loaded on the top of the scaffolds through pipette tips (in case of SFnet scaffolds, on the side without the net). 4 hours after seeding, SF and SFnet scaffolds were moved into a Transwell Polycarbonate Membrane Permeable Support (Corning, US) with a diameter of 6.5 mm and a membrane pore size of 8 µm fitted in a 24-well plate. The unseeded side was carefully maintained in contact with the porous

membrane. Then, 150  $\mu\text{l}$  of medium was added in the transwell, while 600  $\mu\text{l}$  of medium was poured into the well underneath.

At the same time, MG63 cells were seeded in tissue-culture 24-well plates at a density of 13000 cells/cm<sup>2</sup> with 600  $\mu\text{l}$  of co-culture medium. 3 days after seeding, the transwells with chondrocyte/scaffold constructs were either put into the wells with the osteoblast layers or maintained in the same culture conditions. Media were changed every day to ensure a sufficient nutrient supply to both cells.

#### 5.2.3.2 Chondrocyte viability

After 11 days of co-culture, the viability of chondrocytes in the SF and SFnet scaffolds was assessed using calcein AM and propidium iodide (PI, Invitrogen, US) to stain live and dead cells, respectively. Samples were washed in PBS and then incubated with 30  $\mu\text{M}$  of PI in PBS for 2 minutes at room temperature. Extra dye was removed by 5 washes in PBS, then sponges were soaked in a solution of 2  $\mu\text{M}$  calcein AM in PBS for 10 minutes at room temperature. Finally, chondrocyte/scaffold constructs were observed using a Nikon Eclipse Ti-E confocal laser microscope: images of both sides of the constructs were taken, then samples were cut along their coronal plane and the center of the scaffolds was observed.

#### 5.2.3.3 Cell proliferation

The proliferation of both osteoblasts and chondrocytes was evaluated on day 0 (start of the co-culture), day 3, day 7 and day 11 using an alamarBlue<sup>®</sup> assay (Invitrogen, US) as described in paragraph 2.2.6. Fluorescence was measured with a Tecan Infinite M200 Pro spectrofluorimeter using 565 nm and 595 nm as excitation and emission wavelengths, respectively.

#### 5.2.4 Statistical analysis

All biological tests were performed on  $N = 3$  samples at each time point. Data were expressed as mean  $\pm$  standard error of the mean and analyzed using GraphPad Prism 5.0 (GraphPad Software). Statistical significance was determined using two-way or one-way ANOVA test after the equality of variances was assessed. P-values  $< 0.05$  was considered statistically significant.

### 5.3 Results and discussion

#### 5.3.1 Scaffold characterization

##### 5.3.1.1 Scanning electron microscopy

The morphology of the nanometric net and the assembled scaffold developed in this study was assessed using a scanning electron microscope and results are reported in figure 5.2. (a) and (b) are images of the electrospun PdlLA/PEG net, which was characterized by a high porosity but a pore diameter less than  $5 \mu\text{m}$ . (c) and (d) corresponded to the bottom side of the silk fibroin sponge, which appeared completely covered by the net without any modifications to its morphology. Interestingly, no shrinkage of the net was observed, even if the assembled scaffolds were washed in distilled water for 3 days at room temperature. The section of the SFnet scaffolds is shown in the last two images, where the net-sponge transition and adhesion is visible.

SEM analysis confirmed that the morphology of the electrospun net of PdlLA/PEG blends is suitable for the purposes of this study, since it is potentially able to ensure solute flow through its high porosity preventing cell migration thanks to the limited pore diameter range [135]. In addition, a complete coverage of the SF sponge with the net was achieved, without modifying the morphology of both scaffolds. The adhesion between fibers and sponges may also have been hindered the shrinkage of the net, but further studies are needed to evaluate this phenomenon for longer time and at  $37^\circ\text{C}$ , which is much closer to the glass transition temperature of the material (see paragraph

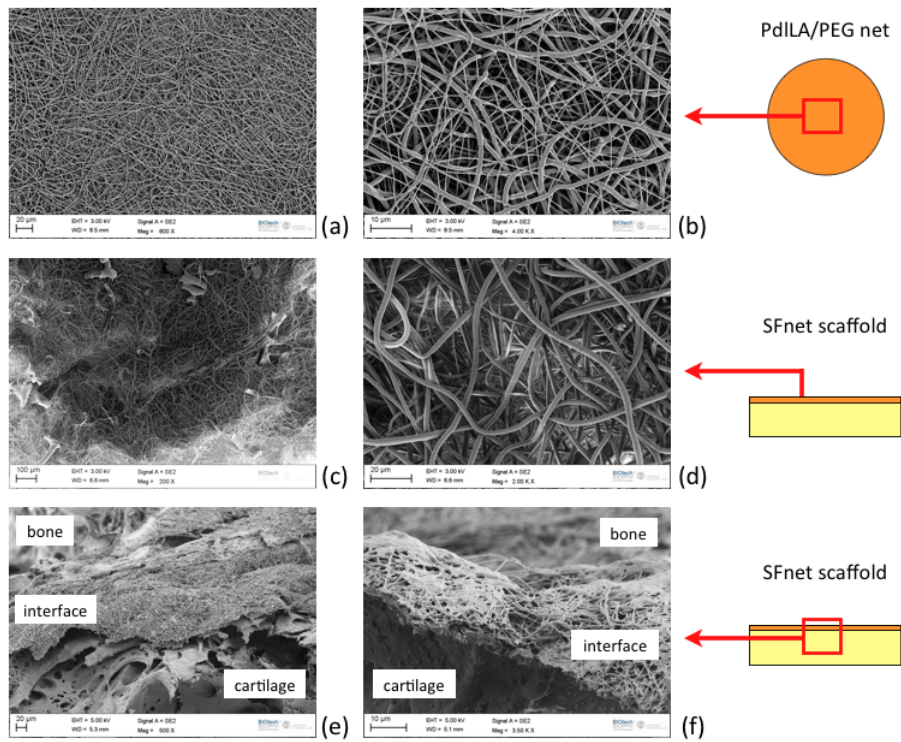


Figure 5.2: Scanning electron micrographs of PdILA/PEG net (a and b), the bottom side of SF sponges covered with the electrospun net (c and d) and details of their section (e and f), where cartilage and bone sides and their interface in the multicomponent scaffold are schematically indicated.

5.3.1.3).

#### 5.3.1.2 Fourier Transform Infrared Spectroscopy

FTIR spectroscopy analysis was performed to evaluate how the addition of PEG, the electrospinning process and/or the presence of residual solvent modified the IR spectra of PdlLA. In figure 5.3 (a), the spectrum of PdlLA before processing is shown. No differences were noticed among spectra of PdlLA before or after electrospinning and with or without PEG, with the only exception of an additional peak at about  $2883\text{ cm}^{-1}$  when PEG was added, as shown in figure 5.3 (b). This peak corresponded to one of the typical bands of PEG, as reported in [136]. In confirmation of that, nets were produced dissolving 30% of PEG with respect to PdlLA weight in the polymer solution and using the same parameters of electrospinning. As a consequence, the intensity of the peak at  $2883\text{ cm}^{-1}$  increased.

Therefore, IR spectra confirmed the addition of PEG in the PdlLA/PEG nets but neither were altered by the electrospinning process, nor revealed the presence of residual solvent.

#### 5.3.1.3 Differential scanning calorimetry

Calorimetric profiles of PdlLA and PdlLA/PEG nets were collected using DSC measurements, to evaluate how the addition of PEG modified the internal stresses of the material and the glass transition temperature  $T_g$ . To that purpose, two subsequent heating scans were performed and results are reported in figure 5.4.

In the first scan of PdlLA nets, an endothermic peak in correspondence to glass transition was observed, indicating a partial recovery of the material due to internal stresses induced by the electrospinning process. Indeed, polymeric chains are stretched during spinning, resulting in tensional stresses that are relaxed during heating because of the increased molecular mobility. In the second scan, only the glass transition is visible at about  $56^\circ\text{C}$ , as for the PdlLA

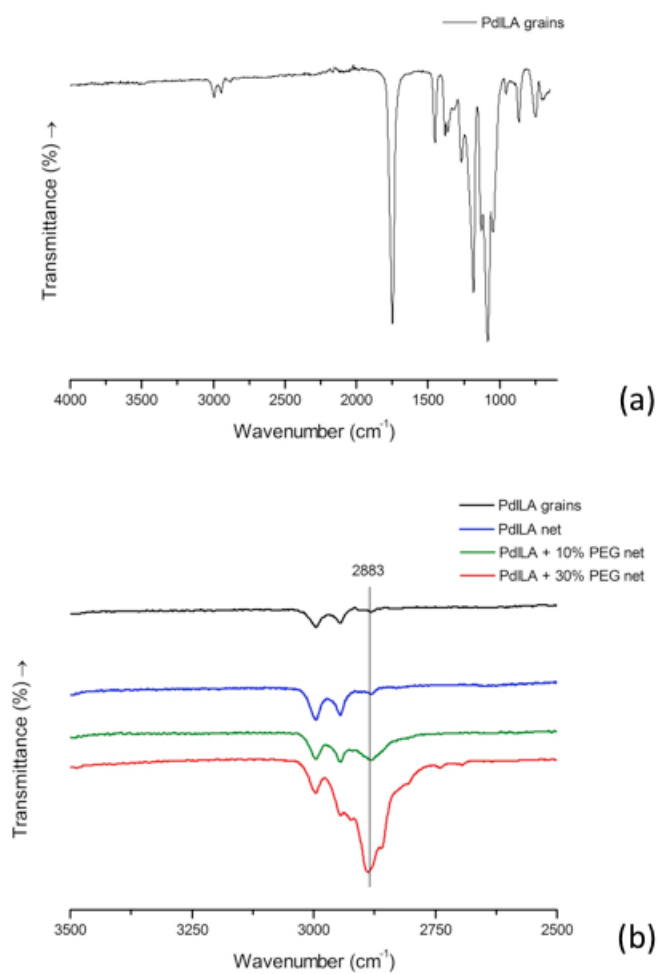


Figure 5.3: FTIR spectroscopy analysis: in (a), the IR spectrum of PdLA grains is reported and subsequently compared in (b) with the IR spectra of PdLA and PdLA/PEG nets at 10% and 30% of PEG in the region of 3500  $\text{cm}^{-1}$  - 2500  $\text{cm}^{-1}$ .

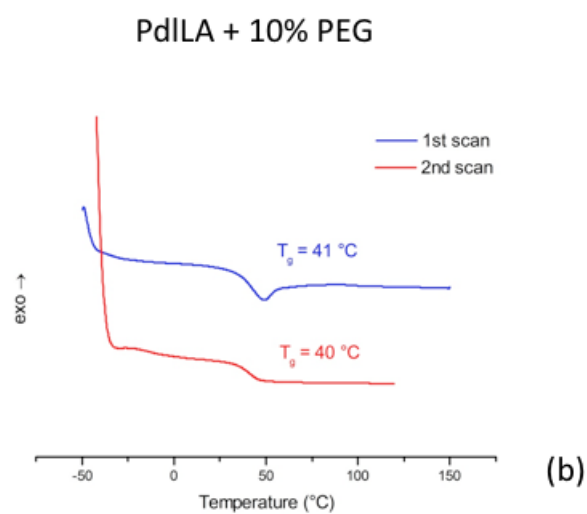
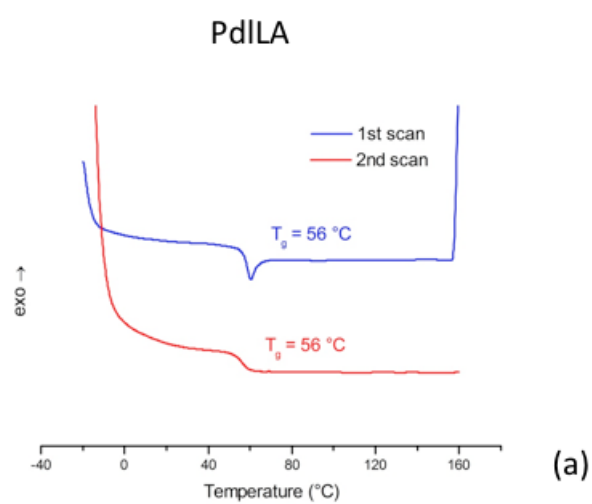


Figure 5.4: Calorimetric profiles of PdILA and PdILA/PEG nets (a and b, respectively). Two subsequent heating scans were performed and the measured glass transition temperatures are indicated.

grains (data not shown).

In the case of PdlLA/PEG nets, the relaxation peak was also detected, but it was superimposed to PEG melting, which increased the broadness of the peak. In addition, glass transition temperature was significantly reduced to about 40°C, suggesting a plasticizing effect by polyethylene glycol.

It has to be mentioned that this decrease of  $T_g$  may be considered a negative effect of PEG addition, because it corresponds to an increase in chain mobility in the material at lower temperatures and thus, it may facilitate material recovery. However, as shown in the SEM pictures (figure 5.2), PEG is effective in preventing net shrinkage. In a recent study where PdlLA/PEG nets were also prepared [137], authors considered the ability of PEG to introduce a certain grade of crystallinity in the material to explain this phenomenon; moreover, PEG chains may physically prevent the movement, opposing to stress relaxation. In addition, PEG may also decrease the residual tensional stresses during electrospinning: therefore, even if the glass transition temperature is lower, less internal stresses are built up during processing and the material recovers less.

### 5.3.2 Co-culture of human articular chondrocytes and osteoblasts

#### 5.3.2.1 Cell proliferation

The proliferation of both osteoblasts and chondrocytes on SF and SFnet scaffolds was evaluated when the co-culture was started, then on day 3, day 7 and day 11. Results are shown in figure 5.5 and 5.6, where cell proliferation is proportional to the collected fluorescence signal.

On both scaffolds with or without net, a slight decrease in chondrocyte proliferation was observed, regardless the presence of MG63 cells. This reduction was not statistically significant with the exception of day 7; however, cell proliferation increased again in all samples on day 11.

No differences in proliferation among scaffolds were detected when co-

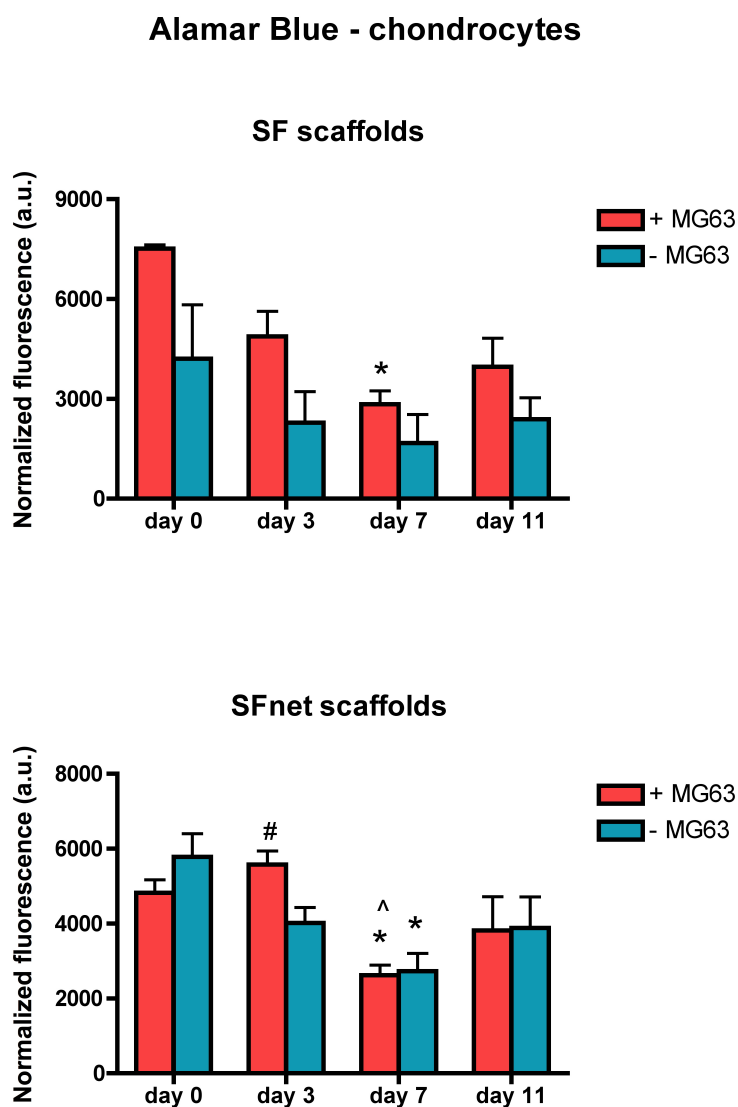


Figure 5.5: Proliferation of chondrocytes on SF and SFnet scaffolds at the beginning of co-culture conditions, on day 3, day 7 and day 11. The number of proliferating cells is proportional to the fluorescence signal. \*  $p < 0.05$  vs day 0, ^  $p < 0.05$  vs day 3, #  $p < 0.05$  vs without MG63.

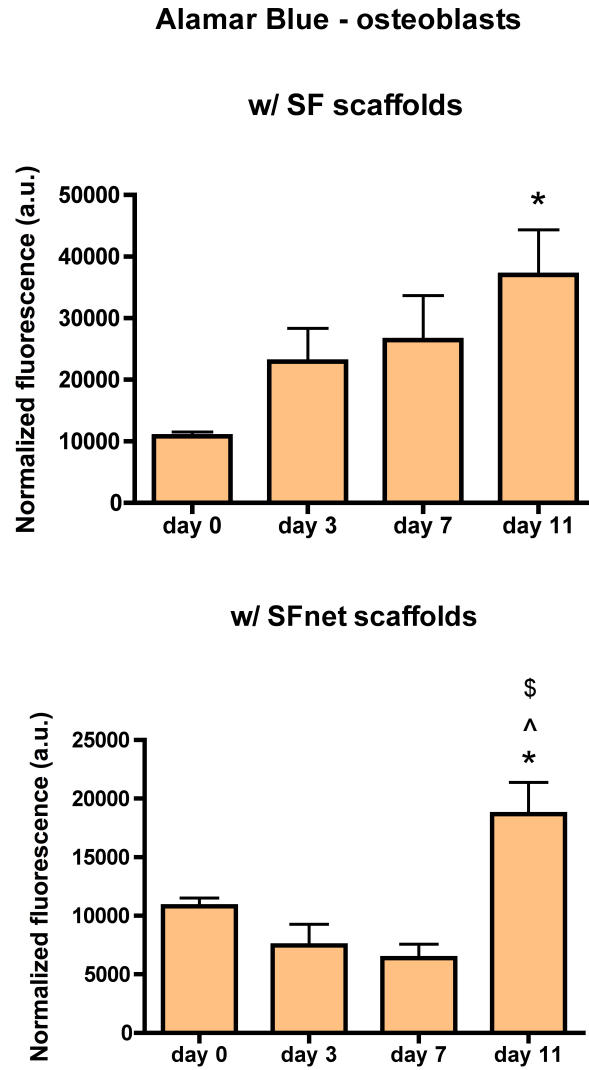


Figure 5.6: Proliferation of osteoblasts in contact with SF and SFnet scaffolds at the beginning of co-culture conditions, on day 3, day 7 and day 11. The number of proliferating cells is proportional to the fluorescence signal. \*  $p < 0.05$  vs day 0, ^  $p < 0.05$  vs day 3, \$  $p < 0.05$  vs day 7.

culture conditions were applied. Only when chondrocytes were cultured on SFnet sponges, an increase of proliferating cells was measured on day 3 when constructs were in contact to MG63 cells, while proliferation decreased on the same scaffolds in the absence of osteoblasts. Nevertheless, the values of proliferation on SFnet samples with or without MG63 cells became similar again on day 7.

Osteoblasts in contact with SF and SFnet constructs proliferated significantly after 11 days of co-culture conditions. However, cell number was significantly lower for MG63 cells cultured with SFnet samples.

On the basis of these results, proliferation of chondrocytes appeared unaffected by the presence of osteoblasts, regardless the scaffold used. However, an increase in seeding homogeneity may be required for both cell types, to avoid discrepancies such in the case of MG63 cells cultured with different sponges. In addition, a better nutrient supply to chondrocytes may be needed to improve their proliferation on the SF and SFnet scaffolds. Indeed, the volume of medium which can be added to the transwells where SF and SFnet scaffolds are placed is limited when compared to the culture conditions used in the studies reported in the previous chapters.

#### 5.3.2.2 Chondrocyte viability

The viability of chondrocytes on SF and SFnet scaffolds after 11 days of co-culture with or without osteoblasts was assessed using a Live/Dead assay and confocal laser microscopy. The collected images for SF and SFnet samples are reported in figure 5.7 and 5.8 respectively. Side A and side B indicate the surfaces of each scaffold. Then, constructs were cut along their coronal plane and a picture in the center of scaffold thickness was taken.

Chondrocytes populated all scaffolds throughout their whole volume, since live cells were detected also in the center of each sample. No differences were noticed with or without the co-culture with osteoblasts. However, a significant number of dead cells was also observed, which confirms the need of a better nutrient supply, as suggested also by proliferation results. In the case of chon-

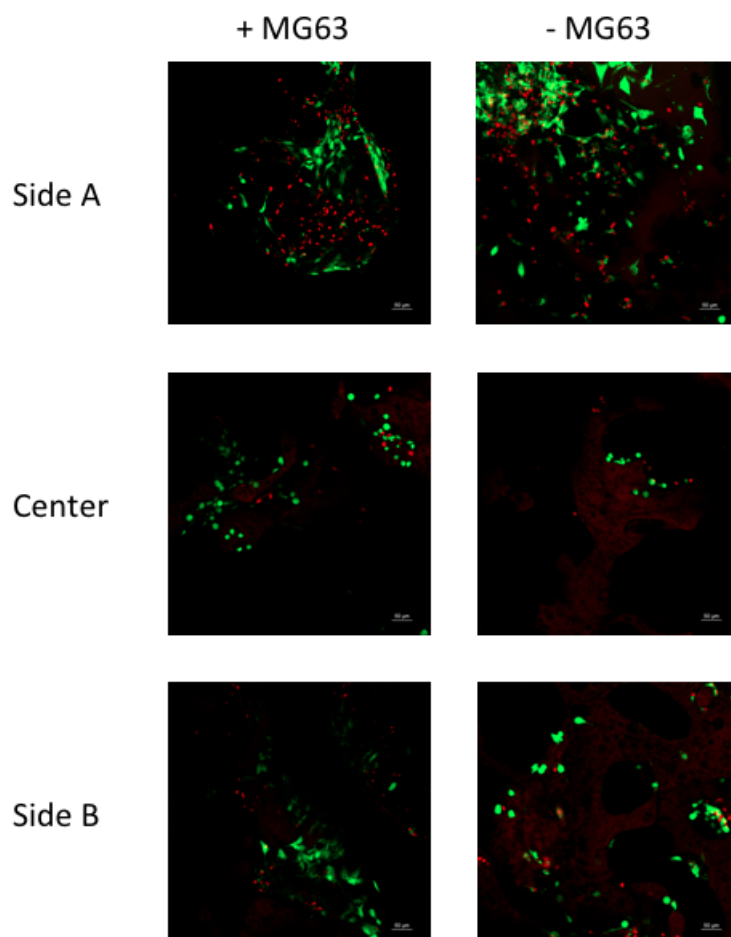


Figure 5.7: Confocal laser microscopy images of chondrocyte/SF scaffold constructs after 11 days of co-culture with or without MG63 cells. Side A and side B refer to the surfaces of each scaffold, while center indicates an image taken in the center of scaffold thickness. Live cells are stained green, while red corresponds to dead cells and fibroin sponges.

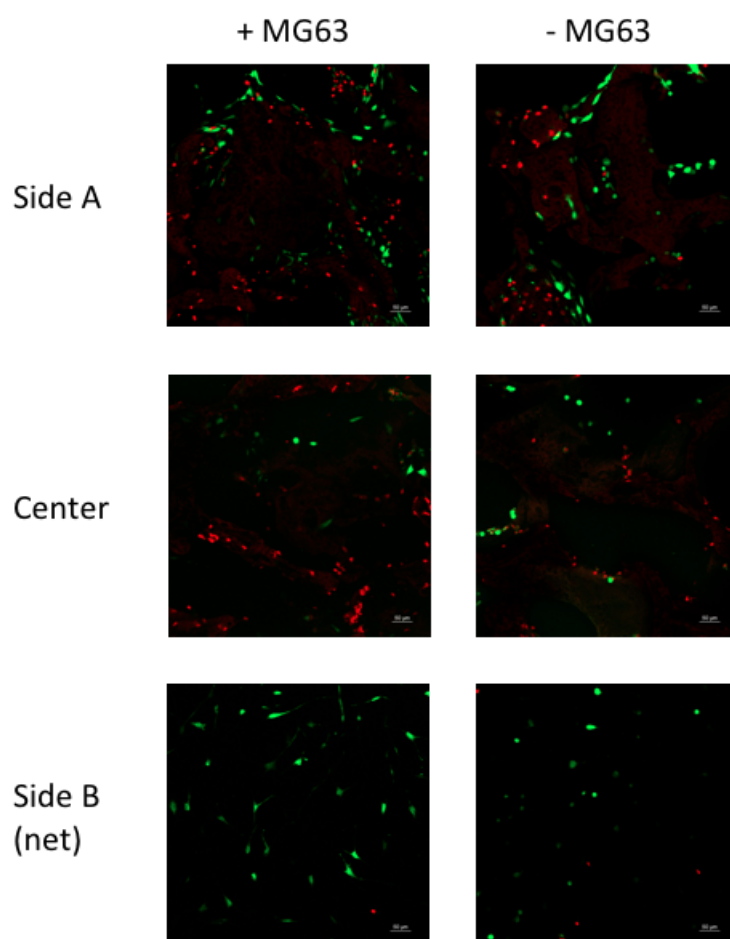


Figure 5.8: Confocal laser microscopy images of chondrocyte/SFnet scaffold constructs after 11 days of co-culture with or without MG63 cells. Side A and side B refer to the surfaces of each scaffold, while center indicates an image taken in the center of scaffold thickness. Live cells are stained green, while red corresponds to dead cells and fibroin sponges.

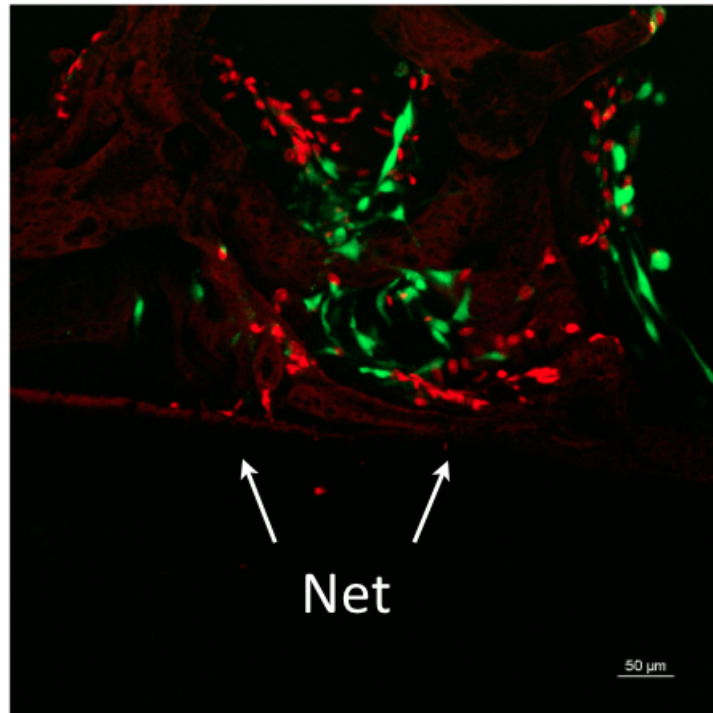


Figure 5.9: Confocal laser microscopy image of the lower part of a SFnet scaffold section. The nanometric net side is indicated by arrows. Live cells are stained green, while red corresponds to dead cells and fibroin sponges.

drocyte/SFnet scaffold constructs, few cells were seen also in correspondence to the scaffold surface with the nanometric net. To confirm that these cells migrated from the seeding side and remained beyond the electrospun net, the lower part of the section of SFnet scaffolds was observed and an image is shown as example in figure 5.9.

It is clear that all chondrocytes were inside the scaffolds and populated the pores of the SF sponge without crossing the nanometric net.

## 5.4 Conclusions

In order to regenerate a functional interface between cartilage and bone, the properties of a scaffold for osteochondral tissue engineering need to be designed following the principles of biomimetics and aiming to translate the physiological complexity into scaffold characteristics. In this perspective, we hypothesized that the restoration of the osteochondral interface can be achieved with a multicomponent scaffold where chondral and subchondral phases are separated by a nanometric net. The role of the net is to ensure the beneficial dialogue among cartilage and bone cells, while preventing cell migration, especially of blood cells which may induce vascularization and cartilage mineralization.

To this purpose, PdlLA/PEG electrospun nets were produced and characterized, showing a high porosity but a limited pore dimension (less than 5  $\mu\text{m}$ ) able to potentially prevent cell migration. In addition, PEG hindered the shrinkage of PdlLA fibers in an aqueous environment, which is one of the main concerns recently reported in literature when PdlLA electrospun nets were employed in tissue engineering applications. Then, PdlLA/PEG nets were successfully assembled to a silk fibroin sponge produced by salt leaching, leading to a complete coverage of its bottom side without modifying the morphology of both scaffolds.

To evaluate the biological properties of the assembled scaffold, a co-culture system was designed and validated. Primary human articular chondrocytes were seeded on SF scaffolds with the PdlLA/PEG net on the bottom side and placed in a commercial Transwell system above a layer of human carcinoma osteoblasts, so that biochemical communications could take place only through the unseeded side covered with the electrospun fibers. Cell proliferation and viability were measured during 11 days of co-culture and unmodified SF scaffolds were used as control to assess the influence of the net on chondrocyte response. Findings were compared to those obtained when the same chondrocyte/scaffold constructs were cultured without osteoblasts.

Results showed that chondrocytes populated all scaffolds throughout the

whole volume, without crossing the electrospun net. However, their proliferation was limited, indicating the need of a better nutrient supply, which may be achieved with suitable dynamic conditions, such as a perfusion bioreactor. In addition, neither the presence of osteoblasts nor the net affected chondrocyte growth.

This preliminary study was a necessary step to verify the effectiveness of the co-culture system used. On this basis, a detailed analysis of chondrocyte gene expression and new cartilage ECM deposition will be performed, to evaluate if the electrospun net can ensure cellular communications among chondrocytes and osteoblasts. In addition, the issue of net degradation has to be addressed: indeed, PdlLA degrades faster than silk fibroin, thus it must be evaluated if its degradation time is compatible with a complete osteochondral interface restoration. Finally, another important point will be analyzed: even if blood cells are prevented to migrate into the chondral side of the multicomponent scaffold, plasma can still permeate the SF-based scaffold used for cartilage regeneration. Therefore, the plasma compatibility of the multiphasic scaffold needs to be assessed, besides the effect of plasma on chondrocyte behavior.

## Chapter 6

### Final remarks

In this research work, a multicomponent scaffold for osteochondral Tissue Engineering was fabricated and characterized. Two strategies were explored to produce the component for cartilage regeneration: first, pure silk fibroin sponges were successfully employed to sustain the chondrogenesis of adipose-derived stem cells *in vitro* and the ability of the resulting cell/scaffold constructs to regenerate cartilage in an *in vivo* model of rat xiphoid critical size defect was demonstrated.

Subsequently, silk fibroin/hyaluronic acid scaffolds were produced at different HA concentrations and with or without cross-linking with genipin. It was shown that both HA and cross-linking modulated scaffold properties: hyaluronic acid influenced fibroin crystallinity and cross-linking degree, while genipin determined the formation of a more interconnected network of the two material components. Moreover, the presence of hyaluronic acid on the scaffold affected the response of articular chondrocytes when cultured in dynamic conditions and at the highest concentration it induced an enhancement of cartilage cell phenotype and a higher ECM deposition with respect to pure fibroin sponges. Further investigations are needed to understand how genipin and HA loss during culture influenced chondrocyte behaviour.

For the regeneration of a functional osteochondral interface, we hypothe-

sized that a nanometric net between the components for cartilage and bone regeneration could ensure the beneficial dialogue among cartilage and bone cells, while preventing cell migration, especially of blood cells which may induce vascularization and cartilage mineralization. Therefore, nets were fabricated by electrospinning of PdlLA/PEG blends, characterized in terms of morphology and thermal properties, then successfully assembled to silk fibroin sponges without any modifications to their morphology.

Finally, a system to co-culture chondrocytes and osteoblasts was designed and validated, so that biochemical communications could take place only through the side covered with the electrospun fibers. Results showed that chondrocytes populated all scaffolds throughout the whole volume, without crossing the electrospun net. However, their limited proliferation indicated the need of a better nutrient supply, which may be achieved with suitable dynamic conditions, such as a perfusion bioreactor.

On the basis of the outcomes presented in this research work, a final multicomponent scaffold will be designed in order to combine the best results obtained. Thus, silk fibroin/hyaluronic acid scaffolds which elicited the best responses on chondrocytes will be cultured with adipose-derived stem cells to assess their potential to sustain chondrogenesis *in vitro*. Then, they will be assembled to the nanometric net and, before moving to an appropriate *in vivo* study, the co-culture system will be used to evaluate how the cellular dialogue with osteoblasts can have beneficial effects on the chondrogenic differentiation of ASCs.

# Bibliography

- [1] R. Lanza, R. Langer, J. Vacanti. *Principles of Tissue Engineering* 3rd edition. Elsevier Academic Press (2007).
- [2] J. B. Park, J. D. Bronzino. *Biomaterials, principles and applications*. CRC Press (2003).
- [3] D. F. Williams. *On the mechanisms of biocompatibility*. *Biomaterials* 29 (2008), 2941–2953.
- [4] W. Swieszkowsky et al. *Repair and regeneration of osteochondral defect in the articular joint*. *Biomolecular Engineering* 24 (2007), 489-495.
- [5] D. Nestic et al. *Cartilage tissue engineering for degenerative joint disease*. *Advanced Drug Delivery Reviews* 58 (2006), 300-322.
- [6] J. S. Temenoff, A. G. Mikos. *Review: tissue engineering for regeneration of articular cartilage*. *Biomaterials* 21 (2000), 431-440.
- [7] A. Redaelli, F. Montevercchi. *Biomeccanica: analisi multiscala di tessuti biologici*. Vol. 13 Collana di Ingegneria biomedica, Patron Editore (2007).
- [8] [http://innovativepharma.com/immagini/articolazione\\_normale.gif](http://innovativepharma.com/immagini/articolazione_normale.gif)
- [9] [http://www-3.unipv.it/webbio/anatcomp/freitas/2009-2010/chart-2\(1\).jpg](http://www-3.unipv.it/webbio/anatcomp/freitas/2009-2010/chart-2(1).jpg)
- [10] <http://www.engin.umich.edu/class/bme456/cartilage/Cart14.jpg>

- [11] <https://casweb.ou.edu/pbell/histology/Images/Slides/Bone/supp.bone.-osteon.40.jpg>
- [12] V. Karageorgiou, D. Kaplan. *Porosity of 3D biomaterial scaffold and osteogenesis*. Biomaterials 26 (2005), 5474-5491.
- [13] T. A. Peters, I. D. McLean. *Osteochondritis dissecans of the patellofemoral joint*. American Journal of Sports Medicine 28 (2000), 63-67.
- [14] C. L. Baker 3rd et al. *Osteochondritis dissecans of the capitellum*. American Journal of Sports Medicine 38 (2010), 1917-1928.
- [15] D. J. Hunter. *Risk stratification for knee osteoarthritis progression: a narrative review*. Osteoarthritis Cartilage 17 (2009), 1402-1407.
- [16] L. Sharma et al. *Epidemiology of osteoarthritis: an update*. Current Opinions in Rheumatology 18 (2006), 147-156.
- [17] W. L. Grayson et al. *Engineering custom-designed osteochondral tissue grafts*. Trends in Biotechnology 26 (2008), 181-189.
- [18] A. E. Beris et al. *Advances in articular cartilage repair*. Injury 36(Suppl 4), S14-S23.
- [19] P. D. Gikas et al. *An overview of autologous chondrocyte implantation*. Journal of Bone and Joint Surgery (British volume) 91 (2009), 997-1006.
- [20] D. Puppi et al. *Polymeric materials for bone and cartilage repair*. Progress in Polymer Science 35 (2010), 403-440.
- [21] I. Martin et al. *Osteochondral tissue engineering*. Journal of Biomechanics 40 (2007), 750-765.
- [22] T. Kimura et al. *Chondrocytes embedded in collagen gels maintain cartilage phenotype during long-term cultures*. Clinical Orthopaedics and Related Research (1984), 231-239.

- [23] S. Wakitani et al. *Mesenchymal cell-based repair of large, full-thickness defects of articular cartilage*. Journal of Bone and Joint Surgery 76 (1994), 579-592.
- [24] M. Nakajima et al. *In vivo mechanical condition plays an important role for appearance of cartilage tissue in ES cell transplanted joint*. Journal of Orthopaedic Research 26 (2008), 10-17.
- [25] T. Gotterbarm et al. *An in vivo study of a growth-factor enhanced, cell free, two-layered collagen-tricalcium phosphate in deep osteochondral defect*. Biomaterials 27 (2006), 3387-3395.
- [26] H. Sa-Lima et al. *Stimuli-responsive chitosan-starch injectable hydrogels combined with encapsulated adipose-derived stromal cells for articular cartilage regeneration*. Soft Matter 6 (2010), 5184-5195.
- [27] S. S. Silva et al. *Novel genipin-cross-linked chitosan/silk fibroin sponges for cartilage engineering strategies*. Biomacromolecules 9 (2008), 2764-2774.
- [28] W. L. Grayson et al. *Spatial regulation of human mesenchymal stem cell differentiation in engineered osteochondral constructs: effects of pre-differentiation, soluble factors and medium perfusion*. Osteoarthritis Cartilage 18 (2010), 714-723.
- [29] C. Chung, J. A. Burdick. *Engineering cartilage tissue*. Advanced Drug Delivery Reviews 60 (2008), 243 - 262.
- [30] L. Wang et al. *Human umbilical cord mesenchymal stromal cells in a sandwich approach for osteochondral tissue engineering*. Journal of Tissue Engineering and Regenerative Medicine 5(9) (2011), 712-721.
- [31] X. Shao et al. *Repair of large articular osteochondral defects using hybrid scaffolds and bone marrow-derived mesenchymal stem cells in a rabbit model*. Tissue Engineering 12 (2006), 1539-1551.

- [32] G. D. Nicodemus, S. J. Bryant. *Cell encapsulation in biodegradable hydrogels for tissue engineering applications*. Tissue Engineering Part B Review 14 (2008), 149-165.
- [33] M. T. Rodrigues et al. *Current strategies for osteochondral regeneration: from stem cells to pre-clinical approaches*. Current Opinion in Biotechnology (2011), doi:10.1016/j.copbio.2011.04.006.
- [34] Z. S. Patel et al. *Dual delivery of an angiogenic and an osteogenic growth factor for bone regeneration in a critical size defect model*. Bone 43 (2008), 931-940.
- [35] J. Glowacki. *Angiogenesis in fracture repair*. Clinical Orthopaedics (1998), S82-89.
- [36] H. P. Gerber, N. Ferrara. *Angiogenesis and bone growth*. Trends in Cardiovascular Medicine 10 (2000), 223-228.
- [37] A. S. Lin et al. *Microarchitectural and mechanical characterization of oriented porous polymer scaffolds*. Biomaterials 24 (2003), 481-489.
- [38] A. Ogose et al. *Comparison of hydroxyapatite and beta tricalcium phosphate as bone substitutes after excision of bone tumors*. Journal of Biomedical Materials Research Part B: Applied Biomaterials 72 (2005), 94-101.
- [39] D. D. Muehrcke et al. *Calcium phosphate cements improve bone density when used in osteoporotic sternums*. Annals of Thoracic Surgery 88 (2009), 1658-1661.
- [40] M. T. Rodrigues et al. *Tissue engineered constructs based on SPCL scaffolds cultured with goat marrow cells: functionality in femoral defects*. Journal of Tissue Engineering and Regenerative Medicine 5 (2011), 41-49.

- [41] H. J. Kim et al. *Bone tissue engineering with premineralized silk scaffolds*. Bone 42 (2008), 1226-1234.
- [42] L. Meinel et al. *Engineering bone-like tissue in vitro using human bone marrow stem cells and silk scaffolds*. Journal of Biomedical Material Research part A 71 (2004), 25-34.
- [43] I. Martin et al. *Osteochondral tissue engineering*. Journal of Biomechanics 40 (2007), 750-765.
- [44] X. Guo et al. *Repair of osteochondral defects with biodegradable hydrogel composites encapsulating marrow mesenchymal stem cells in a rabbit model*. Acta Biomaterialia 6 (2010), 39-47.
- [45] M. Kayakabe et al. *Transplantation of autologous rabbit BM-derived mesenchymal stromal cells embedded in hyaluronic acid gel sponge into osteochondral defects of the knee*. Cytotherapy 8 (2006), 343-353.
- [46] E. Filova et al. *Composite hyaluronate-type I collagen-fibrin scaffold in the therapy of osteochondral defects in miniature pigs*. Physiological Research 56 (suppl. 1) (2007), S5-S16.
- [47] J. H. Ahn et al. *Novel hyaluronate-atelocollagen/beta-TCP-hydroxyapatite biphasic scaffold for the repair of osteochondral defects in rabbits*. Tissue Engineering part A 15 (2009), 2595-2604.
- [48] E. Kon et al. *Orderly osteochondral regeneration in a sheep model using a novel nano-composite multilayered biomaterial*. Journal of Orthopaedics Research 28 (2010), 116-124.
- [49] D. Xue et al. *Osteochondral repair using porous poly(lactide-co-glycolide)/nano-hydroxyapatite hybrid scaffolds with undifferentiated mesenchymal stem cells in a rat model*. Journal of Biomedical Research part A 94 (2010), 259-270.

- [50] G. Zhou et al. *Repair of large articular osteochondral defects using hybrid scaffolds and bone marrow-derived mesenchymal stem cells in a rabbit model*. Tissue Engineering 12 (2006), 3209-3221.
- [51] X. Wang et al. *Tissue engineering of biphasic cartilage constructs using various biodegradable scaffolds: an in vitro study*. Biomaterials 25(17) (2004), 3681-3688.
- [52] R. Tuli et al. *Human mesenchymal progenitor cell-based tissue engineering of a single unit osteochondral construct*. Tissue Engineering 10 (2004), 1169-1179.
- [53] D. Schaefer et al. *In vitro generation of osteochondral composites*. Biomaterials 21 (2000), 2599-2606.
- [54] T. Cao et al. *Scaffold design and in vitro study of osteochondral coculture in a three-dimensional porous polycaprolactone scaffold fabricated by fused deposition modeling*. Tissue Engineering 9(suppl. 1) (2003), S103-S112.
- [55] S. Wakitani et al. *Autologous bone marrow stromal cell transplantation for repair of full-thickness articular cartilage defects in human patellae: two case reports*. Cell Transplant 13 (2004), 595-600.
- [56] J. Fan et al. *Synovium-derived mesenchymal stem cells: a new cell source for musculoskeletal regeneration*. Tissue Engineering part B Reviews 15 (2009), 75-86.
- [57] J. Ringe et al. *Human mastoid periosteum-derived stem cells: promising candidates for skeletal tissue engineering*. Journal of Tissue Engineering and Regenerative Medicine 2 (2008), 136-146.
- [58] A. G. Mikos et al. *Engineering complex tissues*. Tissue Engineering 12 (2006), 3307-3339.

- [59] H. Cheng et al. *In vitro generation of an osteochondral interface from mesenchymal stem cell-collagen microspheres*. *Biomaterials* 32 (2011), 1526-1535.
- [60] N. H. Dormer et al. *Osteochondral interface tissue engineering using macroscopic gradients of bioactive signals*. *Annals of Biomedical Engineering* 38 (2010), 2167-2182.
- [61] J. P. Spalazzi et al. *Osteoblast and chondrocyte interactions during coculture on scaffolds*. *Engineering in Medicine and Biology Magazine* 22(5) (2003), 27-34.
- [62] J. Jiang et al. *Co-culture of osteoblasts and chondrocytes modulates cellular differentiation in vitro*. *Biomedical and Biophysical Research Communications* 338 (2005), 762-770.
- [63] R. Nakaoka et al. *Regulation of chondrocyte differentiation level via coculture with osteoblasts*. *Tissue Engineering* 12 (2006), 2425-2433.
- [64] L. C. Gerstenfeld et al. *Chondrocytes provide morphogenic signals that selectively induce osteogenic differentiation of mesenchymal stem cells*. *Journal of Bone Mineralization Research* 17 (2002), 221-230.
- [65] C. Vepari, D. L. Kaplan. *Silk as a biomaterial*. *Progress in Polymer Science* 32 (2007), 991-1007.
- [66] G. H. Altman et al. *Silk-based biomaterials*. *Biomaterials* 24 (2003), 401-416.
- [67] A. C. MacIntosh et al. *Skeletal tissue engineering using silk biomaterials*. *Journal of Tissue Engineering and Regenerative Medicine* 2 (2008), 71-80.
- [68] H. J. Jin, D. L. Kaplan. *Mechanism of silk processing in insects and spiders*. *Nature* 424 (2003), 1057-1061.

- [69] <http://thurj.org/as/2011/01/1358/>
- [70] R. Valluzzi et al. *Orientation of silk III at the air-water interface*. International Journal of Biological Macromolecules 24 (1999), 237-242.
- [71] C. Viney. *Natural silks: archetypal supramolecular assembly of polymer fibers*. Supramolecular Science 4 (1997), 75-81.
- [72] H. Yamada et al. *Identification of fibroin-derived peptides enhancing the proliferation of cultured human skin fibroblasts*. Biomaterials 25 (2004), 467-472.
- [73] R. E. Unger et al. *Endothelialization of a non-woven silk fibroin net for use in tissue engineering: growth and gene regulation of human endothelial cells*. Biomaterials 25(21) (2004), 5137-5146.
- [74] C. Li et al. *Electrospun silk-BMP-2 scaffolds for bone tissue engineering*. Biomaterials 27(16) (2006), 3115-3124.
- [75] V. Karageorgiou et al. *Bone morphogenetic protein-2 decorated silk fibroin films induce osteogenic differentiation of human bone marrow stromal cells*. Journal of Biomedical Material Research part A 71(3) (2004), 528-537.
- [76] S. Sofia et al. *Functionalized silk-based biomaterials for bone formation*. Journal of Biomedical Material Research 54(1) (2001), 139-148.
- [77] A. Motta et al. *Fibroin hydrogels for biomedical applications: preparation, characterization and in vitro cell culture studies*. Journal of Biomaterial Science Polymer Edition 15(7) (2004), 851-864.
- [78] L. Qiang et al. *Preparation of 3-D regenerated fibroin scaffolds with freeze drying method and freeze drying/foaming technique*. Journal of Material Science: Material in Medicine 17 (2006), 1349-1356.

- [79] U. Kim et al. *Three-dimensional aqueous-derived biomaterial scaffolds from silk fibroin*. *Biomaterials* 26 (2005), 2775-2785.
- [80] Y. Wang et al. *In vitro cartilage tissue engineering with 3D porous aqueous-derived silk scaffolds and mesenchymal stem cells*. *Biomaterials* 26(34) (2005), 7082-7094.
- [81] S. Hofmann et al. *Cartilage-like tissue engineering using silk scaffolds and mesenchymal stem cells*. *Tissue Engineering* 12(10) (2006), 2729-2738.
- [82] Y. Wang et al. *Cartilage tissue engineering with silk scaffolds and human articular chondrocytes*. *Biomaterials* 27(25) (2006), 4434-4442.
- [83] Y. Wang et al. *The synergistic effects of 3-D porous silk fibroin matrix scaffold properties and hydrodynamic environment in cartilage tissue regeneration*. *Biomaterials* 31 (2010), 4672-4681.
- [84] L. Meinel et al. *Bone tissue engineering using human mesenchymal stem cells: effects of scaffold material and medium flow*. *Annuals of Biomedical Engineering* 32(1) (2004), 112-122.
- [85] H. J. Kim et al. *Influence of macroporous protein scaffolds on bone tissue engineering from bone marrow stem cells*. *Biomaterials* 26(21) (2005), 4442-4452.
- [86] L. Meinel et al. *The inflammatory responses to silk films in vitro and in vivo*. *Biomaterials* 26(2) (2005), 147-155.
- [87] I. Dal Pra et al. *De novo engineering of reticular connective tissue in vivo by silk fibroin nonwoven materials*. *Biomaterials* 26(14) (2005), 1987-1999.
- [88] H. S. Yoo et al. *Hyaluronic acid modified biodegradable scaffolds for cartilage tissue engineering*. *Biomaterials* 26 (2005), 1925-1933.

- [89] S. Yamane et al. *Feasibility of chitosan-based hyaluronic acid hybrid biomaterial for a novel scaffold in cartilage tissue engineering*. *Biomaterials* 26 (2005), 611-619.
- [90] H. Tan et al. *Injectable in situ forming biodegradable chitosan-hyaluronic acid based hydrogels for cartilage tissue engineering*. *Biomaterials* 30 (2009), 2499-2506.
- [91] S. Tang et al. *Fabrication and characterization of porous hyaluronic acid-collagen composite scaffolds*. *Journal of Biomedical Material Research part A* 82 (2007), 323-335.
- [92] S. Tang, M. Spector. *Incorporation of hyaluronic acid into collagen scaffolds for the control of chondrocyte-mediated contraction and chondrogenesis*. *Biomedical Materials* 2(3) (2007), S135-S141.
- [93] M. Garcia-Fuentes et al. *The effect of hyaluronic acid on silk fibroin conformation*. *Biomaterials* 29 (2008), 633-642.
- [94] R. S. Tuan et al. *Adult mesenchymal stem cells and cell-based tissue engineering*. *Arthritis Research and Therapy* 5 (2003), 32-45.
- [95] G. Im et al. *Do adipose tissue-derived mesenchymal stem cells have the same osteogenic and chondrogenic potential as bone marrow-derived cells?* *Osteoarthritis Cartilage* 13 (2005), 845-853.
- [96] D. English, M. Q. Islam. *Mesenchymal Stem Cells: Use in Cartilage Repair*. *Current Rheumatology Reviews* 5 (2009), 24-33.
- [97] H. R. Moyer et al. *A new animal model for assessing cartilage repair and regeneration at a nonarticular site*. *Tissue engineering Part A* 16 (2010), 2321-2330.
- [98] R. L. Mauck et al. *Regulation of cartilaginous ECM gene transcription by chondrocytes and MSCs in 3D culture in response to dynamic loading*. *Biomechanics and Modelling in Mechanobiology* 6 (2007), 113-125.

- [99] R. Portner et al. *Bioreactor design for tissue engineering*. Journal of Bioscience and Bioengineering 100 (2005), 235-245.
- [100] Tarng et al. *A novel recirculating flow-perfusion bioreactor for periosteal chondrogenesis*. International Orthopaedics (2011), doi: 10.1007/s00264-011-1291-x.
- [101] E. J. Sheehy et al. *Chondrocytes and bone marrow-derived mesenchymal stem cells undergoing chondrogenesis in agarose hydrogels of solid and channelled architectures respond differentially to dynamic culture conditions*. Journal of Tissue Engineering and Regenerative Medicine 5 (2011), 747-758.
- [102] R. S. Tigli et al. *Chondrogenesis in perfusion bioreactors using porous silk scaffolds and hESC-derived MSCs*. Journal of Biomedical Materials Research A 96 (2011), 21-28.
- [103] K. Liu et al. *The dependence of in vivo stable ectopic chondrogenesis by human mesenchymal stem cells on chondrogenic differentiation in vitro*. Biomaterials 29 (2008), 2183-2192.
- [104] W. Wang et al. *In vivo restoration of full-thickness cartilage defects by poly(lactide-co-glycolide) sponges filled with fibrin gel, bone marrow mesenchymal stem cells and DNA complexes*. Biomaterials 31 (2010), 5953-5965.
- [105] N. Indrawattana et al. *Growth factor combination for chondrogenic induction from human mesenchymal stem cell*. Biochemical and Biophysical Research Communications 320 (2004), 914-919.
- [106] B. P. Toole. *Hyaluronan in morphogenesis*. Cell and Developmental Biology 12 (2001), 79-87.

- [107] F. Gao et al. *Preparation and characterization of hyaluronan oligosaccharides for angiogenesis study*. Journal of Biomedical Materials Research Part B 78 (2006), 385-392.
- [108] C. Tempel et al. *Hyaluronic acid as an anti-angiogenic shield in the preovulatory rat follicle*. Biology of Reproduction 63 (2000), 134-140.
- [109] A. L. Raines et al. *Hyaluronic acid stimulates neovascularization during the regeneration of bone marrow after ablation*. Journal of Biomedical Materials Research Part A 96 (2011), 575-583.
- [110] Y. Ren et al. *Preparation and characterization of fibroin/hyaluronic acid composite scaffold*. International Journal of Biological Macromolecules 44 (2009), 372-378.
- [111] M. Garcia-Fuentes et al. *Silk fibroin/hyaluronan scaffolds for human mesenchymal stem cell culture in tissue engineering*. Biomaterials 30 (2009), 5068-5076.
- [112] X. Hu et al. *Biomaterials from ultrasonication-induced silk fibroin-hyaluronic acid hydrogels*. Biomacromolecules 11 (2010), 3178-3188.
- [113] M. Yang et al. *The influence of rat mesenchymal stem cell CD44 surface markers on cell growth, fibronectin expression, and cardiomyogenic differentiation on silk fibroin – hyaluronic acid cardiac patches*. Biomaterials 31 (2010), 854-862.
- [114] H. Koo et al. *Antiinflammatory effects of genipin, an active principle of gardenia*. European Journal of Pharmacology 495 (2004), 201-208.
- [115] H. Koo et al. *Anti-inflammatory evaluation of gardenia extract, geniposide and genipin*. Journal of Ethnopharmacology 103 (2006), 496-500.
- [116] S. S. Silva et al. *Genipin-modified silk-fibroin nanometric nets*. Macromolecular Bioscience 8 (2008), 766-774.

- [117] C. Ko et al. *Type II collagen-chondroitin sulfate-hyaluronan scaffold cross-linked by genipin for cartilage tissue engineering*. Journal of Bio-science and Bioengineering 107 (2009), 177-182.
- [118] H. Meyer. *The ninhydrin reaction and its analytical applications*. Bio-chemical Journal 67 (1957), 333-340.
- [119] Z. Lin et al. *Swelling behaviors, tensile properties and thermodynamic interactions in APS/HEMA copolymeric hydrogels*. Frontiers of Materials Science 1(4) (2007), 427-431.
- [120] N. A. Peppas et E. W. Merrill. *Hydrogels as swollen elastic network*. Journal of Applied Polymer Science 21(7) (1977), 1763-1770.
- [121] C. Migliaresi et al. *Physical characterization of microporous poly(2-hydroxyethyl methacrylate) gels*. Journal of Biomedical Materials Research 15 (1981), 307-317.
- [122] A. N. De Belder et K. O. Wik. *Preparation and properties of fluorescein-labelled hyaluronate*. Carbohydrate Research 44 (1975), 251-257.
- [123] H. Jin et al. *Biomaterial Films of Bombyx Mori Silk Fibroin with Poly(ethylene oxide)*. Biomacromolecules 5 (2004), 711-717.
- [124] Q. Hua et al. *Internalization of hyaluronan by chondrocytes occurs via receptor-mediated endocytosis*. Journal of Cell Science 106 (1993), 365-375.
- [125] D. W. Hutmacher. *Scaffolds in tissue engineering bone and cartilage*. Biomaterials 21 (2000), 2529-2543.
- [126] A. Motta et al. *Serum protein absorption on silk fibroin fibers and films: surface opsonization and binding strength*. Journal of Bioactive and Compatible Polymers 17 (2002), 23-35.

- [127] R. Servaty et al. *Hydration of polymeric components of cartilage – an infrared spectroscopic study on hyaluronic acid and chondroitin sulfate*. International Journal of Biological Macromolecules 28 (2001), 121-127.
- [128] A. Motta et al. *Stabilization of Bombyx mori silk fibroin/sericin films by crosslinking with PEG-DE 600 and genipin*. Journal of Bioactive and Compatible Polymers 26 (2011), 130-143.
- [129] C. H. Lohmann et al. *Pretreatment with platelet derived growth factor-BB modulates the ability of costochondral resting zone chondrocytes incorporated into PLA/PGA scaffolds to form new cartilage in vivo*. Biomaterials 21 (2000), 49-61.
- [130] B. D. Boyan et al. *Regulation of growth plate chondrocytes by 1,25-dihydroxyvitamin D3 requires caveolae and caveolin-1*. Journal of Bone and Mineral Research 21 (2006), 1637-1647.
- [131] R. W. Forsey et J. B. Chaudhuri. *Validity of DNA analysis to determine cell numbers in tissue engineering scaffolds*. Biotechnology Letters 31 (2009), 819–823.
- [132] J. P. Bretauiere et T. Spillman. *Alkaline phosphatases. Methods of enzymatic analysis*. Verlag Helvetica Chimica Acta (1984), 75–92.
- [133] C. Wang et al. *Cytocompatibility study of a natural biomaterial crosslinker—Genipin with therapeutic model cells*. Journal of Biomedical Materials Research B 97B (2011), 58-65.
- [134] J. Hendriks et al. *Co-culture in cartilage tissue engineering*. Journal of Tissue Engineering and Regenerative Medicine 1 (2007), 170–178.
- [135] J. Rnjak-Kovacina et al. *Tailoring the porosity and pore size of electrospun synthetic human elastin scaffolds for dermal tissue engineering*. Biomaterials 32 (2011), 6729-6736.

- [136] I. Pasquali et al. *Measurement of CO<sub>2</sub> sorption and PEG 1500 swelling by ATR-IR spectroscopy*. *Journal of Supercritical Fluids* 45 (2008), 384–390.
- [137] W. Cui et al. *Evaluation of electrospun fibrous scaffolds of poly(DL-lactide) and poly(ethylene glycol) for skin tissue engineering*. *Materials Science and Engineering C* 29 (2009), 1869-1876.



# Acknowledgements

This doctoral thesis would not have been possible without the constant support of my supervisor Dr. Antonella Motta, whose encouragement, suggestions and helpfulness led me to this important result.

I owe my gratitude to Prof. Claudio Migliaresi for his constructive advices and the great opportunities he offered to me during these three years of work at BIOtech.

I am deeply thankful to Dr. Barbara D. Boyan and Dr. Zvi Schwartz for providing me the extraordinary possibility to spend seven months working at the Parker H. Petit Institute of Bioengineering and Bioscience at the Georgia Institute of Technology in Atlanta (US). This stimulating and challenging experience made me grow both personally and professionally. I would also like to acknowledge their financial support to participate in the TERMIS-NA Congress in Orlando (US) in 2010.

I would like to thank my amazing colleagues, who accompanied me through one of the toughest period of my life, offering me a practical support and a whole-hearted friendship. A special thank to my desk partners during the last few months (you know what I am talking about). Last, but not least, I would like to thank Eleonora and Matteo for giving me an essential hand in the most difficult time, with genuine affection.

I am heartily grateful to my friends, who have always been there for me to share problems, doubts, choices and the satisfaction for the goal I achieve today. I would like to thank Elena, who has always believed in me, Laura, Eleonora

and Laura, who have constantly supported me throughout these years.

I would like to thank my family, mamma Loreta, papà Franco, Alessandro, Lorenzo and Alberto, for the continuous encouragement and backing. A particular thank to my sister Deborah, who has always been a guide with her advices and affection.

Finally, I would like to thank Stefano, who has taken care of me, lovely and unconditionally.